# NONINVASIVE IMAGING OF THE LUNG IN MODELS OF ASTHMA AND COPD

# NONINVASIVE IMAGING OF LUNG PATHOLOGY AND PHYSIOLOGY IN MURINE MODELS OF ASTHMA AND COPD

By BRIAN N. JOBSE, B.Sc. (H)

A Thesis Submitted to the School of Graduate Studies in Partial Fulfillment of the Requirements for a Philosophical Doctorate

McMaster University PHILOSOPHICAL DOCTORATE (2012)
Hamilton, Ontario (Medical Sciences)

TITLE: Noninvasive Imaging of Lung Pathology and Physiology in Murine Models of Asthma and COPD
AUTHOR: Brian N. Jobse, B.Sc. Honours (McMaster University)
SUPERVISOR: N. Renée Labiris
NUMBER OF PAGES: ix, 130

## ABSTRACT

Obstructive lung diseases limit airflow and gas exchange and have a major impact on a patient's long-term health. Asthma and chronic obstructive pulmonary disease (COPD) are the most prevalent obstructive lung diseases and represent a major burden on healthcare systems worldwide. It is now accepted that the pathologies associated with these diseases are heterogeneous in nature, and as the function of the lung is determined by its three-dimensional structure, methods to volumetrically evaluate the lung are important tools in furthering the study of these pathologies.

Three-dimensional imaging methodologies, such as computed tomography (CT) and single photon emission computed tomography (SPECT), are used clinically in the diagnosis of lung disease, but results are not commonly quantified. In addition, asthma and COPD develop slowly over time and diagnosis normally takes place after the underlying pathologies are well established. Experimental models in small animals, such as rats and mice, allow for the study of disease pathogenesis in a controlled setting and development of quantitative imaging practices for these models provides translational tools for relating results back to the clinic.

In this thesis, CT densitometry and ventilation/perfusion (V/Q) SPECT are explored as methods to investigate models of asthma and COPD. CT densitometry is shown to be capable of quantifying allergic inflammation in an asthma model but is of less use in a model of COPD, predominantly due to the relative amounts of inflammation present. However, V/Q imaging is shown to be quite sensitive to the effects of cigarette smoke in a model of COPD and has been used to better understand how pathologies associated with COPD contribute to gas exchange limitation in the lung.

The models, imaging techniques, and analysis methods described in this work provide insight into chronic obstructive lung disease and allow for future investigations into how pathologies affect gas exchange. Further, the characterization of the models described in this thesis allows for drug efficacy studies to be performed, both on established and novel treatments. Future research into asthma and COPD will benefit further from the use of three-dimensional imaging methodologies because they provide volumetric information on structure and function and can act as a translational bridge between clinical disease and preclinical animal models.

## ACKNOWLEDGEMENTS

I would like to begin by thanking my family, both natural and acquired, for their support over the years and for never questioning what to some could be considered the foolhardy undertaking that is a Ph.D. My friends, who know who they are, have also had an impact by keeping me relatively sane. Thank you for believing in me.

I would also like to acknowledge the many excellent teachers and tutors I've had over the years, without whose help I would not have made it this far. A particular thank you to Dr. W.P. Sheffield and V. Bhakta for their patience and the chance to find that I could excel in a laboratory setting. Dr. J. Johnson needs special mention as the person who taught me how to be a graduate student and has been a resource whenever I have needed her insight. To C. Saab, thank you for putting up with me throughout my training and for making the imaging aspect of research a lot of fun. To R. Rhem, I could not have managed to overcome the hurdles involved in this research without your problem solving, your constant good attitude, and your ability to chat about anything under the sun. To the other graduate students and technicians that have made my experiences bright, thank you!

To my Supervisory Committee, you have guided me to the edge of scientific knowledge and have had the patience to listen while I described confusing findings in an equally confusing manner. Dr. T. Farncombe, thank you for making the time to explain topics in medical physics whenever I had a question. Dr. M. Jordana, thank you for believing in my abilities and for giving me the opportunity to succeed. Dr. M. Stämpfli, thank you for treating me like a member of your lab and for all the advice. Dr N.R. Labiris, thank you for having so much patience, for the opportunities you gave me, and for your guidance; keeping me on track is a challenge at the best of times and you've done admirably.

Finally, to my wife Lauren, thank you so much for standing by me through all of my trials and tribulations in graduate school. You don't even know what a difference your love has made. I could somehow manage to do it all over again with you by my side, but please don't make me.

# TABLE OF CONTENTS

## LIST OF FIGURES AND TABLES

## LIST OF COMMON ABBREVIATIONS AND SYMBOLS

ANOVA – Analysis Of Variance
BAL – Bronchoalveolar Lavage
BALT – Bronchial Associated Lymphoid Tissue
BN – Brown Norway (rat)
COPD – Chronic Obstructive Pulmonary Disease
CS – Cigarette Smoke
CT – Computed Tomography
eV – Electron Volt
$^{18}$FDG – $^{18}$Fluorodeoxyglucose
$FEV_1$ – Forced Expiratory Volume over 1 second
FRC – Functional Residual Capacity
FVC – Forced Vital Capacity
GINA – Global Initiative for Asthma
GOLD – Global initiative for chronic Obstructive Lung Disease
Gy – Gray (mGy – milliGray)
H&E – Haemotoxylin & Eosin
HDM – House Dust Mite
HU – Hounsfield Unit
HVC – Hypoxic Vasoconstriction
IgE – Immunoglobulin class E
IL-1 – Interleukin 1
kV – kilovolt
LAA – Low Attenuation Area
Log – Base 10 Logarithm
LPS – Lipopolysacharride
MAA – Macroaggregated Albumin
MBq – MegaBecquerel
MIGET – Multiple Inert Gas Elimination Technique
MLI – Mean Linear Intercept
MRI – Magnetic Resonance Imaging
$^{13}N_2$ – $^{13}$Nitrogen Gas
PBS – Phosphate Buffered Saline
PET – Positron Emission Tomography
PFT – Pulmonary Function Test
PMT – Photomultiplier Tube
PPE – Porcine Pancreatic Elastase
ROI – Region of Interest
SPECT – Single Photon Emission Computed Tomography
$^{99m}$Tc – $^{99m}$Technetium
TLR-4 – Toll-like Receptor 4
TLV – Total Lung Volume
TV – Tidal Volume
Veh – Vehicle Control
VLA – Volume of Low Attenuation
V/Q – Ventilation/Perfusion
$\infty$ – Infinity
$\rho_{lung}$ – Mean Lung Density Value

# PREFACE

This thesis contains three peer-reviewed articles and one manuscript for which I am the first author. While there are other contributing authors, I was responsible or involved in the experimental design, experimental execution, data collection, data analysis, writing, editing, and submission of these works.

In the second chapter, I was responsible for all of the above aspects of work. Other authors contributed to all of these areas as well, but I was involved in the acquisition of all images and specimens, the analysis of all data, and the writing of the journal article.

Some of the data contained in the third and fourth chapters were collected previously to my work on the project, but I was involved in the final stages of data collection through to the final analysis. The analysis techniques, in and of themselves, represent a major contribution as many of these quantification methods had to be envisioned, programmed, and tested; the majority of this work was completed by myself in conjunction with Rod G. Rhem. Again, while other authors contributed to various aspects of the work in the third and fourth chapters, all data analysis and submission of the work was my responsibility.

Finally, the fifth chapter explores various aspects of obstructive lung disease and, again, I was primarily involved in all steps of design, experimentation, analysis, and writing. Other authors contributed to experimental execution, data analysis, and editing but, overall, this thesis represents original work for which I was primarily responsible.

# Chapter 1
# Introduction

## 1.00 – Overview

The advance of medical treatment for human disease is firmly rooted in the ability to translate scientific progress into the clinical setting. As the burden of disease in Canada, and in much of the world's population, shifts from infectious pathologies to chronic, non-communicable disorders [1] the scope of our current inability to prevent or treat many of these conditions has become more apparent. It is therefore important to continue efforts to characterize and understand the biological functions of the human body in health and disease and to develop new methods and tools to aid in this venture.

Lung disease is a research area where a better understanding of both pathologies and pathogenesis is required. Two chronic lung diseases, in particular, have been increasing in morbidity and mortality over the past decades: Asthma affects over 300 million worldwide [2] while Chronic Obstructive Pulmonary Disease (COPD) is responsible for at least 2.5 million deaths annually worldwide [3]. While these diseases have high prevalence in our society, very few treatment options are available and there are even fewer options to reverse the course of disease [2,4]. With the increasing incidence of these diseases comes a long-term strain on the healthcare system. These pulmonary diseases cause airflow obstruction on a daily basis and are associated with episodic exacerbations that endanger lives and create a significant burden on emergency healthcare systems [5,6]. Unfortunately, as these diseases develop slowly over time, the early pathology is rarely detected or assessed and is therefore extremely difficult to study in a clinical context. In addition to this lack of information regarding the pathogenesis of disease, the current methods to assess disease severity fail to differentiate the heterogeneous pathologies underlying the airflow obstruction [7,8]. Earlier diagnosis of these diseases may allow for prevention of irreversible lung damage.

Medical imaging has the potential to add substantial insight into these lung diseases, due to strengths in identifying pathology, tracking disease progression and allowing for longitudinal cohort studies to better understand pathogenesis. This half-century old diagnostic field is comprised of several non-invasive technologies that provide volumetric images of anatomical structure or physiological processes in the body. Due to the complexity of these images, and the associated methods and computing power necessary to analyze them, this field, up to the present, has been primarily qualitative in nature, relying on trained specialists to interpret findings on an individual basis. Through the continued evolution of imaging techniques and computing methods these powerful methodologies can now begin to be harnessed to provide the information that is necessary to understand the pathogenesis and constituent structural and functional abnormalities of chronic respiratory diseases.

Though volumetric medical imaging has been used clinically for several decades in diagnostic practice, translation of these techniques to small animal research is a relatively recent advance [9]. Small animal models of disease, usually in rats or mice, are used to investigate the molecular and physiologic mechanisms contributing to disease. These models are especially useful where ethical considerations limit experimental design or when a disease takes years to develop in humans. The results obtained from studies in small animal models provide a glimpse into the possible mechanisms underlying human disease and can be used for preclinical screening of therapeutic interventions. The use of imaging technologies in preclinical settings provides the same benefits in understanding pathologies and pathogenesis and extends the ability to experimentally determine the biological mechanisms contributing to disease [10]. In addition, due to the nature of preclinical research as a quantitative field and the general lack of quantitative analysis in clinical imaging, small animal research models are now also serving as venues for the testing of new approaches to disease measurement.

Because so many of the biological and physiological pathways are evolutionarily conserved between mammalian species [11], preclinical imaging provides an important opportunity to translate findings in the laboratory to results in the clinic. At present, imaging research abilities in both small animals and humans are not widespread and many clinical abilities have yet to be applied to preclinical models; however, this avenue represents a significant step in research potential. Through development of novel small animal imaging methodologies and analysis techniques it is my belief that debilitating chronic pulmonary diseases, such as asthma and COPD, can be better understood, and ultimately can be better diagnosed, treated, and even prevented.

## Section 1.1 – The Lung in Health and Disease

### 1.10 – Lung Structure, Function, and Physiology

The lung is a vital organ that facilitates gas exchange for molecules necessary for proper metabolic function. All cells within the body require molecules such as adenosine triphosphate (ATP) as an energy source, and the majority of cells require oxygen to produce ATP efficiently [12]. The process of oxidative phosphorylation, taking place in mitochondria, is responsible for the production of most of the ATP produced in the body and this process uses oxygen as an end-stage electron acceptor, converting the molecular oxygen to water. Carbon dioxide is another important gas in the body as it is produced at various points in cellular metabolism prior to oxidative phosphorylation [13]. Both oxygen and carbon dioxide are therefore integral to metabolism, and, as the body never stops metabolizing fuel sources, a constant supply of oxygen and constant removal of carbon dioxide is required. The cardiovascular system is responsible for transporting oxygen to cells and removing carbon dioxide. The lungs form a

fundamental part of this system as the location where oxygen is absorbed into the body and carbon dioxide is expelled into the outside environment. The act of breathing is therefore responsible for controlling the partial pressures of these gases within the lung and bloodstream [14].

The lung is made up of several components that form the lower respiratory tract. The primary airway is the trachea, which bifurcates into the major bronchi and these, in turn, bifurcate into still smaller airways. In humans, there are approximately 23 generations of airway before the respiratory zone of the lung, which is comprised of alveolar ducts and alveoli [12]. This branching pattern allows for a large amount of surface area that can be used for gas exchange. The alveoli are comprised of a single epithelial layer covered with a thin liquid layer known as surfactant that acts to help regulate the structure through reduction of surface tension [14]. Immediately adjacent to the alveolar epithelial cells are endothelial cells of the pulmonary capillary beds through which blood flows. The entire cardiac output of blood comes from the heart, through the pulmonary artery, which branches in a manner similar to the airways to become the alveolar capillary beds, and then reverses this branching pattern to become the pulmonary vein, which then returns to the heart.

Gas exchange is therefore reliant on both ventilation of the alveoli and perfusion of the capillary beds. The beating of the heart forces blood through all bodily blood vessels and perfusion of the lung capillary beds is achieved by this action. Ventilation of alveoli is reliant on the flow of air into the lung. To achieve ventilation the diaphragm and muscles of the chest wall move away from the lungs causing a negative pressure in the space between two pleural sacs surrounding the lungs. Gases follow the properties of fluid dynamics, moving from volumes of high to low pressure, so once a negative pressure is created within the thorax air rushes in to fill the void [14]. This difference in pressures is also responsible for movement of oxygen molecules into the deoxygenated blood and the movement of carbon dioxide into the alveoli. While at rest, breathing out air is a passive process. The lungs, as well as the chest wall, have elastic recoil and so force air out until equilibrium is reached. Exhalation during exercise retains the passive recoil properties but adds an additional, muscle-driven component [14].

The airways provide the means by which to move air from the oropharynx to the alveoli. Airways are stiffened and strengthened by structural components such as collagen and fibronectin, among others [15], and the larger airways, such as the trachea and major bronchi, have support from rings of cartilage [12]. In addition, larger airways are also surrounded by a layer of smooth muscle. These structural elements are required to ensure the airways stay open to the movement of air under the pressures exerted in the act of breathing; without airways, efficient movement of gases into the alveoli would not be possible [12]. Movement of air through the airways is dependent on the resistance of the system. For each airway the resistance is determined by the relative amounts of

laminar and turbulent flow and is heavily dependent on the luminal diameter of the airway in question. The resistance of any one path through the lung can be summed as all of these resistances are in series. Therefore, the movement of air into the alveoli of the lung is greatly affected by the structure and condition of the airways [14].

Finally, the lung has several defence mechanisms to protect against various insults. Particulate matter that enters the trachea normally impacts against the wall of one of the major airways; the larger the particle, the more likely impaction and sedimentation become. These large particles are removed through mucocilliary clearance [12]. The major airways are lined with a layer of mucous produced by goblet cells within the epithelium. This mucous layer is carried, by the beating of tiny cilia, toward the top of the trachea where the offending material and mucous is swallowed into the esophagus. Other defense mechanisms are immune in nature: macrophages phagocytize any foreign small particulate that deposits outside the range of the mucocilliary clearance and either innate and/or adaptive immune responses are triggered by any invading pathogen recognized [16]. In a healthy individual, these immune mechanisms only respond when needed and only to the degree necessary to rid the lung of the pathogen and return it to a sterile condition.

### 1.11 – Obstructive Lung Disease

Obstructive lung diseases are defined as afflictions wherein the respiratory flow rate is obstructed. This physiological definition widely applies to such lung diseases as asthma, chronic obstructive pulmonary disease (COPD), cystic fibrosis, pulmonary fibrosis, and many other subtypes and related syndromes. All of these conditions together affect over 3 million in Canada alone causing a significant, long-term burden on healthcare systems [17]. Of these diseases, asthma affects over 2.7 million while COPD affects over 750 thousand in Canada [17]. The morbidity and mortality associated with these diseases have been increasing over time [2,4].

In the case of asthma, the increase in prevalence is linked to an increase in allergy rates but it is unknown what is driving this increase in atopy in the population. Possible contributors include genetic predisposition, pollution and toxin exposure, and interaction with commensal and infectious microorganisms [2,18,19,20]. Allergy develops when the immune system of the body recognizes a normally innocuous molecule, such as pollen, as a threat and begins to mount inflammatory responses involving the adaptive arm of immunity [21]. Various cell types begin to respond to the allergen as if it were an invading microbe or parasite, causing airway inflammation and resulting in the various upper respiratory tract symptoms associated with allergy such as mucus secretion, sneezing, and nasal congestion. In asthma, this process also takes place in the lower respiratory tract where the mucus and inflammation cause narrowing of the airways and impede airflow into the lungs [22]. In addition, asthmatics have increased smooth muscle and structural components around their major airways,

known generally as airway remodelling [15]. Upon exposure to allergen, or other triggers, the smooth muscle layers contract to close the airways even further, a process referred to as bronchoconstriction. Physiologically, the combination of inflammation, mucus, and active airway constriction lead to obstruction of airflow into the lungs; therefore, the larger, major airways generally contribute most to airflow limitation during an asthmatic attack as this is the general site of structural remodelling and muscle contraction. Asthma is defined as a reversible airflow obstruction as therapeutic intervention, or time away from the allergen, can potentially return airflow to normal [2].

COPD, on the other hand, is physiologically defined as a non-reversible airflow obstruction. This is because the airflow limitation is caused by changes to the lung structure that do not generally resolve over time [4]. These changes include destruction of the alveolar surface complex, known as emphysema, and fibrosis of the small airways [4]. Thus, the smallest airways and end-units of the lung structure generally contribute most to the airflow obstruction in COPD. While there are several causes of COPD, by far the most common is exposure to cigarette smoke [4]. Repeated exposure to cigarette smoke causes low-level inflammation and a skewed inflammatory profile [23]. Many other issues stem from smoke exposure such as altered expression of genes, cellular damage and death, and lowered resistance to infectious agents. In many aspects, COPD resembles an accelerated aging process of the lungs [24]. These changes, in tandem with the inflammation, eventually result in pathologies such as emphysema and small airway fibrosis, among others. Furthermore, infectious agent-induced exacerbations of the inflammatory response in the lungs cause more severe airflow obstruction, are a major cause of hospitalization, and could very well contribute to the pathogenesis of the disease [25,26]. Ultimately, this chronic and debilitating disease affects between 15 and 50 percent of smokers, with increasing incidence with increasing age [4,27]. The increase in COPD morbidity and mortality is therefore linked to the prevalence of cigarette smoking and the aging population in many countries.

While a combination of corticosteroids, to dampen inflammation, and bronchodilators, to relax smooth muscle and open airways, are generally efficacious in asthmatics, these treatments do not work for every patient and do not cure what can be a lifelong disease [2]. In COPD, the inflammation is generally insensitive to corticosteroid therapy and no therapeutics exist to address the structural pathologies [28]. In both of these chronic diseases the pathogenesis is unclear and more investigation is needed to properly define the patient population and to characterize the underlying pathologies [2,4,7,8]. Overall, asthma and COPD are major healthcare concerns that need to be addressed so as to manage the associated healthcare costs, to reduce the overall prevalence, and to provide better care and therapeutic intervention for afflicted individuals.

## 1.12 – Pathobiology of Atopic Asthma

Asthma is commonly associated with atopic, or allergic, immunological responses to aeroallergens. There are many aeroallergens associated with allergic asthma including plant pollens, fungal spores, animal dander, and factors associated with insects such as cockroaches and house dust mites (HDM) [2]. Allergic airway disease begins with sensitization to an aeroallergen and investigation into the mechanisms of allergic sensitization is ongoing. However, initial immune reactions can be associated with the allergens themselves as, for example, when proteolytic action of house dust mite faecal proteins damage airway epithelial layers and invoke repair and defense mechanisms [29]. Genetic predisposition is known to play a role and environmental factors have also been implicated in this process [2,18,20,30]. It is now also becoming clear that other immunological events, such as the inflammation brought on by viral infection, can alter the response to otherwise tolerated levels of potential allergens [19]. Though there are many potential mechanisms at play during sensitization and they have yet to be fully elucidated, all allergic disease must begin with immune sensitization wherein the adaptive arm of the immune system develops recognition of the allergen as a target for later response [22]. In the case of actual pathogens this adaptive response serves to quickly recognize and eliminate any repeat infection [16], but in the case of allergen where there is no threat to the well being of the individual, the adaptive response only serves to damage the surrounding lung tissue.

The prevalence of airway allergy has been growing over the last generations and now affects a significant proportion of the population [31]. For many these allergies are a nasal nuisance or a slight disability, but for those where allergy progresses to allergic airway disease it becomes a chronic and potentially life-threatening lower-respiratory tract condition [22]. Exposure to allergen in an atopic asthmatic causes robust inflammation in the major airways where the allergen impacts upon the epithelial layer. This inflammation is triggered both by innate mechanisms, such as recognition of bacterial content by receptors recognizing ancient pathogen-associated molecular patterns (PAMPs) and, more importantly, by adaptive responses that recognize the protein content of the allergen itself [21]. This adaptive recognition is co-ordinated through T-lymphocytes, which specifically recognize an antigen and generally serve to prime other immune cells. Also at play are B-lymphocytes and related cells, which produce and release immunoglobulins (Ig), or antibodies, against the specific antigen. These antibodies, which include several classes indicative of allergy, bind to their target and are in turn recognized by various other immune cell types, each of which has a different response depending on its type and current environment. Two of these cell types, namely mast cells and eosinophils, are thought to be important in asthma as they release cytotoxic compounds into their environment given the correct conditions and the presence of antigen-bound IgE class antibodies. All of these immune cell types, as well as structural cells in the airways, release compounds known as cytokines, which act as mediators to prime or signal other cells, and chemokines, which act to recruit

other cells to the area of inflammation. In addition to the cellular component of inflammation, many proteins are present within an oedematous infiltrate. While there are mechanisms that eventually calm this storm of mediator and cellular activity, continued exposure to the allergen means continued inflammation [21]. As inflammation cannot necessarily act in a completely specific manner, damage is inflicted upon the structural cells and components of the lung during the inflammatory episodes common in asthmatics.

Remodelling of the airway walls is the next broad step in the development of asthma and is likely initiated by the inflammatory environment described previously [15]. During airway remodelling additional layers of structural extracellular matrix proteins, such as collagen and fibronectin, are laid down. This is generally associated with activation/differentiation of fibroblasts into myofibroblasts [15]. Also involved in the remodelling process is the thickening of the smooth muscle layer surrounding major airways. There is no current consensus on the biological relevance of this thickening process but, once remodelling has taken place, the airways are capable of greatly reducing their diameter and, along with inflammation and mucus in the airway, greatly restrict airflow into the lung [15]; resistance to airflow in an airway is related to the radius to the inverse fourth power meaning that the large changes to airway diameter possible in asthma can lead to severely limited airflow.

### 1.13 – Pathobiology of Chronic Obstructive Pulmonary Disease

The majority of patients suffering from chronic obstructive pulmonary disease (COPD) are, or were, long-term smokers of cigarettes [4]. Other forms of COPD are caused by exposure to high levels of certain particulates or biofuel smoke. Further, genetic mutation in the α1-antitrypsin gene can produce deficiency in this key anti-protease, which in turn can result in irreversible airflow obstruction [32]. However, cigarette smoke exposure is the principal underlying cause in up to 90 percent of cases [17]. The definition of COPD is physiological and there are several lung pathologies involved in the airflow limitation present in this chronic disease. Each patient may have differing amounts of these differing pathologies; current wisdom separates COPD into numerous phenotypes based on characteristics described by clinical, physiological and radiological outcomes as well as exacerbations, systemic inflammation, and comorbidities [8]. These patients ultimately have severe gas exchange impairment due to both airflow limitation and the fact that the gas exchange units of the lung become compromised. Only those aspects of disease associated with cigarette smoke exposure will be discussed further and only as they apply to the local environment of the lung.

Cigarette smoke is comprised of aerosol and gaseous components. Over 4700 substances have been identified in cigarette smoke including many known carcinogens and various other harmful molecules [33]. Gases such as nitric oxide, among others, are known to interfere with the pulmonary vascular response and several components cause inflammation upon interaction with the

airway and alveolar epithelial layers [34,35]. While the impact of some of these components is known to some degree, the biological consequences of such a diverse chemical milieu interacting with a mucosal tissue with an incredibly large surface area is complicated and unpredictable. Three of the primary pathologies associated with prolonged exposure to cigarette smoke are neutrophilic inflammation, small airway fibrosis, and emphysema [21]. While these conditions are present in patients with COPD, non-affected smokers may also have them to some degree, though not enough to severely affect lung function [35].

Inflammation is an immune response generally responsible for fighting off infectious or parasitic agents [16]. As the homeostasis of the immune response is dependent on a large number of signalling molecules, many of which have redundant capacities, the precise mechanisms behind cigarette smoke-induced inflammation are still being investigated. It has now been established in the mouse that this inflammation is interleukin 1 (IL-1) as well as toll-like receptor 4 (TLR-4) dependent [36]. IL-1 is a primary inflammatory cytokine involved in almost all immune reactions and TLR-4 is a receptor for lipopolysaccharide (LPS), a component found on the surface of gram-negative bacteria and a danger signal to the immune system [16]; tobacco smoke is known to contain LPS, likely from bacteria on the surface of the tobacco leaves prior to combustion [37]. Continued exposure to cigarette smoke leads to inflammation and a skewed inflammatory profile with the presence of neutrophils, a cytotoxic cell-type, as a hallmark [35]. Prolonged exposure also leads to secondary lymphoid structures forming in the lung, known as bronchial associated lymphoid tissues (BALT), a central point for antigen presentation and adaptive immune cell activation [38]. Eventually, this altered inflammatory environment persists, even after smoking cessation, along with the presence of antibodies targeted against self-antigens, meaning that COPD may be, in part, an autoimmune disorder [39,40]. Inflammation is associated with both cellular and oedematous infiltrates which both can act to obstruct small airways by decreasing luminal diameter [23].

Small airway fibrosis is a pathology likely stemming from small airway inflammation, though the link between inflammation and fibrosis is unclear [35]. Fibrosis refers to the accumulation of fibrotic material, generally structural proteins or other structural molecules such as collagen, fibronectin, or others. Thus, fibrosis caused by prolonged cigarette smoke exposure is a form of scar tissue formation, likely caused by the ongoing inflammation around the small airways. Due to the addition of these structural elements the affected airways become less pliable and less adaptive, and may lose luminal diameter, causing airflow obstruction [23].

Emphysema, on the other hand, is a loss of alveolar tissue that results in air trapping [23]. Again, the precise links between cigarette smoke and emphysema are not yet established, but inflammation is the probable culprit, at least insofar as initiation of the process. Alveolar regions are made up of pulmonary

capillaries covered by alveolar mucosal epithelial layers. The protein elastin is an essential component of the alveoli, giving them elastic recoil that is important to the process of breathing [14,41]. Several inflammatory proteinases, including members of the matrix metalloproteinase family and elastase, are capable of breaking down elastin and other structural components of the alveoli, leading to the loss of alveolar tissue [42]. With this tissue loss comes the loss of the associated elastic properties, meaning there is less force present to push air out of these regions. In addition, airways, especially small airways, are held open in part by tethering forces produced from elastic recoil of alveolar regions [14]. Therefore, emphysema formation leads to air trapping but could also affect the stability of neighbouring airways not directly associated with the airspace enlargement.

Together, inflammation, small airway fibrosis and emphysema are likely responsible for much of the airflow obstruction seen in COPD patients [23]. As each patient has different genetics, a different history of smoking, and a different history of illness and lung infection, there are many different combinations and variations of the pathologies described. Over time, these pathologies worsen and lead to both airflow obstruction and gas exchange limitation. It is also becoming clear that COPD is under-diagnosed, as people associate their loss of breath with age, and that many of these pathologies, once established, continue in the absence of cigarette smoke [4].

## Section 1.2 – Medical Imaging of the Lung

### 1.20 – Imaging Modalities Overview

Medical imaging has its roots in the first documented x-ray image, a radiograph of a human hand produced by Wilhelm Röntgen in 1895, and the subsequent use of x-ray images to diagnose a variety of ailments [43]. Other imaging modalities were developed to address different needs, most within the past half century. While two-dimensional, or planar, imaging methods are still used for a variety of purposes, three-dimensional, or volumetric, imaging methods are much more powerful as they more accurately describe the object, or patient, being imaged. Examples of planar imaging methods still currently in use include x-ray and gamma scintigraphy; the images produced from these methods are summations across the body. Common volumetric imaging methods include computed tomography (CT), single photon emission computed tomography (SPECT), positron emission tomography (PET), and magnetic resonance imaging (MRI). Some of these methods were derived from previous planar methods, as is the case with SPECT being a 3D version of gamma scintigraphy and CT being a 3D version of x-ray, while others are inherently volumetric, such as MRI. However, all volumetric data is ultimately stored electronically as a 3D matrix, and any particular plane within the matrix can therefore be viewed.

CT images are produced from a series of rotating planar x-ray images while SPECT images are produced from a series of rotating planar gamma scintigraphy images. X-ray images are produced by differential x-ray absorption, or attenuation, while gamma scintigraphy images are produced by collecting gamma rays created from radioactive events coupled to a molecule of interest [44]. These techniques will be described in greater detail in following sections due to their importance to the work described in this thesis.

PET images, on the other hand, are produced by determining a line of response between two coincident gamma photons created during an annihilation event between a positron and an electron. To accomplish this, the positron-emitting isotope must be coupled to, or integrated into, a biological molecule of interest; once delivered into a patient, the biological molecule traffics to a specific target. Decay of the isotope, through a process known as β+ decay, produces the positron, as well as a non-important neutrino, in the general location of the biological target. After annihilation, the two 511keV gamma photons created travel at the speed of light approximately 180 degrees to each other [44]. The process by which these photons are collected, amplified, and recorded is paralleled in SPECT imaging and will be detailed later. The important difference is that PET imaging uses a 360-degree collection system around the patient so as to detect both coincident photons. During reconstruction of the image, lines of response can be drawn between the detection points of the coincident photon pairs to create a volumetric map of the annihilation events. PET imaging uses isotopes of biologically relevant elements such as carbon, nitrogen, and fluorine but these isotopes have relatively short half-lives and require a cyclotron for production. Currently, PET is used for several applications but the most common diagnostic tests utilize $^{18}$Fluorodeoxyglucose ($^{18}$FDG), a labelled analog of glucose. Within the lung, this molecule is used in screening for lung cancer [45] and can be used to visualize neutrophilic inflammation [46], as both cancerous cells and neutrophils uptake glucose at a high rate and the $^{18}$FDG accumulates in cells without being metabolized [44]. Of relevance to this thesis, PET imaging can also be used to perform ventilation-perfusion scans with the use of $^{13}N_2$, providing data on perfusion, diffusion, and relative ventilation [47]. This technique has been used to investigate the impact of cigarette smoke on the lung [48] and has also has been used to assess both asthma and COPD [49,50].

MRI is another modality that can be used to image the lung. Briefly, a magnetic field is produced and atoms in the body with a net spin, I.E., the hydrogen in water molecules, line up to the field. A radio signal, which is a form of electromagnetic energy, is then applied, causing the molecules to go out of alignment with the magnetic field. The machinery then monitors the resultant induced voltage caused by the rotating magnetic moments of the affected atoms as they precess back to magnetic field alignment, a process known as free induction decay. A magnetic field gradient is used to spatially localize the resonance signal, allowing information to be gathered for any particular plane of the body. Atoms in different environments, I.E., different organs or other

situations, will have different processions and these differences will be detected, producing an image of these environments for the magnetic gradient plane being monitored. This process is then repeated for as many planes as necessary to gather the appropriate volumetric data [51]. There are many variations in molecules measured, radio signal used, magnetic field strength, and feedback measurement techniques employed, so the possibilities for medical tests are vast. Both anatomical and functional images are possible with this technique. However, MRI machines require additional infrastructure and expertise compared to other modalities, so their use is limited to major centres. Importantly, in regards to lung imaging, MRI is not particularly suited to collecting images of the lung due to the lack of signal, compared to other water-rich tissues [51]. Hyperpolarized gases, such as helium and xenon, can be used but this again requires specialized infrastructure and expertise. Nevertheless, studies using these technologies can be performed in the lung [52,53]. For example, MRI with hyperpolarized helium has been used to characterize progression of COPD [54] and to investigate methacholine challenge in asthmatics [55].

While all of the modalities discussed are capable of imaging the lung, each technique has advantages and disadvantages, making it more or less suitable for an organ or from an infrastructural view. For the lung, CT, PET, and SPECT can image the entire organ and are not particularly limited by the structure of the lung itself, as is the case with MRI. CT and SPECT are of particular relevance to this thesis as they were the modalities used to study the lung. Furthermore, the anatomical imaging offered by CT is complementary to the functional information that can be obtained through SPECT, making the use of these technologies very advantageous.

### 1.21 – Computed Tomography

Computed tomography is a volumetric imaging method developed by Hounsfield et al. and described in 1973 [56]. To produce a CT image, planar x-ray images, or projections, must first be acquired. Both a source of x-rays and a detector are necessary to produce these projections. The projections themselves describe the densities through which the x-rays must pass.

X-rays are produced in a vacuum by directing high energy electrons from a cathode towards a target anode, such as tungsten, and are described by wavelengths roughly between $10^{-8}$ and $10^{-13}$ m on the electromagnetic spectrum [57]. As the electrons pass by the atoms of the anode they change direction and slow. Energy must be conserved and, thus, photons are released from the slowing electrons; this process is known as bremsstrahlung radiation, or braking radiation. The photons generated will have an energy distribution in kiloelectron volts (keV) less than the original electron energies in kilovolts (kV). Allowing the escape of these photons, which will have energies above 100eV [44], in a specified direction then produces an x-ray beam [57].

As the x-ray photons pass through a subject there is a chance that they will be absorbed or scattered, a process known as attenuation. Attenuation is dependent on the density of molecules within any volume of space that the photon must pass through. As different tissues have different densities they each produce a different degree of attenuation [44]. If an x-ray beam is consistent across the area being imaged, then the number of x-ray photons that reach the far side of the subject depends on the sum of densities through which they had to pass [58]. A detector then collects photons that were not attenuated.

The original detectors for x-ray images were simple photographic film. CT images require computed reconstruction, and therefore require an electronic image. After passing through a subject, the x-rays strike a scintillation material. Within the crystal structure of the scintillation material the energy of the x-ray photon is absorbed and re-emitted as a multitude of lower-energy photons. Modern CT systems use photodiodes to collect the scintillation photons. Within the photodiode the signal and location of photon impact is converted to an electrical signal. Recording many signals from the photodiode thus produces an electronic x-ray projection image [57].

To produce a CT image a series of x-ray projection images are collected in short intervals 360 degrees around the subject. These projections are then reconstructed, generally by a procedure called filtered back-projection. Basically, back-projection takes a single projection and applies the attenuation values uniformly across the underlying matrix. The frequency data of each projection is applied from the appropriate angle whence it was acquired, resulting in a total frequency distribution of the subject. This data is then transformed into the final volumetric CT attenuation image, the matrix units representing the average for the total set of projections [44,57].

The CT image is then calibrated into Hounsfield units (HU) by setting the value of water to 0 and the value of air to -1000 [57]. This calibration step is necessary because different CT configurations or equipment will produce different CT units within the reconstructed image. Conversion to HU allows for comparison of images taken at different times, in different locations, or with different system settings. The final resolution of the CT image depends on many factors, including the original x-ray beam energy and its coherence, the amount of photon scattering within the subject, the size and shape of the collimator, the number of projections acquired, the scintillation material employed, the sensitivity and resolution of the photodiodes, and the reconstruction software and methodology used [57]. Using various strategies, medical CT machines can now produce extremely high-quality images in a relatively short amount of time with relatively minimal radiation dose compared to older machines. While the materials and technology used in CT machines have advanced over the years, the basic principles remain the same today.

Within the lung, CT can be used to measure tissue destruction (emphysema) or tissue build-up (fibrosis) in the parenchyma. Out of these two, only measurement of emphysematous lesions is a widely accepted clinical test due to ease of use and reproducibility. CT images can also provide information on wall thickness and luminal diameter of the airways, measures that are especially useful in diseases such as asthma. Furthermore, similar techniques can be applied to the pulmonary vasculature to provide diameter measurements. This type of index is of use in the study of COPD [52]. Additionally, CT can be used in conjunction with xenon gas to image ventilation in the using a dual-energy technique that exploits the photon absorption of the xenon [59]. Finally, CT angiography is a routine procedure that can be performed in cases of suspected pulmonary embolism. This technique requires the injection of a radio-dense contrast agent to depict the location and severity of occlusions in the pulmonary vasculature [60].

### 1.22 – Single Photon Emission Computed Tomography

Single photon emission computed tomography (SPECT) is a volumetric nuclear medical imaging technique that has developed from planar gamma scintigraphy. Similar to PET imaging, SPECT utilizes radioisotopes coupled to a biological molecule of interest, or a tracer of a biological process. This tracer is delivered to the patient, by various means depending on the medical test, and the distribution of the radioactivity in the body is determined by the specifics of the tracer and its interaction with the patient's tissues [44]. The isotopes employed in SPECT are generally of relatively high atomic weight, and so are generally coupled to relatively large biological molecules or tracers. While this large size limits the biological processes that could potentially be imaged by this technique, their ease of use due to relatively long half-lives is useful for patient interaction and for shipping the activity to distant centres. The radioisotopes used primarily decay to a more stable state through isomeric transition, releasing a gamma photon in the process. These photons have energies above 100eV, depending on the specific isotope being used, and because of their high energies they do not interact strongly with tissues; therefore, many of these gamma photons pass through the subject for possible collection by the SPECT detectors. It is important to note that these single emission photons escape the subject from the point of decay in all directions [44].

Similar to CT, a scintigraphic material is used to collect the photons exiting the subject. First, however, the photons must pass through a collimator, which is essentially a honeycomb of a dense material such as lead, so that only photons on a relatively straight path from the original source will be collected. Once through the collimator the photons can strike the scintillation material. Instead of photodiodes, SPECT detectors utilize an array of photomultiplier tubes (PMTs) to amplify the signal from an event to adequate levels due to the relatively low signal from gamma ray transmission possible in nuclear medicine techniques. The collision of a photon from the scintillation crystal striking the cathode of the PMT sets free an electron. This electron is directed towards a dynode that releases further electrons upon impaction of the original electron. PMTs contain

a series of these dynodes, multiplying the original incident photon signal to levels that can be detected by the circuitry attached to the final anode. Recording many signals from the array of PMTs thus produces an electronic projection image [44].

Normally, there are two detectors on either side of the subject, though other configurations are possible. After a certain amount of time, or after recording a set number of radioactive events, the detectors rotate to another orientation and eventually projections are acquired 360 degrees around the subject. Instead of back-projection, a computerized process known as iterative reconstruction is normally used to produce the final volumetric image. This process starts with an approximation within a matrix, which is compared against the data from the projections. The system then estimates a pattern that would better fit the data and again the data are compared to this new pattern. This process continues until the estimated image fits the projection data with good fidelity while limiting the reproduction of artifacts such as background scatter [61].

Data collected by SPECT describes the number of radioactive events within any of the matrix elements of the final image. The quality of the final image is dependent on the amount of radioactivity used and the number of counts collected, the type of detector and collimator employed, the characteristics of the PMT array, and the reconstruction software used [44]. As SPECT only supplies data on the distribution of the biological tracer, coupling this technique to an anatomical imaging methodology such as CT is highly advantageous.

SPECT imaging is currently used for three major purposes in regards to the lung. The first is the assessment of inhaled drug distribution [62]. The isotopes used in SPECT cannot easily be coupled to the drugs themselves to provide uptake information, but the delivery of the drug to the lung can be traced by adding an isotope-labelled compound to the delivery system, allowing for an assessment of the initial deposition. The second major use is the collection of information on the rate of mucocilliary clearance, which can be investigated by acquiring successive SPECT images after delivery of an isotope-labelled compound to the airways that is not systemically absorbed E.G., sulphur colloid [62]. Finally, physiological information regarding ventilation and perfusion within the lung can be acquired by using radiolabelled tracers of these processes. Scanning of this type is a standard diagnostic test in cases of suspected pulmonary embolism [63]. This technique will be expanded upon in section 1.34.

## Section 1.3 – Measurement of Lung Disease

### 1.30 – Measurement Overview

Lung disease is measured, both diagnostically and for research purposes, by various means of varying invasiveness to the patient. Tissue sampling is possible to view the structure or inflammatory state of the lung, either through excision of

diseased lung or biopsy with the aid of a bronchoscope. In another bronchoscope related manoeuver, bronchoalveolar lavage (BAL) can be collected from a region of lung and the inflammatory environment measured [64]. Sputum can also be induced, if necessary, to yield similar outputs [65]. The current gold standard approach is physiological in nature and seeks to determine the maximum forced rate of airflow out of the lungs, though others, such as the 6-minute walk test, exist to test the endurance of gas exchange [66]. Finally, imaging methodologies are playing an increasingly important role in measuring lung disease due to their non-invasive nature, ability to look at the entire lung, and ability to track biological processes. Many of these methods are complementary to each other but progress in some areas, especially within imaging fields, will be truly valuable so as to better understand and diagnose the wide variety of lung diseases. Basic descriptions of how these techniques are commonly used to assess the lung follow.

### 1.31 – Sputum, Bronchoalveolar Lavage, and Excised Tissue

There are many biological indicators of lung disease that can be measured through sampling of cellular material or fluids. The techniques required to collect specimens are generally invasive, either employing a bronchoscope or surgery to obtain a sample, and are therefore difficult to obtain regularly from patients [67]. In addition, a tissue sample taken in this manner is not necessarily representative of the state of the rest of the lung. Sputum is one source of biological materials that can be used to help determine the inflammatory state of the airways and whether any pathogens are present [68]. While sputum collection is noninvasive, it represents a pooled sample of airway inflammation and it is therefore not possible to determine the location of inflammation. In some cases patients can produce sputum easily, but experimental control patients or those unable to easily produce sputum can be induced to do so by inhaling hypertonic saline. Cellular, protein, and microbial/viral components within the sputum can then be measured to provide inflammatory information and to provide evidence of infection. Bronchoalveolar lavage, or BAL, is another method of gathering fluids containing the same sorts of measures available with sputum; however, BAL is performed with the aid of a bronchoscope and is effectively a wash of the outlying airways and alveolar regions [68]. Again, this means that BAL taken from human patients is only indicative of the environment in the region from which the BAL was gathered. While similar measures can be determined from both BAL and sputum samples, the methods used result in samplings of different environments within the lung.

Excised tissue is another means by which to gather information on the environment within the lung, but, as this requires surgery, it is only collected in cases of severe disease, especially when a portion of diseased lung is removed to increase the performance of the remaining lung tissue [69], or during a post-mortem. Excised tissue can either be homogenized, or ground up, so that protein indicators can be examined, or the tissue can be sectioned, mounted, and stained to allow cellular and morphometric analysis. This is common in cases of severe

emphysema, where tissue excision improves the respiratory mechanics of the patient and morphometric analysis of the collected tissue provides a quantifiable example of the degree of airspace enlargement [70]. This pathology is measured by the mean linear intercept, or MLI; a basic technique performed on high magnification images where the distance between alveolar septa is measured based on gridlines drawn across the sample [71]. This technique is labour intensive, and may or may not accurately reflect the disease status of the entire lung.

### 1.32 – Spirometry

Spirometry is the current gold standard for lung function testing and diagnosis of chronic respiratory disease. Also known as a type of pulmonary function test (PFT), this methodology measures the force and flow rate that a patient can produce during exhalation. Pressure-volume relationships in the lung can be described and can indicate how much compliance the lung has, an indicator of stiffness, and can also point to problems in the overall flow of air into and out of the lungs [72]. More commonly, at least in diagnostic practices, the forced expiratory volume over 1 second, or $FEV_1$, is used as a major indicator of disease when its value falls below a predicted value based on age and patient size. In fact, this measure is the basis for the diagnostic definition of both asthma and COPD. The forced vital capacity, or FVC, referring to the total amount of air a person can forcibly expel from their lungs from full inspiration, is also used, often as a ratio with $FEV_1$, to further delineate the altered function observed in diseases such as asthma and COPD. To diagnose a patient with obstructive lung disease, a predicted value of $FEV_1$ would be found based on age, weight, and gender. The $FEV_1$ is actually measured and expressed as a percentage of the predicted value. Currently, a percent of predicted $FEV_1$/FVC ratio of 0.7 or less denotes airflow obstruction [72]. A fast-acting bronchodilator is then administered and the patient retested. In asthma, the percent predicted $FEV_1$ would increase due to the reversible nature of the obstruction. In COPD, however, the percent predicted $FEV_1$ would not change as the nature of the obstruction is irreversible [72].

Unfortunately, in many cases diagnosis takes place well after the establishment of disease has occurred, at least partially due to the insensitivity of PFTs [73]. This is most apparent in diseases of the small airways as these airways, in a healthy lung, are only responsible for approximately 10-15% of total airway resistance measured at the mouth; a large degree of obstruction across many of the small airways is thus required before the impact on spirometric measures is apparent [23]. Because of this limitation, pathogenesis and progression of incipient disease is difficult to study and treatments targeting early disease processes cannot be implemented. In addition, PFTs quantify the global degree of airflow limitation but fail to address regional lung function or physiological changes caused by the various underlying pathologies that make up the disease [74]. In other words, PFTs are unable to differentiate between pathologies. The social and economic implications of these chronic conditions are expected to

increase [75] while the ability to evaluate the underlying pathogenesis within the lung remains indirect and insensitive to early disease.

### 1.33 – Anatomical Imaging

Many pathologies affecting lung function can also be visualized with anatomical imaging. Within the lungs, x-ray images are a common tool as the healthy lung parenchyma is relatively uniform across the entire organ, so that abnormalities appear as areas of greater or lesser density compared to normal tissues. Three-dimensional imaging methods are now preferable, as planar x-ray images cannot differentiate overlapping features along the axis in which the image was acquired. Both CT and MRI are capable of acquiring volumetric anatomical images of the lung but CT is better suited to this purpose due to characteristics of the methodology itself [52]. The combination of air and tissue within the lung provides great disparity for x-ray absorption, and therefore can provide excellent contrast in the final image.

CT is becoming an important tool for both the diagnosis and investigation of chronic lung diseases. For asthma, CT can be used to assess inflammation within the lung and, in particular, the altered structure of the major airways through measurement of airway diameter and airway wall thickness [52]. However, while these techniques are used in research they are not standard in clinical practice. In COPD, CT is used to describe the presence and amount of emphysema present in the lungs [76] and can act as a guide for lung resection surgery [69]. Contemporary CT systems can also investigate the structure of the small airways [77], a benefit in studying all lung diseases, as these small airways are crucial to lung function.

At present, CT or other anatomical images of the lung are rarely quantified. Generally, a radiologist assesses these images and the results are reported back to the primary physician. However, the data are not further utilized or investigated. One particular area where quantitative techniques are becoming more regularly employed is the identification of emphysematous areas in COPD patients. Emphysematous volumes attenuate fewer x-ray photons than the surrounding tissue and so have lower densities in the resulting CT image. A simple threshold, normally -950HU or the HU value at the lower $15^{th}$ percentile in humans, can be applied to quantify the volumes of low attenuation (VLA), also known rather erroneously as low attenuation areas (LAA) [76,78].

Research using CT to investigate obstructive lung disease have recently demonstrated that quantification of airway wall thickness in asthma is possible, though no consensus has yet been reached on correlation with disease severity or algorithms employed [79]. In COPD, results from CT have shown that terminal bronchiole narrowing and destruction precedes emphysematous lesion formation [77]. Recently, CT findings have demonstrated that airway tethering forces play an important role in the apparent increases of airway wall diameter, a measurement normally thought to reflect remodelling [80]. CT has also been used

to longitudinally investigate the progression of emphysematous lesions [81]. In addition, a technique assessing the differences between respiratory-gated CT images has shown promise for providing a biomarker of disease progression in COPD [82]. Clearly, the use of CT, and potentially MRI, in anatomical imaging of obstructive lung disease provides important tools that provide greater insight into these diseases.

### 1.34 – Ventilation/Perfusion

While $FEV_1$ is currently the gold standard of lung function testing, it is an incomplete measurement of lung function without assessments of ventilation and perfusion. Ventilation of alveoli (V) and blood perfusion of the associated pulmonary capillary beds (Q) are the two physiological processes ultimately responsible for gas exchange within the lung. Both ventilation and perfusion are determined by the resistance to flow along the airways or vessels through which the air or blood must travel prior to the possibility of gas exchange in an alveolar region [14]. As such, any pathology present within the lungs could impact either, or both, of these processes and lead to a decline in gas exchange capability. It is also important to note that mechanisms exist to ensure that ventilation and perfusion are as tightly matched as possible I.E., regions of high ventilation have high perfusion and regions of low ventilation have low perfusion. Pulmonary hypoxic vasoconstriction (HVC) is primarily responsible for this homeostasis but the multiple mechanisms underlying the response require further research [83]. Pulmonary HVC is conserved across many animal species and is a reaction in response to low oxygen pressure in an alveolar region. The multiple sensing mechanisms of HVC include, but are not limited to, changes in reactive oxygen species concentrations, changes in the concentrations of electron carriers, and changes to the mitochondrial environment. These mechanisms detect this lack of oxygen and act on the calcium influx of the surrounding blood vessels, causing them to contract and restricting blood flow to those regions of hypoxia, thus equalizing the ventilation-perfusion ratio [84]. Finally, in addition to the physiological processes of ventilation and perfusion, diffusion of gas must take place between the alveolar air space and the blood. This effect is commonly measured clinically by the lung diffusion of carbon monoxide, or $D_{LCO}$, which utilizes the inspiration of a small amount of carbon monoxide to determine diffusion capacity [85].

Measurement of ventilation and perfusion can be accomplished by several methods. One such method is the multiple inert gas elimination technique, or MIGET [86]. By injecting a patient with six gases of differing diffusion coefficients and monitoring the levels of these gases within the blood and in the exhaled breath, V/Q ratios for the lung can be established. Diffusion of gas from the blood into the alveoli and its subsequent washout through exhalation allows for a determination of gas exchange capability. The technique depends on the specific diffusion coefficients of the gases used and requires sophisticated calculations to determine the distribution of V/Q. Unfortunately, the expertise and equipment required for this type of test is not widespread and the results

represent a global measurement, or a measurement of the lung as a whole, with no possibility of regionalization.

Functional imaging techniques, on the other hand, offer the advantages of regionalization, though there are many measurement possibilities and, at present, few examples of quantitative evaluation. MRI can be used to measure ventilation properties with the aid of hyperpolarized gases. Further, perfusion can be examined by use of contrast agents injected into the blood [87]. Examples of recent research using MRI to investigate the lung include the assessment of asthmatics after methacholine challenge [55], several evaluations of patients with COPD [54,88,89], and an observation of collateral ventilation in COPD [90]. Radio-dense gases, such as Xenon, can be used in a similar manner with CT, though they are generally limited to studies of ventilation alone. Recent preliminary research has used inhaled Xenon gas in conjunction with CT to investigate asthma [91] and COPD [92]. Further, Krypton has now also been used in patients with COPD to show ventilation abnormalities [93].

PET, in conjunction with a soluble radioactive gas such as $^{13}N_2$, can also be used to trace perfusion, diffusion, and relative ventilation for the lung [94]. Since PET imaging collects data for the entire field of view simultaneously, a large portion of the lung can be imaged in real time as the radioactive nitrogen moves through the system. Coupled to anatomical imaging, such as CT, this technique also provides regionalization; transmission data from the PET scan can also be used, though anatomical detail is lacking in comparison to CT. A current drawback of PET V/Q is the necessity of cyclotron facilities on site, due to the short half-lives of the required radioisotopes. Another daunting problem is the vast amount of data collected representing the three processes of gas exchange referred to previously; PET V/Q images represent dynamic processes for which quantification methods have yet to be developed. While there are several technical issues surrounding this methodology, given time and resources it could be the most biologically accurate and useful V/Q measurement. PET imaging using $^{13}N_2$ has been used to investigate V/Q relationships in both asthma [50,95] and COPD [49], though clinical research appears to have been limited to a few small studies.

V/Q by SPECT, on the other hand, is a well-established methodology commonly used for diagnosis of pulmonary embolism [96]. As such, medical centres equipped with nuclear imaging facilities can easily accommodate this technique. In addition, $^{99m}$Technetium, the isotope most commonly employed, has a half-life of approximately 6 hours, allowing for ease of use. To complete a V/Q by SPECT a ventilation tracer, such as $^{99m}$Tc-labelled Technegas$^{TM}$, is delivered via the respiratory tract and a SPECT image acquired; this image describes the pattern of ventilation. A perfusion tracer, such as $^{99m}$Tc-labelled macroaggregated albumin (MAA), is then delivered via intravenous injection. The MAA traffics through the veins, through the heart, through the pulmonary arteries, and lodges in the pulmonary capillary beds. The same radioisotope may be used as long as the

relative quantity of the perfusion activity overwhelms that used for ventilation. A SPECT image of the distribution of the MAA thus describes pulmonary perfusion. Co-registration of the V and Q images allows for calculation of V/Q ratios and the addition of an anatomical image, such as CT, allows for regionalization. One limitation of this method is the lack of information regarding diffusion, meaning it may not be accurate in the study of diseases that impact diffusion distance, such as idiopathic pulmonary fibrosis. This technique is easily employed but, to date, quantification efforts have been minimal. SPECT V/Q imaging has been shown to be consistent with results from MIGET, indicating that this method accurately depicts gas exchange capability [97]. $^{99m}$Technegas/$^{99m}$Tc-MAA V/Q SPECT has not seen use in asthmatics to measure both ventilation and perfusion, but similar methodologies have demonstrated the potential for measurements in asthma [98,99,100]. In COPD, SPECT V/Q has been shown to be sensitive to pathological changes [101] and easily detects emphysematous lesions [102].

## Section 1.4 – Pre-clinical Experimental Systems

### 1.40 – Modelling Overview

Animal modelling, also known as pre-clinical modelling, refers to the use of organisms other than humans as surrogates for studying human anatomy, physiology, and molecular biology in health and disease. Experimental systems in animals are advantageous in that they allow for the testing of hypotheses that would not be ethical, or even possible, in humans. In Canada, the Canadian Council for Animal Care is the body that governs and enforces codes of ethical behaviour pertaining to the use of animals of all varieties in experimental systems; the vast majority of pre-clinical investigation takes place in flies, fish, and rodents [103]. Rodents are of particular use to pre-clinical investigation of human disease because, as mammals, they are biochemically quite similar to humans. In addition, they are small enough and have a generation time useful in experimentation. These animals are bred for the sole purpose of scientific experimentation so that all subjects are as similar as possible to allow for interpretability of results. Many experiments are carried out *in vivo*, and tissues and samples are collected at the appropriate time points. From an experimental design standpoint, this means that many mice are needed to provide sufficient numbers and controls at all time points necessary in the experimentation. If the measurements are terminal, which is common, comparisons of data are never from the same subject, limiting the interpretability of disease progression or drug efficacy studies.

Since rodent models became a workhorse of scientific disease experimentation, many strains of rats, mice, and other rodents have been developed. Each of these strains has particular characteristics that make them useful for study in particular areas of research. Further, as the molecular mechanisms behind health and disease are elucidated by experimentation, gene-knockout strains have been

developed for many genes of interest. These strains allow for specific proteins and pathways to be targeted so as to allow for better understanding of their roles in the biochemistry of a complex organism. While animal models never completely replicate the disease being modelled, they are particularly useful for studying specific pathways or pathologies. Even the simplest model, if appropriately carried out and interpreted, can provide valuable insight into human life.

### 1.41 – Asthma Models

Up until a decade ago there was one primary model of allergic airway disease in mice and other rodents. To produce this model, mice were first exposed to ovalbumin, an innocuous egg protein, intraperitoneally and in the presence of an immune adjuvant, normally alum. The adjuvant caused the immune system to react to an otherwise harmless protein. After several sensitization injections, mice were then exposed to ovalbumin via inhalation [104]. This exposure leads to eosinophilic inflammation around the airways similar to that observed in human asthma patients [104]. However, repeated exposure to ovalbumin in this system results in immune tolerance [105], a situation that is not consistent with allergen exposure in humans. While useful for studying the precise interactions of immune cells due to the simplicity of the 'allergen', this model does not represent mucosal airway sensitization or the complexity of immune interactions present with exposure to true allergens [104].

Mice are not inherently allergic to the same substances that many humans become allergic to, but it is possible to sensitize animals to human allergens. Work in BALB/c mice described some of the mechanisms by which allergens such as house dust mite (HDM) and ragweed could produce allergic airway inflammation without the need for an adjuvant [106,107,108]. The sensitization was carried out via intranasal delivery so the immune conditions more closely model the human disease. It is important to note that the preparations of HDM and ragweed do contain bacterial components, but at least the adjuvant properties of these components could also be present in the initiation of human asthma. In fact, toll-like receptor 4, a pattern recognition receptor integral to immune activation against the bacterial endotoxin lipopolysaccharide, has been shown to be required for the immune activation observed in HDM models [109]. In addition, where repeated ovalbumin exposure lead to immune tolerance, repeated HDM exposure lead to airway remodelling [108,110], recapitulating the human disease. While no model will ever perfectly reflect the human condition, these models of actual human allergens have provided a means by which further research into the pathogenesis could take place.

These models have also been adapted to other rodents such as guinea pigs and rats [104,111,112]. For allergic sensitization, Brown Norway (BN) rats are quite useful as a model as they tend to mount T-helper 2, or $T_H2$, immune responses [113]. This type of immune response is commonly associated with the development and continuation of allergy, and BN rats have been shown to be

susceptible to allergic inflammation induced by HDM [112]. The characteristics of an HDM model in BN rats are quite similar to that seen in BALB/c mice.

### 1.42 – COPD Models

There are several *in vivo* models of COPD, but, especially as the human disease is extremely heterogeneous, no one model has yet to describe more than a few of the associated pathologies [104]. Airspace enlargement is perhaps the simplest pathology to mimic, and this can be accomplished with various genetic knockouts or by delivering enzymatic or inflammatory agents that degrade the structure of the alveoli. Examples include SMAD3 knockouts, repeated exposure to lipopolysaccharide, and exposure to porcine pancreatic elastase [104,114,115,116,117]. It must be noted, however, that the distribution of emphysema in these models may not reflect that observed after many years of exposure to cigarette smoke or human α1-antitrypsin deficiency. Nevertheless, these models provide a lung structure or lung environment that perhaps behaves similarly to that seen in human patients.

Neutrophilic inflammation can be modelled by exposing animals to immune triggers, such as LPS [118], and several transgenic models can cause inflammation and emphysema [119,120,121], but no one situation can recapitulate the milieu of substances found in cigarette smoke. Exposure to cigarette smoke is therefore likely the most accurate etiological model of this disease [104]. Inflammatory effects on the lung due to cigarette smoke exposure occur within days but the characteristics of this inflammatory state change over time [122]. COPD has been described as an accelerated aging of the lung tissues [24], and so it is important to consider the effect of aging on the subjects as well. Some models of cigarette smoke exposure have recently been carried out as far as six months [123,124,125], a substantial amount of time in the life of a mouse and a very long duration for a mouse model. This inflammation tends to be represented by T-helper 1, or $T_H1$, and $T_H17$ T-cell responses and neutrophils are the hallmark innate immune cell present in this inflammation, though alveolar macrophages and other cell types also play important roles [39].

Exposure to cigarette smoke also eventually causes airspace enlargement in mice, though it is very mild in comparison to the previously mentioned models or cases seen in severe COPD [104]. What is not abundantly clear is whether cigarette smoke exposure in rodents leads to the small airway fibrosis observed in human COPD patients. Gene expression of profibrotic mediators is increased in the small airways of mice after six months of cigarette smoke exposure, though changes to the airways themselves were not obvious [126]. It is possible that an even greater length of exposure is required to demonstrate effects similar to that seen in humans. It also appears that mucus production is not a major consequence of cigarette exposure in mice [127], while this is a common feature in human patients. Overall, cigarette smoke exposure is potentially the best model basic research has to address the underlying mechanisms associated with the same exposure in humans.

## Section 1.5 – Pre-clinical Imaging

### 1.50 – Small Animal Imaging Overview

As described previously, imaging methodologies offer information by which to diagnose and investigate lung disease that is not accessible by any other means. The regionalization of data within the lung is one such advantage, but the non-invasive nature of these tests is another. Because an animal does not need to be sacrificed for imaging data, that same animal can be used at a later time-point; this situation allows for greater insight into the experimental model and lends strength to statistical tests of the data.

Due to the small size of rodents and other small animals, imaging machines must be scaled down so as to be capable of providing resolutions similar to those obtained in humans. Small animal versions of CT, SPECT, PET, and MRI systems have been produced and refined over the past decade [10,128]. These scaled-down machines work in the same way as their larger counterparts, but with much smaller spaces for the subject and several other modifications to allow for volumetric picture elements, or voxels, in the range of 10-200 microns, depending on the system, subject, and modality.

Pre-clinical imaging is sometimes referred to as translational imaging; a reference that describes that human imaging data from a particular technique, with a particular modality, will be paralleled by information available in small animal imaging. This allows for the use of pre-clinical systems to predict the outcome of human trials, a useful ability in both the screening of therapeutic compounds and the investigation of biological structure and function in health and disease [10].

### 1.51 – Quantification

One very important aspect of pre-clinical imaging that is lacking in the more established human equivalent is the process of quantification. For diagnostic purposes, human imaging needs only to be interpreted by a trained radiologist or nuclear medicine physician. However, for scientific research quantification is preferred over qualitative assessment. Quantification of the imaging data produced in small animal experiments is therefore the best avenue to further scientific understanding.

In addition, it can be easily argued that three-dimensional images are too complex for humans to interpret properly without the aid of data processing. While obvious anatomical or physiological issues may be obvious to someone trained to look for them, low-level or widespread issues may go unnoticed without image quantification. Also, quantification ensures that the attributes of the data are known, and can therefore be compared against other results and other quantification methods. For example, an abnormality may be found in an image but the size, shape, location, and intensity of that abnormality cannot be known without quantification. Further, results garnered by quantification of

images can be used in the comparison to the quantitative results from other, non-imaging methods.

Quantification of imaging data is still in its infancy as any output must first be conceived, performed, and validated prior to general use. Considering the staggering number of possibilities for quantification in specific diseases, and animal models thereof, it is no wonder that this will be a slow but rewarding process. Validation of quantified outputs is somewhat easier to accomplish in animal models as experiments can be designed specifically to address any possible concerns.

### 1.51 – Preclinical Imaging of the Lung

Over the last few years preclinical imaging has gained popularity for the investigation of chronic lung disease. CT, MRI, PET, and SPECT have all seen use in the *in vivo* investigation of various pulmonary pathologies in murine models. Of these modalities, CT has been used most extensively, likely because CT measures density and the lung provides good contrast with this technique. Therefore, disease models causing large changes in lung density are most commonly used. In addition to the article investigating allergic inflammation contained in Chapter 2, preclinical CT imaging has recently been used to investigate airway remodelling in an OVA model of allergic airway disease to characterize remodelling [129]. Also, models of emphysema [130,131] and pulmonary fibrosis [132,133] have been used to demonstrate the ability of CT to investigate these pathologies in murine models.

MRI has also seen use in imaging the lungs of small animals. Hyperpolarized helium has been used to characterize bronchoconstriction [134], and to perform qualitative ventilation/perfusion in a surgical model of airway obstruction [135]. MRI has also been of use without hyperpolarized gas to characterize models of pulmonary embolism [136], fibrosis [137], allergic inflammation [138], and emphysema [139].

In regards to nuclear imaging of lung disease models in small animals, not including cancer research, $^{18}$FDG-PET has been used to study neutrophilic lung inflammation [140] and has recently been used to characterize lung regeneration after pneumonectomy in mice [141]. SPECT, on the other hand, has been used in small animals to characterize new methods to measure lung perfusion [142] and, recently, a bacterial substrate labelled with iodine has been shown to reflect infection but not sterile inflammation [143]. The methodology described in Chapter 3 to measure V/Q in the lungs of mice is another example of SPECT use in small animals.

While these applications only represent some examples of the use of three-dimensional imaging modalities in murine models of lung disease [144], they demonstrate that preclinical imaging is a valuable tool that can be used to investigate pathology, drug distribution, and intervention efficacy.

## Section 1.6 – Paradigm, Hypothesis, and Objectives

### 1.60 – Central Paradigm

Chronic obstructive lung diseases are commonly modelled through the use of laboratory mice and rats but data collection, as it pertains to the lung, is normally terminal. Three-dimensional imaging modalities have the capacity to provide information from within the lung *in vivo*. Therefore, the use of imaging modalities in models of chronic lung disease will allow for noninvasive insight into the lung environment, and its function, not available by any other means.

### 1.61 – Hypothesis

Imaging methods, such as CT and V/Q SPECT, will be sensitive to pathological changes within the lung and will allow for quantitative analysis of disease conditions *in vivo*. Furthermore, results acquired by imaging methods will be indicative of the results obtained through standard biological sampling methods.

### 1.62 – Objectives

**Objective 1:** Investigate the use of CT imaging to noninvasively quantify robust inflammatory processes taking place in the lung using a rat model of allergic airway disease.

**Objective 2:** Develop and validate V/Q SPECT in a preclinical methodology and determine the suitability and sensitivity of V/Q imaging to subtle pulmonary pathologies in a model of cigarette smoke exposure.

**Objective 3:** Define the relative contributions of pathology to V/Q mismatching within the smoke-exposed lung environment through the use of additional models for inflammation and airspace enlargement.

## Section 1.7 – Summary

### 1.70 – Potential for Imaging in the field of Lung Disease

Lung disease is a broad field that includes both acute and chronic conditions. Many of these conditions are caused or complicated by microbial and viral infections. Further considerations, such as atopy or autoimmunity, also impact the respiratory system. Thus, lung disease is an extremely complex problem. Our understanding of the lung is still, in some ways, quite preliminary, mainly due to the complex structure to function relationship present and the sheer possibilities for environmental exposure to foreign substances. It has been established, for example and in both mice and humans, that viral infection can alter the amount of antigen necessary to bring about allergic sensitization [19,145]. This example illustrates the interplay possible between the specific environment and immune regulation. Because the lungs of each human are impacted by different stimuli

and can react differently to those stimuli the specifics of each case are needed to understand the whole scope of the problem.

Imaging has the potential, and has already been put to use, to better characterize lung disease. The lung is an organ in which the volumetric movement of tissue is a primary mechanism of its function. As such, three-dimensional methods are necessary to fully explore the function of this organ. Volumetric methods also have other advantages in research and for diagnostic purposes. As non-invasive methods, imaging techniques provide a means by which to gather structural, functional, or cellular information not accessible otherwise. Further, because of their digital nature, volumetric images can easily be analyzed for any particular piece of information contained within the image; as long as the technique itself hasn't changed, data acquired previously can be reanalyzed to answer a different question. This characteristic also means that before- and after-images can be compared for a subject, increasing the information available for diagnostic practices. Overall, volumetric imaging offers data that promises to increase our understanding of the lung in both health and disease.

Unfortunately, there are still several limitations that must be overcome before imaging methods can reach their full potential. One such limitation is the lack of quantification present in current research and diagnostic practices. While some conditions are simple to view by eye, some are widespread or create only small perturbations to the system. With quantitative practices, the sensitivity and specificity of results can both be improved. This will, however, require great efforts into producing the knowledge and technology necessary to quantify different diseases volumetrically. Another limitation is the availability of imaging. Not all imaging modalities, or specific techniques for a modality, are available at all centres, and some require major infrastructure. Finally, due to the relatively high cost of imaging, relevant possibilities for impactful tests and techniques must be found and validated so that the full potential of imaging in clinical practice can be reached. This process will take considerable time and effort, but could ultimately change the face of healthcare and the morbidity and mortality of lung disease in our society.

### 1.71 – Overview of Work Completed

The work contained in this thesis speaks to the use of volumetric imaging methodologies in the context of chronic lung disease. To provide quantification of pathologies, anatomical imaging was first used in a rat model to define regions of interest surrounding the lungs. The techniques employed to this end were then used throughout all following work. Anatomical imaging by CT also allowed for the quantification of robust allergic inflammatory processes in the lung. Functional information regarding ventilation and perfusion within the lung was also used to characterize and quantify chronic lung disease states, though this was done in models of COPD and in mice. The methodology of V/Q imaging and quantification was described and validated with a proof-of-concept in aged mice. Next, the effects of prolonged cigarette smoke exposure on V/Q

mismatching was described and compared to measurements of the inflammatory state and alveolar structure. Finally, the lung dysfunction associated with prolonged smoke exposure was further characterized by investigating the impact of smoke cessation, and the roles of inflammation and airspace enlargement in V/Q mismatching. In addition to several advances in methodologies, this work demonstrates the ability of volumetric imaging techniques to quantify and investigate various pathologies in the lung. Through their use, greater understanding of lung structure and function, in both health and disease, is possible.

# CHAPTER 2
# Evaluation of allergic lung inflammation by computed tomography in a rat model *in vivo*

## 2.0 – Overview of Chapter 2

The first article of this thesis is entitled "Evaluation of Allergic Lung Inflammation by Computed Tomography in a Rat Model *in vivo*". For the CT machinery available, a rat model was suitable to allow for good resolution in the lungs. Therefore, the house dust mite-driven allergic airway sensitization protocol, developed in mice, was adapted to Brown Norway rats. This process required much in the way of optimizing, but the end result was a consistent model that produced robust allergic inflammation along the airways.

Segmentation procedures for the lungs in CT images were also optimized so that data reliably demonstrated the condition of the lung. Both lung and thoracic segmentations were utilized for different purposes. In addition, the processing of baseline scans, acquired before any experimentation occurred, allowed for the subtraction of the original lung state providing a means to compare these different segmentation operations and a subject-by-subject tracking of disease pathology.

These procedures and experimental abilities allowed for a volumetric characterization of an allergen dose response. Further, this dose response was evaluated across multiple experimental time-points, indicating that the immune responses develop differently depending on the dose of allergen administered. CT imaging results were also compared against measures from biological sampling to provide a more complete description of the inflammation. Fundamentally, this was the first use of CT to noninvasively quantify and describe the level of inflammation in the lungs of rats or mice. This work also provides a foundation for further studies using CT to noninvasively assess the volumetric impact of intervention strategies or exacerbatory stimuli.

This article was published in the June 2009 issue of the European Respiratory Journal. Reproduced with permission of the European Respiratory Society.
Eur Respir J June 2009 33:1437-1447; published ahead of print January 22, 2009, doi:10.1183/09031936.00087508

Eur Respir J 2009; 33: 1437–1447


# Evaluation of allergic lung inflammation by computed tomography in a rat model *in vivo*

B.N. Jobse*, J.R. Johnson*, T.H. Farncombe#, R. Labiris", T.D. Walker*, S. Goncharova* and M. Jordana*

AFFILIATIONS
*Dept of Pathology and Molecular Medicine, Division of Respiratory Diseases and Allergy, Centre for Gene Therapeutics, McMaster University, #Dept of Nuclear Medicine, Hamilton Health Sciences, McMaster University, and "Dept of Medicine, Firestone Institute for Respiratory Health, McMaster University, Hamilton, ON, Canada.

CORRESPONDENCE
M. Jordana
Dept of Pathology and Molecular
Medicine, Division of Respiratory
Diseases and Allergy, Centre for
Gene Therapeutics, MDCL 4013
McMaster University
1200 Main Street West
Hamilton, ON
Canada L8N 3Z5
Fax: 1 9055226750
E-mail: jordanam@mcmaster.ca

Received:
June 09 2008
Accepted after revision:
January 04 2009

SUPPORT STATEMENT
This research was partially funded by the Canadian Institutes of Health Research (CIHR; Ottawa, ON, Canada). M. Jordana holds a Senior Canada Research Chair on the ''Immunobiology or Respiratory Diseases and Allergy'' and J.R. Johnson was a holder of a CIHR doctoral award.

STATEMENT OF INTEREST
None declared.

## 2.1 – ABSTRACT

The ability of micro-computed tomography (CT) to noninvasively evaluate allergic pulmonary inflammation in an experimental model was investigated. In addition, two image segmentation methods and the value of respiratory gating were investigated in the context of this model. Brown Norway rats were exposed to one of four doses of house dust mite (HDM) extract (0, 0.15, 15 or 150 μg) delivered intratracheally every 24 h for 10 days. CT scanning was performed at baseline and after several longitudinal HDM exposures. Both thoracic- and lung-segmentation methods yielded similar results when standardization practices were employed. While tissue histology correlated well with CT images, cell counts from bronchoalveolar lavage depicted greater inflammation than did density measures from CT images. Evidence from representative CT slices and transaxial density distribution indicated that inflammation was primarily associated with major airways and extended into the periphery from these focal points. Respiratory gating demonstrated that images of the inspiratory state provided greater contrast of inflammatory processes. Lastly, decreases in tidal volumes indicated significant mechanical respiratory changes in animals exposed to both 15 and 150 μg. In summary, CT image segmentation can extract pertinent data on *in vivo* allergic airway/lung inflammation. Furthermore, respiratory gating provides additional contrast and insight into these quantification practices.

## 2.2 – INTRODUCTION

Research in experimental models of disease, particularly *in vivo*, is an essential endeavour, especially as it pertains to revealing disease pathogenesis and developing assessment tools. However, these types of studies also have significant drawbacks. In particular reference to models of asthma, data analyses have largely relied on the invasive collection of biological samples such as bronchoalveolar lavage (BAL) and lung tissues. Unfortunately, these techniques demand the sacrifice of many animals. In addition, the data obtained from these measurements are generally extrapolated to the lung as a whole, whereas it is plausible that they are evaluating only one compartment or a small and distinct volume within the lung. Importantly, in reference to kinetic studies, the need to terminate animals at each designated time-point precludes performing longitudinal studies in the same group of animals.

In this context, micro-computed tomography (CT) is quickly becoming a useful tool for the investigation of lung diseases in small animals. Its usefulness relies on the ability to anatomically and functionally measure processes in the lung across an experimental protocol. Progress has already been made using this imaging modality in studies of fibrosis and emphysema [1–3]. With respect to asthma, research utilising CT immediately following sacrifice, i.e. *ex vivo*, has elegantly contributed to establishment of the role of airway closure on hyperreactivity in mice undergoing acute allergic inflammation [4]. The ability to acquire CT data in a model of allergic asthma *in vivo* would be a step towards

noninvasive assessment, utilising the same tools that are available in humans [5, 6]. The main objective of the present study was to investigate whether CT could be useful to noninvasively and sequentially evaluate experimental allergic lung/airway inflammation. A secondary objective was to evaluate several volume extraction methodologies and display parameters that have recently been reported in other lung disease models. In particular, segmentations of the thoracic cavity versus the lung proper were investigated, in order to determine whether results could be compared between these two contrasting methods. Furthermore, we wished to explore whether we could gain functional information by gating CT images on the respiratory cycle [7]. Our laboratory has extensive experience in the use of house dust mite (HDM) in models of allergic asthma in mice [8–10]. However, in this report we chose to study Brown Norway (BN) rats in order to increase technical resolution. Some of the results presented here have been previously reported in abstract form [11].

## 2.3 – MATERIALS AND METHODS

**Animals**

5-week-old female BN rats, weighing ~90 g, were purchased from Charles River Laboratories (Montreal, QC, Canada). Rats were housed under specific pathogen-free conditions on a 12:12-h light:dark cycle and were acclimatised to housing conditions for 1 week prior to experimentation. The experiments described in this study were approved by the Animal Research Ethics Board of McMaster University (Hamilton, ON, Canada).

**Allergen administration**

Rats were exposed, under isoflurane-induced anaesthesia, to purified HDM extract (Greer Laboratories, Lenoir, NC, USA) by intratracheal intubation. The procedure was performed with a laryngoscope while rats were suspended supine, by the teeth, at 35° from horizontal. A 3.5-cm PE20 endotracheal tube (1.09 mm outer, 0.38 mm inner diameter (Becton Dickenson and Co., Sparks, MD, USA)) on a 25G needle was used to deposit allergen (or vehicle) ~1.5 cm into the trachea; allergen was allowed to distribute freely through the lung. Groups of rats received 0, 0.0015, 0.15 or 1.5 μg□mL$^{-1}$ of HDM, corresponding to delivered doses of 0 (vehicle control), 0.15, 15 and 150 μg of HDM protein in 100 μL sterile saline. Exposure took place daily for 10 consecutive days.

**Collection and measurement of specimens**

Sample sizes were six, ten, seven and six for allergen dose groups 0, 0.15, 15 and 150 μg, respectively; these sample sizes represent data pooled from two separate experiments. Rats were sacrificed and BAL was collected ~48 h after the final allergen exposure (24 h post imaging). In brief, the lungs were removed and the trachea was cannulated with a polyethylene tube (Becton Dickenson and Co.). The lungs were lavaged twice with 1 mL PBS; ~1 mL of the total instilled fluid was consistently recovered. Total cell counts were determined using a haemocytometer. After centrifugation, cell pellets were resuspended in PBS and

slides were prepared by cytocentrifugation (Shandon Inc., Pittsburgh, PA, USA) at 9.66g for 2 min. Hema3 (Fisher Scientific Co., Kalamazoo, MI, USA) was used to stain all slides. Differential counts of BAL cells were determined from at least 500 leukocytes using standard haemocytological procedures to classify the cells as neutrophils, eosinophils, lymphocytes or macrophages/monocytes. Additionally, blood was collected by cardiac puncture and serum was obtained by centrifugation in Capiject tubes (Terumo Medical Corp, Elkton, MD, USA). Total immunoglobulin (Ig)E from sera was determined with a rat IgE ELISA (Kamiya Biomedical, Seattle, WA, USA). Finally, lung tissue was fixed in 10% formalin and embedded in paraffin; 3-mmthick sections were stained with haematoxylin and eosin (HE).

**CT image acquisition, respiratory gating and standardisation**

All HDM dose groups were composed of four rats for CT scanning. All imaging was performed on spontaneously breathing animals anaesthetised with 1.5% isoflurane at 1 $L \cdot min^{-1}$. CT images were acquired on an X-SPECT (Gamma Medica, Northridge, CA, USA) within the McMaster Centre for Pre-Clinical and Translational Imaging at McMaster University (Hamilton, ON, Canada). CT acquisition was performed at a voltage of 75 kVp and a current of 220 mA. Two rotations of 1,024 continuous projections (2,048 projections total, ~10 min scan time) were collected and post-acquisition respiratory gating was applied with RespGate software (RespGate, Hamilton, ON, Canada), as described by FARNCOMBE [12]. Images were reconstructed using a Feldkamp cone beam reconstruction algorithm into 512x512x512 arrays (0.155-$mm^3$ voxels) producing images for peak inspiratory and expiratory states as well as an ungated image reconstructed from all 2,048 projections. Calibration of each image for Hounsfield Unit (HU) scaling was performed using a water-filled tube included in the scan. For each CT scan, rats received 166 mGy of deposited energy; this value was calculated by D.R. Boreham and N. Phan (Dept of Medical Physics and Applied Radiation Sciences, McMaster University) from work in mice using thermoluminescent dosimeter chips (Harshaw TLD-100, Global Dosimetry, Irvine, CA, USA) on the same CT equipment used in the present study. As HDM exposures were carried out at 24-h intervals, scans were performed just prior to the first exposure and 20 h following the third, seventh and tenth exposures; these scans are henceforth referred to as baseline, 3, 7, and 10 days (end-point) of exposure, respectively.

**CT image processing**

CT images were processed with Amira software (Version 3.1; Visage Imaging, Andover, MA, USA). Two methods of volume segmentation, as described by others [1–4, 13], were performed, in order to assess the advantages of and similarities between these methods. In Method 1, the thoracic volume was segmented by defining a region of interest that encapsulated the entire lung by manually outlining the ribcage and chest wall using characteristic landmarks and interpolation. A representative thoracic volume is shown in figure 2.1a. In Method 2, lung volume was segmented by a semi-automatic process where a

computer-assisted volume selection of -1000– -50 HU was further subjected to manual alterations as required to include all lung regions and exclude all non-lung regions that may have been selected. This volume selection process included blood vessels as well as a small volume of tissue immediately surrounding the lung, but excluded the heart. A representative lung volume is shown in figure 2.1b. Method 1 was applied on respiratory-gated data as well as ungated data, while Method 2 was used only on ungated data due to a lower signal-to-noise ratio in gated data sets, particularly in inspiratory state images because of fewer associated projections. To simplify the use of volume expansion tools used in Method 2, digital Gaussian filtering (kernel 3, sigma value 1) was employed to smooth the three-dimensional, ungated, HU-calibrated CT images. Images from respiratory gating did not undergo digital filtering; Method 1 did not require a filtering procedure if no image artefacts were present and Method 2 was not applied to gated images. Density histograms were produced with 26 bins describing a range from -1,025 to 275 HU (50 HU·bin$^{-1}$). Thoracic air volumes were calculated by determining the air volume in each bin based on the HU value, followed by summation of the total amount of air in each density bin for the entire thoracic volume. All histogram data (ungated and gated) were expressed as a percentage of the total lung volume for standardization purposes. This total represents all voxels in Method 2 but only the calculated number of air voxels in Method 1. For a given animal and exposure, baseline histograms were subtracted from exposure time-point histograms to produce data demonstrating the difference from baseline. Axial distribution histograms were produced in Amira using the ''volume-by-slice'' component, based on a threshold of -350 HU. These histograms were expressed as the percentage of volumes greater than -350 HU in each slice, divided by the total volume of that slice (to account for varying slice volumes throughout the lung). These axial density curves contain ~5% error in lung length due to the averaging of data between animals. Group averages were obtained and a scale based on percentage of average lung length produced. Mean lung density values ($\rho_{lung}$) were obtained for ungated data with the method described by SIMON [13]. Maximal HU ($HU_{max}$ ) values for histograms of gated images were determined by use of Minitab software (Minitab, Inc., State College, PA, USA). Tidal volumes were calculated by subtracting expiratory state air volume from inspiratory state air volume, after determining the total air volume for each image.

**Data analysis**

Data are expressed as the mean or the mean±SEM. Results were interpreted using an unpaired t-test or one-way ANOVA with Dunnett's *post hoc* test. All statistical analysis was performed in Graphpad Prism software (Graphpad Software Inc., La Jolla, CA, USA). For ANOVA tests, repeated criteria were used for longitudinal CT data, while nonpaired criteria were used for comparisons between groups.

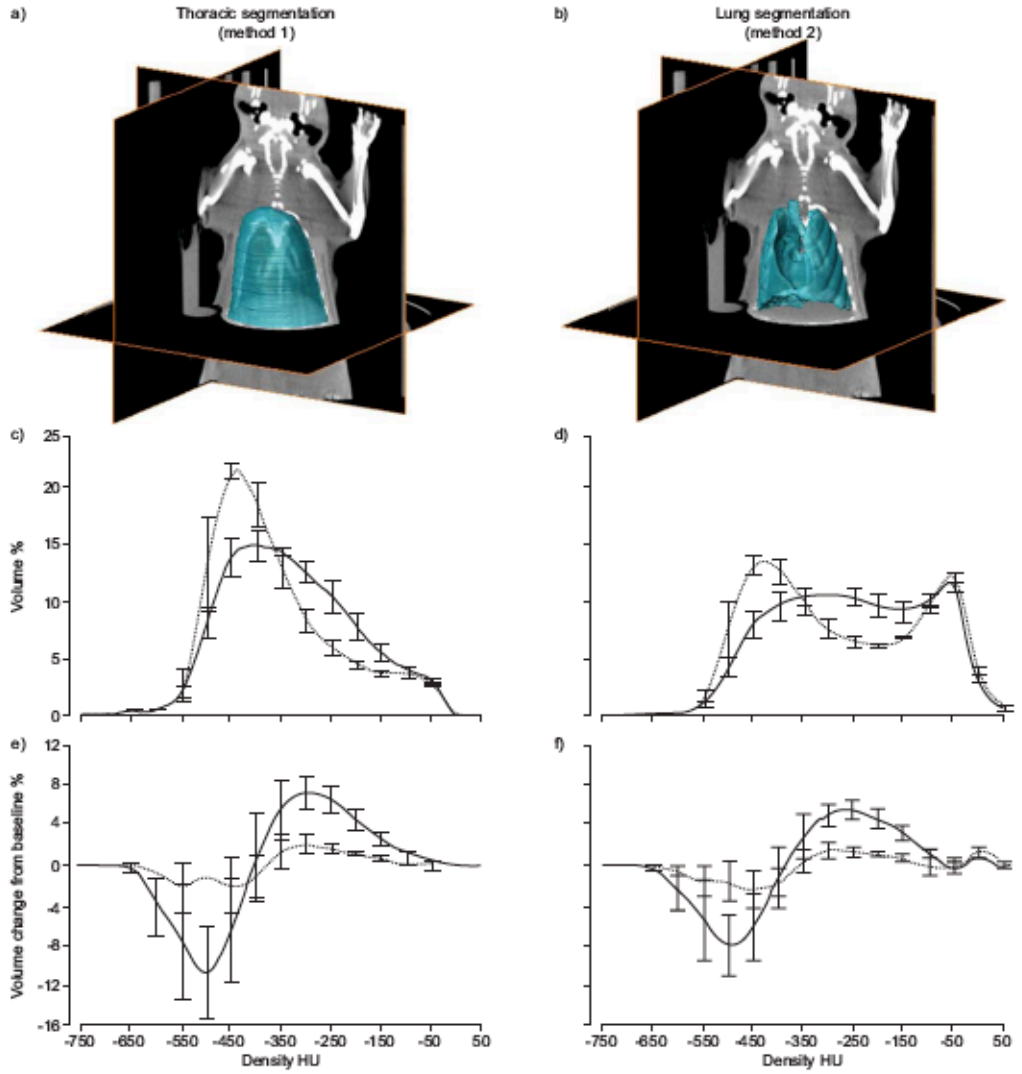


FIGURE 2.1
Computed tomography (CT) volume segmentation and analysis methods. CT-derived histogram analysis obtained with two segmentation methods. **a, c and e)** Volume selection by thoracic segmentation (Method 1). **b, d and f)** Volume selection by lung segmentation (Method 2). For each volume selection method, volume standardised histograms (c and d) and change from baseline histograms (e and f) are shown. HU: Hounsfield Units. Dotted line: animals exposed to vehicle control; Solid line: animals exposed to 150 μg of house dust mite extract for 10 days. n=4 in each group. Error bars represent SEM.

## 2.4 – RESULTS

BAL, tissue histology and serum were collected for comparison with CT scanning after the 10 days' exposure time-point. Exposure for 10 days to vehicle control, or 0.15, 15 or 150 μg of HDM, demonstrated a significant increase in total cell numbers in the groups exposed to 15 and 150 μg of HDM (fig. 2.2a). Similarly, increases were seen in eosinophils and mononuclear cells for the 15 and 150 μg groups (fig. 2.2b and c) but not in neutrophils (data not shown); a statistically significant increase in mononuclear cells was observed only in animals exposed to 150 μg of HDM. Total serum IgE, as a marker of systemic sensitisation, was significantly elevated in animals exposed to 150 μg but the response did not reach statistical significance in those exposed to 15 μg (fig. 2.2d). HE-stained histological sections from animals exposed to 15 and 150 μg depicted increased inflammatory infiltrate around blood vessels as well as both major and peripheral airways; these changes were particularly robust in the 150 μg HDM group (fig. 2.2e–l).

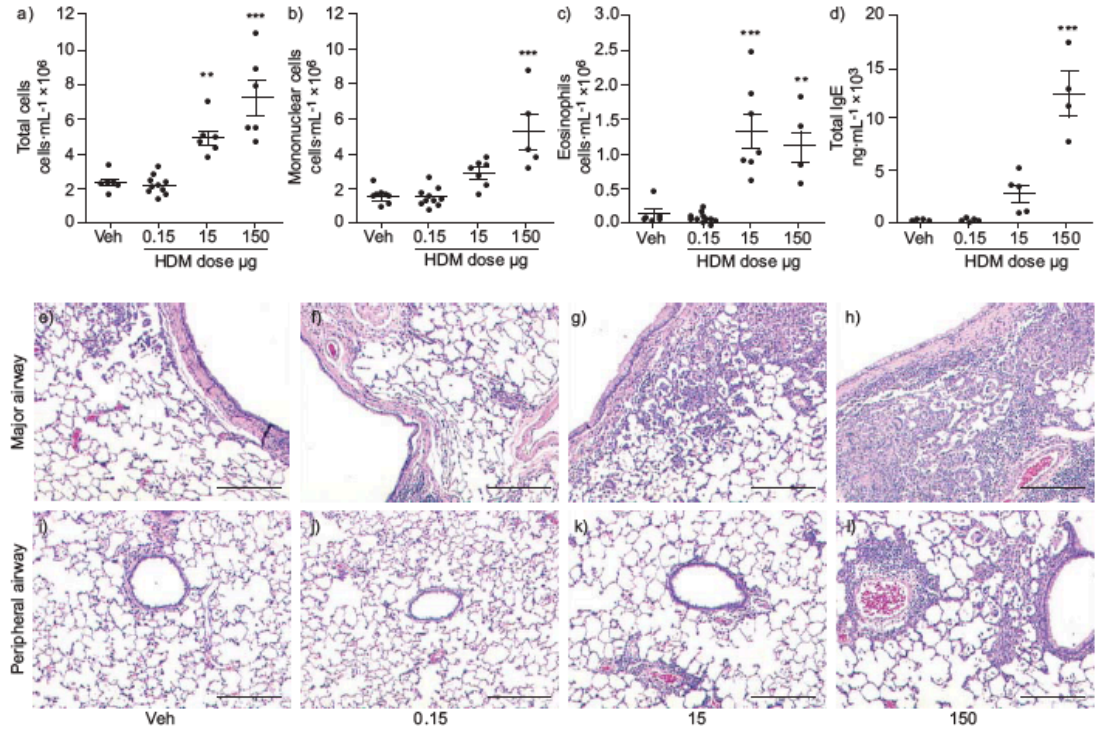


FIGURE 2.2

Biological data pertaining to the 10-day house dust mite (HDM) model in Brown Norway rats. Samples from animals exposed to vehicle control (Veh), or 0.15, 15 or 150 μg of HDM, were collected 48 h after the final HDM exposure. **a)** Total cells, **b)** total mononuclear cells and **c)** total eosinophils in the bronchoalveolar lavage from each dose group after 10 days' HDM exposure. **d)** Total immunoglobulin (Ig)E measured by ELISA indicating systemic sensitisation. Sample size is indicated in the dot plots. **e–l)** Representative images from histological sections stained with haematoxylin and eosin for each dose group; major (e–h) and peripheral (i–l) airways are shown for each dose. **: $p<0.01$ versus Veh; ***: $p<0.001$ versus Veh. Scale bars=1 mm.

Two methods of image volume segmentation were employed to analyse the data obtained from CT scanning (fig. 2.1a and b). Based on ungated CT images, histograms were produced and displayed as the percentage of total lung-associated volume for a given density bin. Representative curves for 10 days' exposure to vehicle control and 150 μg of HDM are shown (fig. 2.1c and d). For each method, histograms from baseline images were then subtracted from 10 days' exposure histograms in order to illustrate the change from baseline (fig. 2.1e and f). For Method 1, histograms represented the density distribution of air volume, whereas histograms produced from Method 2 described the density distribution of the entire segmented volume, which included densities greater than 0 HU, i.e. voxels containing no component of air. Given that ~95% of the segmentation volume from Method 2, describing both normal lung tissue and inflammation, was associated with density values less than 0 HU, and based on the similarities between histogram curves from both methods, it is possible to conclude that both Method 1 and Method 2 produce similar results for this model if the change from baseline is established (fig. 2.1e and f).

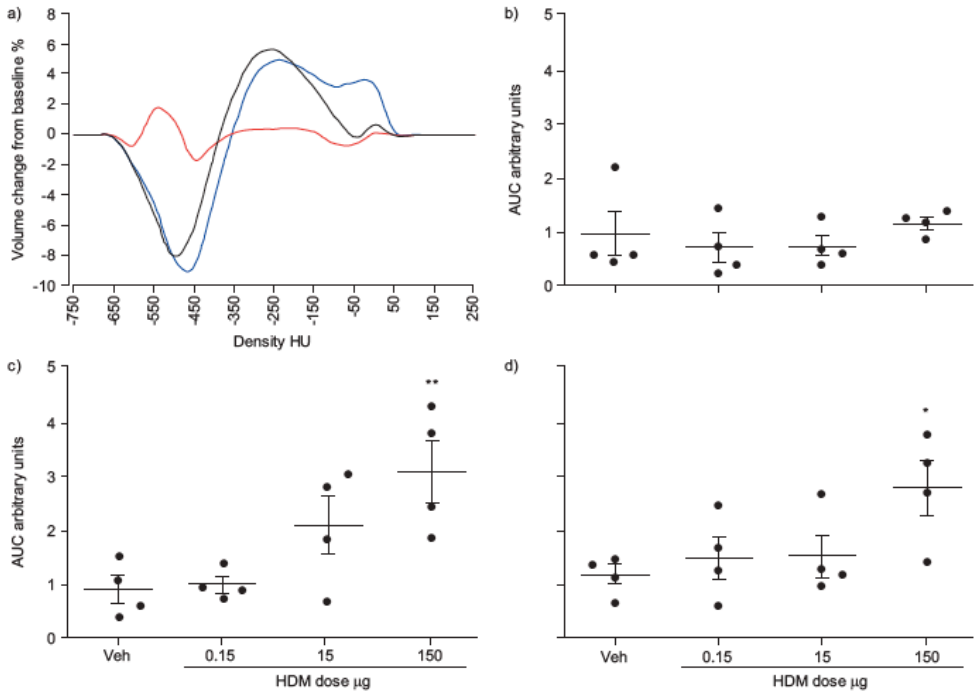


FIGURE 2.3
Ungated computed tomography data for house dust mite (HDM) extract dose groups during the 10-day exposure protocol. **a)** Difference from baseline histogram curves for the group exposed to 150 μg of HDM, detailing volume-density changes taking place after 3 days (red line), 7 days (blue line) and 10 days (black line) of HDM exposure. Curves represent group averages. HU: Hounsfield Units. **b–d)** Values produced by integration of the change from baseline histogram curves. The integrals of the absolute values of the curve were calculated for each animal at b) 3 days, c) 7 days and d) 10 days for all HDM doses; these values represent total change as defined by area under the curve (AUC). Veh: vehicle control. N=4 in each group. *:$p<0.05$ versus Veh; **:$p<0.01$ versus Veh.

The ability to take measurements across multiple time-points allowed for a longitudinal assessment of the state of the lung in the same subject animal. Histograms depicting change from baseline for the group exposed to 150 μg of HDM, after 3, 7 and 10 days of exposure, indicated that increased densities were greatest after 7 days, particularly in the highest density bins (fig. 2.3a). The magnitudes of these density changes were quantified by finding the integral (area under the curve) of the absolute values of the curve for each animal and at each time-point (fig. 2.3b–d). Only the group exposed to 150 μg of HDM showed a significant difference versus the vehicle control; however, a dose-dependent response was observed at the 7 days' exposure time-point in the group exposed to 15 μg of HDM.

CT slice images from representative animals, at the 10-day time-point, allowed for an anatomical assessment of the illustrated the density differences observed in the whole lung and reflected those seen in the representative images (fig. 2.4c). These curves indicated that, while lower doses of HDM appeared to have some effect on overall lung densities, 150 μg elicited a dramatic decrease in densities less than -350 HU and a reciprocal increase in densities greater than -350 HU. For the purpose of understanding the morphological and spatial significance of different densities, a threshold of -350 HU was found to be useful for distinguishing between normal, air-filled volumes (-1,000– -350 HU) and volumes associated with inflammation as well as structural and functional components (-350– 100 HU), as seen in two colour density maps (fig. 2.4h–k). Low-density volumes, i.e. those volumes associated with high air content, were largely diminished in animals exposed to 150 μg of HDM. In addition to a single threshold (two-colour), the volumes with values greater than -350 HU were further divided to provide a more detailed map of densities, seen in four-colour density maps (fig. 2.4l–o). The changes in density due to HDM exposure appeared to extend from major blood vessels, enveloping nearby airways and forming a decreasing gradient towards the lung periphery, indicating that inflammation was primarily associated with the major airways and vessels.

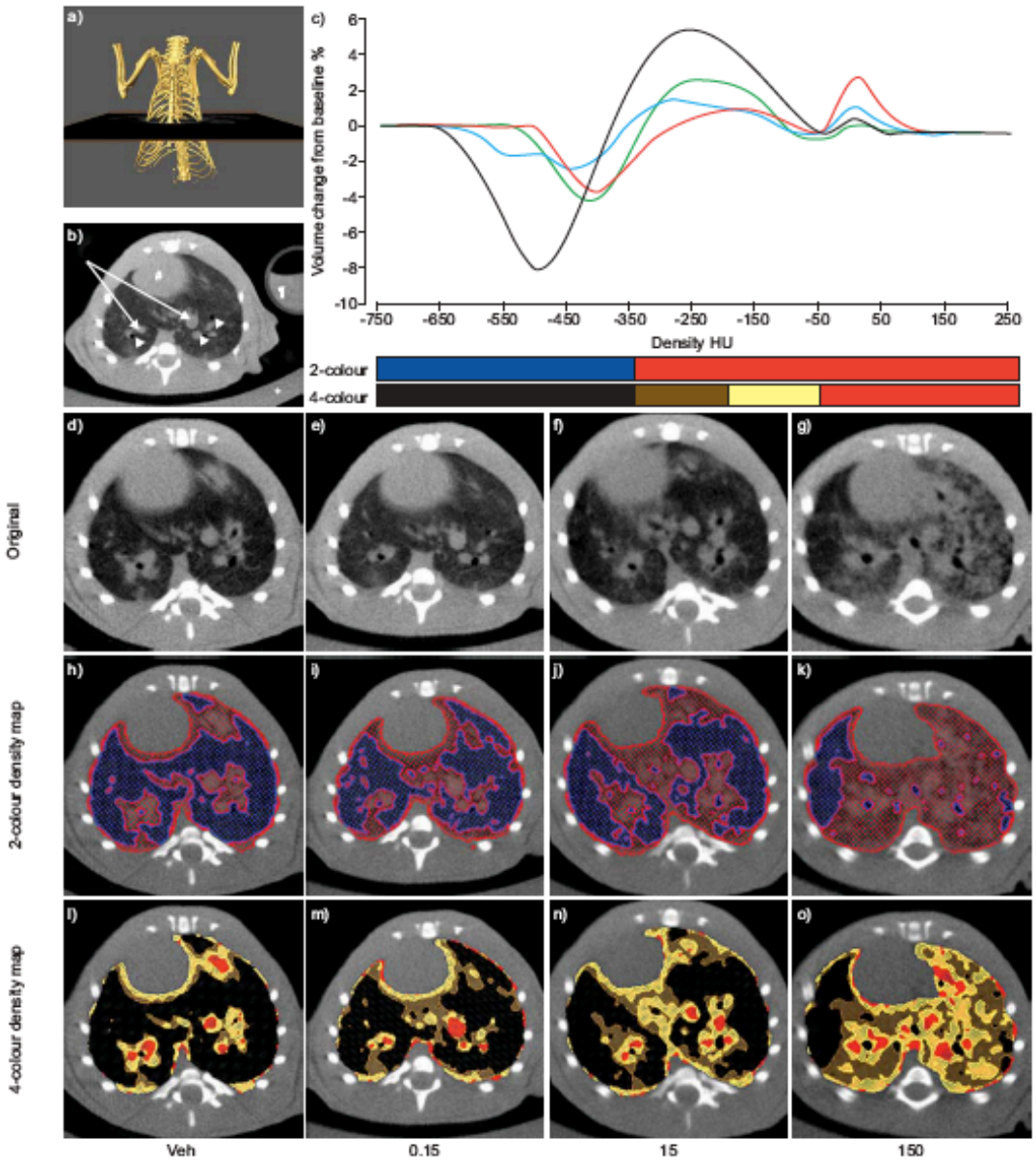


FIGURE 2.4

Representative axial computed tomography (CT) slices and whole lung histograms from house dust mite (HDM) extract dose groups at 10 days' exposure. **a and b)** CT image features. a) The method used to ensure images from separate animals were acquired from approximately the same position in the lung. b) Representative CT slice. Arrows: large blood vessels; arrowheads: large airways; #: heart; ¶: water-filled tube for the calibration of images into Hounsfield Units (HU); +: animal support platform. **c)** Difference from baseline histogram curves for all dose groups after 10 days of HDM exposure. Blue line: vehicle control; red line: 0.15 µg HDM; green line: 15 µg HDM; black line: 150 µg HDM. The colour scales featured below the graph indicate HU thresholds as shown in the two- and four-colour density-mapped duplicates in (d–o). **d–o)** Representative images for each dose group with colour-mapped duplicate images illustrating d–g) original, and h–k) two or l–o) four thresholds. d, h and l) vehicle control (Veh); e, i and m) 0.15 µg HDM; f, j and n) 15 µg HDM; g, k and o) 150 µg HDM.

The distribution of increased lung densities after 10 days in rats exposed to 150 μg of HDM was assessed by several approaches. To determine the location of increased densities, the percentage of high-density volume, based on a threshold of -350 HU, was calculated from each axial slice and plotted against the percentage of lung length for both baseline and 10-day exposure scans in the same group of animals (fig. 2.5a). From these data it was apparent that increased densities, due to HDM exposure, were relatively consistent throughout the lung, from apex to diaphragm. Representative CT slices depicted increased densities throughout the central lung; position was indicated by noting the percentage of the distance from the trachea to the base of the lung (fig. 2.5b–d). Representative three-dimensional modelling, again using a threshold of -350 HU, illustrated the widespread loss of low-density volumes and the association of these losses with central lung structures (fig. 2.5e and f). Total lung density values, $\rho_{lung}$, provided whole lung density means, and were compared with baseline values for all time-points investigated (fig. 2.6). These values reinforced the appraisal that both 15 and 150 μg of HDM were capable of causing increased lung densities over the course of the protocol.

Post-acquisition respiratory gating was performed on CT projections to provide inspiratory and expiratory images. Gated images then underwent thoracic volume segmentation (Method 1), as described in the Materials and Methods section. Histograms, displayed as percentage of total thoracic air volume, indicated both a broadening of the curve and a shift in the peak density value ($HU_{max}$) towards higher densities in animals exposed to 150 μg HDM for 10 days (fig. 2.7c and d). $HU_{max}$, as a measure of overall density change in air-containing compartments, was not significantly altered between the vehicle control group and the group exposed to 150 μg of HDM for the expiratory state; however, the difference between these groups became highly significant for the inspiratory state (fig. 2.7e). Tidal volumes, calculated by subtracting total expiratory air volume from total inspiratory air volume, revealed results in the dose–response and scanning time-points not easily observed by other means. The groups exposed to both 15 and 150 μg of HDM displayed significantly decreased tidal volume after 10 days of exposure when compared with baseline values (fig. 2.7f). In addition, 7 days of exposure to 150 μg of HDM also significantly decreased the tidal volume, while 15 μg HDM showed a similar response. Furthermore, exposure to 0.15 μg of HDM seemed to affect the tidal volume, although this change did not reach statistical significance and only appeared after 10 days of exposure. Notably, these tidal volume changes coincided with a substantial loss of both inspiratory and expiratory volume in groups exposed to 15 and 150 μg of HDM for 7 days, whereas at 10 days' exposure lung volumes resembled those seen at baseline (data not shown) but still displayed a large loss of tidal volume indicating a more complicated pathology, possibly including airway closure and gas trapping.

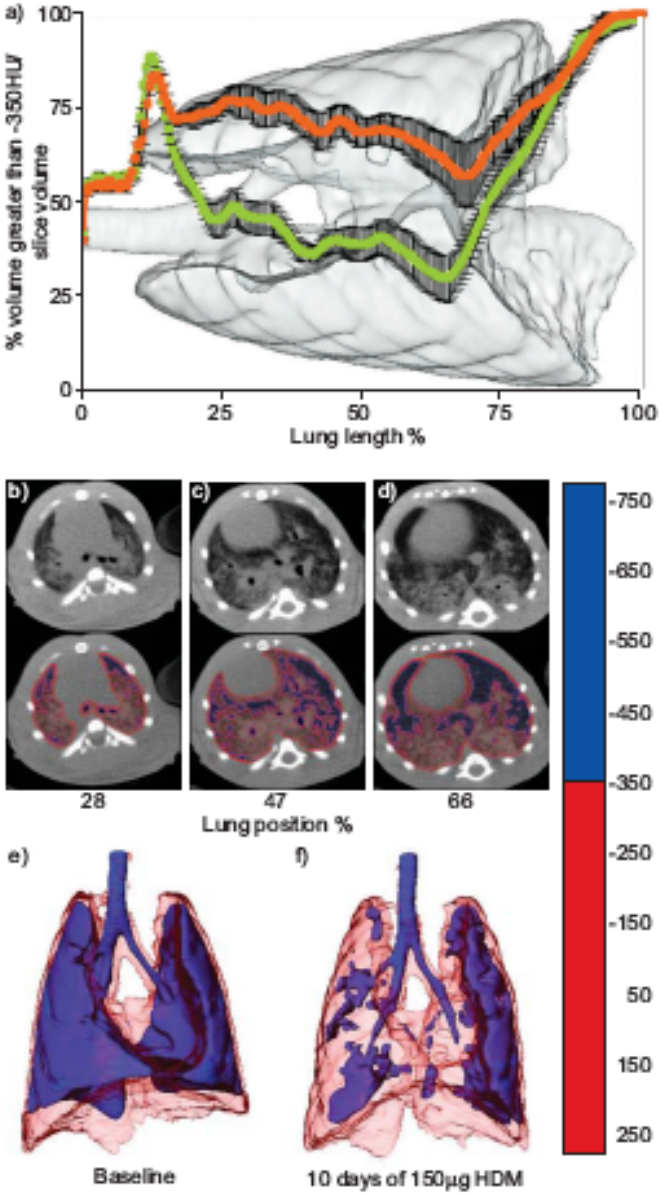


FIGURE 2.5
Distribution of increased density volumes in ungated data. **a)** Measurement of the axial location of density values greater than -350 Hounsfield Units (HU). Curves represent the percentage of volume with values greater than -350 HU in each slice, standardised by the total volume of the slice from which they were obtained, for the same group of rats (n=4) at baseline (green) and 10 days' exposure to 150 µg of house dust mite (HDM) extract (orange). The background image is from one representative animal. Error bars represent SEM. **b–d)** Evenly spaced axial slices denoted by their relative positioning in the lung, with two-colour density-mapped duplicates, from a representative animal. b) 28%, c) 47% and d) 66% of the distance from the trachea to the base of the lung. The colour scale featured on the right indicates HU thresholds used. Three-dimensional lung images from one representative animal at **e)** baseline and **f)** after 10 days of exposure to 150 µg of HDM. Refer to the colour scale for HU mapping thresholds.

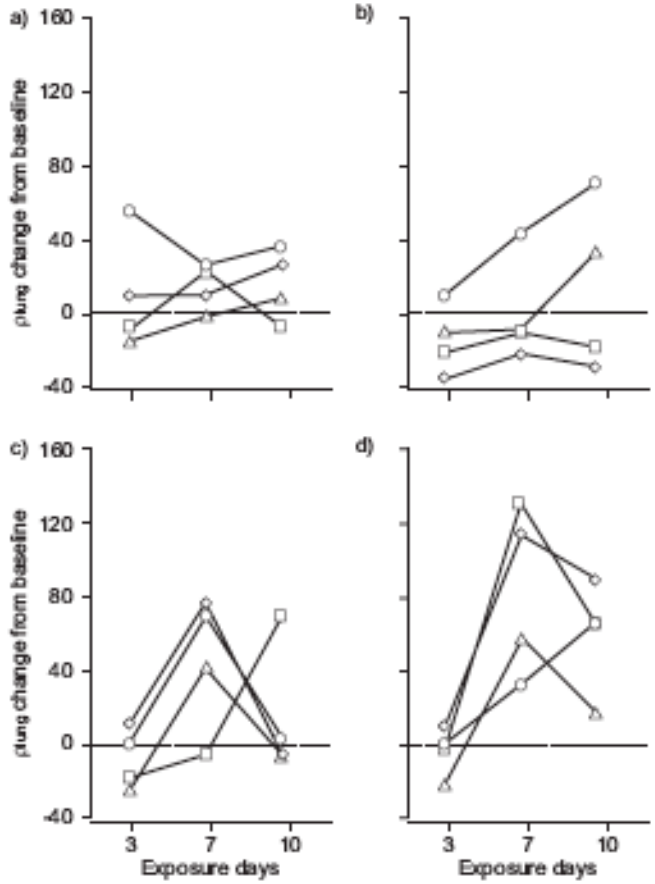


FIGURE 2.6

The difference in mean density values ($\rho_{lung}$) from baseline after 3, 7 and 10 days of house dust mite (HDM) extract exposure for all dose groups. **a)** vehicle control; **b)** 0.15 μg HDM; **c)** 15 μg HDM; **d)** 150 μg HDM. These values indicate the extent and timing of the inflammatory response. Distinct animals in each group are represented by different symbols. Statistics are not shown as baseline values were used in the standardisation of data, and no between-groups comparison is presented.

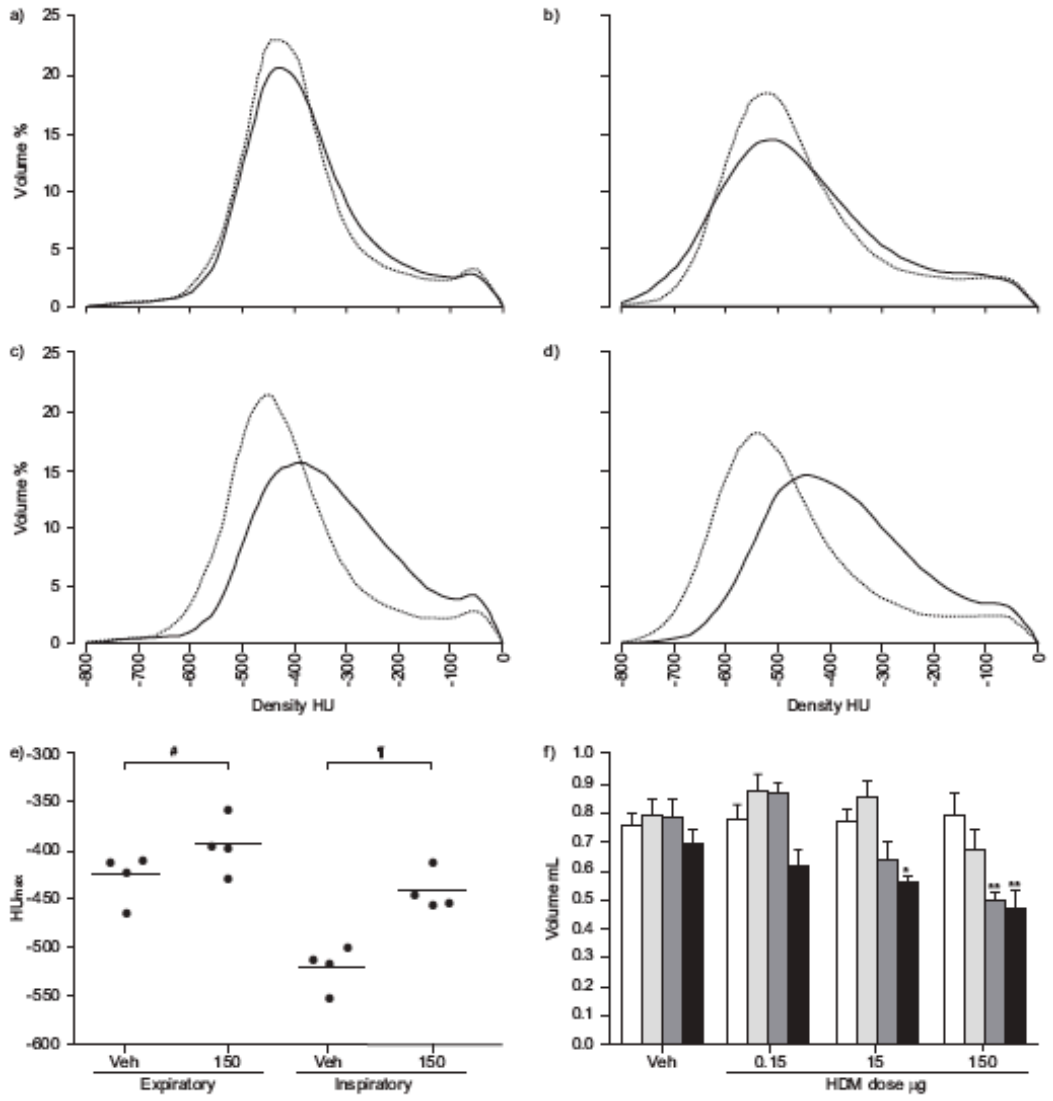


FIGURE 2.7

Tidal computed tomography data from respiratory gating. Data were obtained using thoracic segmentation (Method 1). **a and c)** Expiratory and **b and d)** inspiratory volume-standardised histograms at baseline (dotted line) and after 10 days of exposure to house dust mite (HDM) extract (solid line). **a and b)** vehicle control (Veh) group; **c and d)** group exposed to 150 µg of HDM. HU: Hounsfield Units. **e)** Comparison of peak histogram density value ($HU_{max}$) for expiratory and inspiratory states between Veh and 150 µg of HDM groups. #: p=0.144; ¶: p=0.002; p-values were calculated by two-tailed t-test. **f)** Tidal volumes for each dose group at each scanning time-point. White: baseline; light grey: 3 days; dark grey: 7 days; black: 10 days *: $p<0.05$ versus baseline; **: $p<0.01$ versus baseline; p-values were calculated by repeated measures ANOVA, n=4.

## 2.5 – DISCUSSION

The ability to noninvasively evaluate pulmonary inflammation is of great interest in experimental asthma as it would facilitate the investigation of issues concerning the onset, evolution and treatment of this disease. A number of imaging technologies are currently available to evaluate lung inflammation but the application of these techniques to allergic inflammation is limited. For example, $^{18}$F-fluorodeoxyglucose, in conjunction with positron emission tomography (PET), is commonly used to assess increased glucose uptake, and therefore metabolism, as a surrogate of inflammatory cell activity [14]. Unfortunately, this technique has not been shown to be a useful assessment of airway inflammation in asthmatics [15], unless under conditions of a segmental allergen challenge [16, 17], most likely because neutrophils, a cell-type with a debatable association to allergic asthma, use more glucose than other cell types when activated [18, 19]. Magnetic resonance imaging has also been used to detect inflammatory changes [20–22] as well as functional disruption after allergen exposure [23] in experimental models of asthma. Although this modality provides superior soft tissue contrast with no known deposition of radiation, CT is more widely available and is more commonly associated with PET and single photon emission CT (SPECT) radio-imaging technologies. These attributes, along with its ability to evaluate anatomical and functional processes by density measurements, make CT a promising technology for assessing inflammatory processes in the lung for at least preclinical and possibly clinical research.

CT has been used in several small animal models of lung disease to date, but there has been little agreement in the methods used to segment and present CT data. Methodological differences could be minimised by employing standardisation techniques, thus allowing for inter-study comparisons. For example, CT histogram data can be standardised by expressing bin volumes as the percentage of total volume, as shown by FROESE et al. [2], and, furthermore, by subtracting baseline values for each animal. As demonstrated in figure 2.1, the results obtained by Methods 1 and 2 were extremely similar in nature once the suggested standardisation methodologies were applied. These practices also allow for greater agreement within a data set, as differences between animals, such as total volume or baseline state of the lung, are partially resolved, thus facilitating longitudinal studies with a relatively small sample size.

The two methods of segmentation used for the current study, namely thoracic and lung segmentation, have both been reported previously in the literature. Thoracic volume segmentation (Method 1) has several advantages, when using basic software for analysis, in that it is considerably faster than lung segmentation, requires minimal user-defined manipulation, and can be used with relatively low-quality CT images. However, this method relies on the principle that all unit volumes (voxels) belonging to lung tissues must have an associated content of air, I.E. they belong to density values less than 0 HU. Lung tissues with values equal to or greater than water are therefore lost. Lung segmentation (Method 2) has its own benefits, principally associated with analysis of regions of

high density within the lung. Removal of bone, heart and other irrelevant tissues from the region of interest allows for the determination of average lung values ($\rho_{lung}$), slice density maps, and three-dimensional volume maps. However, in comparison with thoracic segmentation, the time required for lung segmentation, the amount of user-defined manipulation required (especially in regions of robust inflammation) and the quality of CT image needed limit its accessibility. We suggest that, for the purposes of assessing pulmonary inflammation in any CT image, thoracic segmentation should always be performed, so that the more user-reliant lung segmentation method can be double-checked.

Based on the change from baseline histogram curves, the current data indicated that the airspace in a BN rat lung was primarily associated with density values less than -350 HU and inflammatory processes with values above -350 HU. It is also important to note the gradient of this inflammation-associated range in relation to pulmonary structure. It appeared that the highest densities (greater than -50 HU) were directly associated with major blood vessels, middle-range densities (-50– -200 HU) were predominantly associated with major airways, and the lowest inflammation-related densities (-200– -350 HU) were peripheral to all higher densities. This distribution, in the context of allergen-induced inflammation of the lung, would seem to indicate that densities decrease with increasing distance from the major blood vessels. Furthermore, histograms produced through the transaxial axis of CT images indicated that densities greater than -350 HU were consistent throughout the lung, from apex to base. These data, in conjunction with representative axial slices and histological sections, indicate that the major conducting airways, and their associated vessels, are the focal point of inflammation in the lung. Thus, it is likely that the localisation and extent of both cellular and oedematous inflammation is determined by the site of interaction of the allergen with the airway mucosa and the proximity to a conducting vessel.

As it pertains to ungated data, exposure to 150 μg of HDM for 7 days resulted in a statistically significant increase in lung densities. Very suggestive changes were also observed in CT images after exposure to 15 μg of HDM for 7 days, although these changes did not reach statistical significance. Interestingly, after 10 days, only the group exposed to 150 μg of HDM continued to show overt and statistically significant change. Appraisal of histogram curves indicated that the difference between days 7 and 10, in groups exposed to both 15 (data not shown) and 150 μg (fig. 2.3a), was caused by a reduction in volumes with densities in the range -100– 100 HU (water is 0 HU). Thus, the comparatively greater increases in density observed at day 7 may reflect a greater contribution of oedematous infiltrate, rather than cellular inflammation, at this time.

When comparing CT data with biological outcomes, we observed a direct relationship between CT images and histological evidence of inflammation. Conversely, BAL findings, if viewed as a measure of the entire lung, were more

pronounced than the equivalent CT-derived values, such as integrals of the absolute change from baseline or $\rho_{lung}$ values. Since the CT-derived values were produced from data incorporating the entire lung, this comparison may suggest that results from BAL primarily evaluate processes surrounding the major airways and do not necessarily reflect the overall status of the periphery. A means of CT image airway segmentation could be developed to limit the diluting effect of peripheral density values, potentially providing a noninvasive BAL-equivalent measurement in allergic airway inflammation models. The divergence between BAL- and CT-derived findings is also probably affected by the relatively small density changes seen in vehicle control animals over the protocol (figs 2.3b–d, 2.4d, h and l, 2.6a and 2.7a and b). This reaction does not appear to be caused by any immunopathology but could be a result of the accumulation of liquid in the alveoli over the course of the protocol or limited pulmonary inflammation, occurring spontaneously, common to BN rats.

While the majority of the work presented was acquired from ungated CT images, post-acquisition respiratory gating was performed to determine the potential value of this methodology in this model of pulmonary inflammation. We found that peak values ($HU_{max}$) for histogram curves were significantly different between vehicle control and 150 μg of HDM for inspiratory but not expiratory CT images. This result indicates that the additional air volume at tidal inspiration provides an increased capability to determine the impact of inflammation on lung volumes, potentially improving the sensitivity of all measurement techniques reported. Unfortunately, segmentation procedures for gated images were restricted to Method 1, as the number of projections acquired in this study did not provide the image quality necessary for Method 2 to be used for further analysis. Projections were limited, especially for the inspiratory gate, because subject animals had a tendency towards a long expiratory phase and short inspiratory phase under anaesthetic. This scenario also skewed ungated images towards expiratory volumes. Therefore, future studies would benefit from an increased projection count so that the measurement methods described for ungated images could be applied to gated data sets. Intriguingly, tidal volumes, also derived from gated images, revealed altered breathing patterns in rats exposed to 15 and 150 μg of HDM, as well as an apparent response after 10 days in rats exposed to 0.15 μg of HDM. The rate of breathing could be determined in further work, in order to shed light on the physiological consequences of this result. Nonetheless, the current findings suggest that tidal volume may directly relate to the extent of inflammatory processes around major airways.

The research presented here was performed to determine the value and sensitivity of CT measurements in assessment of inflammatory events occurring in the lung as a result of exposure to HDM, a common and complex aeroallergen. In summary, we have shown that differences in the extent of inflammation can be extracted from CT images, and that this noninvasive modality is suitable for longitudinal evaluation of allergic airway inflammation. We suggest that future *in vivo* studies of pulmonary inflammation utilise standardisation practices,

respiratory gating and thoracic segmentation in addition to lung segmentation. Our findings provide a platform for further studies to evaluate intervention strategies and other asthma-related processes such as airway remodelling, and for investigations of existing or novel radiolabelled molecular markers for use with PET or SPECT. We propose that the noninvasive assessment of asthma in humans will directly benefit from advances in imaging methods and molecules tested in disease models.

## 2.6 – ACKNOWLEDGEMENTS

The authors gratefully thank C. Saab and R. Rhem for their expertise in and contribution towards all imaging aspects of experimentation; K. Ask, G. Martin, N. Stieber and E. Archer for their technical assistance; M. Kiriakopoulos and M. Colbert for secretarial support; and D.R. Boreham and N. Phan for dosimetry calculations (all McMaster University, Hamilton, ON, Canada).

## 2.7 – REFERENCES

1 Johnson KA. Imaging techniques for small animal imaging models of pulmonary disease: micro-CT. Toxicol Pathol 2007; 35: 59–64.
2 Froese AR, Ask K, Labiris R, et al. Three-dimensional computed tomography imaging in an animal model of emphysema. Eur Respir J 2007; 30: 1082–1089.
3 Labiris R, Ask K, Farkas L, et al. Comparison between conventional and ''clinical'' assessment of experimental lung fibrosis. J Transl Med 2008; 6: 16.
4 Lundblad LK, Thompson-Figueroa J, Allen GB, et al. Airway hyperresponsiveness in allergically inflamed mice: the role of airway closure. Am J Respir Crit Care Med 2007; 175: 768–774.
5 de Jong PA, Mu¨ ller NL, Pare´ PD, et al. Computed tomographic imaging of the airways: relationship to structure and function. Eur Respir J 2005; 26: 140–152.
6 Sung A, Naidich D, Belinskaya I, et al. The role of chest radiography and computed tomography in the diagnosis and management of asthma. Curr Opin Pulm Med 2007; 13: 31–36.
7 Simon BA, Christensen GE, Low DA, et al. Computed tomography studies of lung mechanics. Proc Am Thorac Soc 2005; 2: 517–521.
8 Cates EC, Fattouh R, Wattie J, et al. Intranasal exposure of mice to house dust mite elicits allergic airway inflammation via a GM-CSF-mediated mechanism. J Immunol 2004; 173: 6384–6392.
9 Johnson JR, Wiley RE, Fattouh R, et al. Continuous exposure to house dust mite elicits chronic airway inflammation and structural remodeling. Am J Respir Crit Care Med 2004; 169: 378–385.
10 Fattouh R, Pouladi MA, Alvarez D, et al. House dust mite facilitates ovalbumin-specific allergic sensitization and airway inflammation. Am J Respir Crit Care Med 2005; 172: 314–321.
11 Johnson JR, Archer EW, Ask K, et al. Noninvasive imaging of lung inflammation and fibrosis in a rat model of chronic allergic asthma. Proc Am Thorac Soc 2006; 3: A344.

12 Farncombe TH. Software-based respiratory gating for small animal conebeam CT. Med Phys 2008; 35: 1785–1792.
13 Simon BA. Non-invasive imaging of regional lung function using X-ray computed tomography. J Clin Monit Comput 2000; 16: 433–442.
14 Chen DL, Schuster DP. Imaging pulmonary inflammation with positron emission tomography: a biomarker for drug development. Mol Pharm 2006; 3: 488–495.
15 Jones HA, Marino PS, Shakur BH, et al. In vivo assessment of lung inflammatory cell activity in patients with COPD and asthma. Eur Respir J 2003; 21: 567–573.
16 Taylor IK, Hill AA, Hayes M, et al. Imaging allergeninvoked airway inflammation in atopic asthma with [18F]-fluorodeoxyglucose and positron emission tomography. Lancet 1996; 347: 937–940.
17 Holmes JH, Sorkness RL, Meibom SK, et al. Noninvasive mapping of regional response to segmental allergen challenge using magnetic resonance imaging and [F-18] fluorodeoxyglucose positron emission tomography. Magn Reson Med 2005; 53: 1243–1250.
18 Jones HA, Clark RJ, Rhodes CG, et al. In vivo measurement of neutrophil activity in experimental lung inflammation. Am J Respir Crit Care Med 1994; 149: 1635–1639.
19 Borregaard N, Herlin T. Energy metabolism of human neutrophils during phagocytosis. J Clin Invest 1982; 70: 550–557.
20 Beckmann N, Tigani B, Ekatodramis D, et al. Pulmonary edema induced by allergen challenge in the rat: noninvasive assessment by magnetic resonance imaging. Magn Reson Med 2001; 45: 88–95.
21 Tigani B, Cannet C, Zurbrugg S, et al. Resolution of the oedema associated with allergic pulmonary inflammation in rats assessed noninvasively by magnetic resonance imaging. Br J Pharmacol 2003; 140: 239–246.
22 Tigani B, Cannet C, Karmouty-Quintana H, et al. Lung inflammation and vascular remodeling after repeated allergen challenge detected noninvasively by MRI. Am J Physiol Lung Cell Mol Physiol 2007; 292: L644–L653.
23 Driehuys B, Walker J, Pollaro J, et al. 3He MRI in mouse models of asthma. Magn Reson Med 2007; 58: 893–900.

# CHAPTER 3
# Imaging Lung Function in Mice Using SPECT/CT and Per-Voxel Analysis

## 3.0 – Overview of Chapter 3

The second article of this thesis is entitled "Imaging Lung Function in Mice Using SPECT/CT and Per-voxel Analysis" and is a methodological description of the ventilation/perfusion technique that was adapted for use in preclinical research. This represents the first use of V/Q imaging in mice and the first statistically analyzed quantification of V/Q images.

The methodology was set out in detail and various measures were presented to characterize lung function in a set of mice. This approach was then validated by taking measurements in a much older set of mice, demonstrating that V/Q matching declines with age, a result expected from scientific knowledge of V/Q in humans. Further, two methods of regionalization were provided to demonstrate the ability of this volumetric methodology to examine specific regions of the lungs, something that is not possible without a volumetric modality.

This article, therefore, demonstrated the ability to apply a sensitive, volumetric and clinically relevant lung function measurement to preclinical models. In addition, it demonstrated the power of volumetric methods to gather information not accessible by other means, such as spirometric-type measures, and, in so doing, added to the literature regarding the change in the distribution of physiological processes in the lung with age.

Publication of this article took place online on the 3rd of August, 2012 in the Public Library of Science One (PLoS One), an open access, online journal.

PLoS One. 2012;7(8):e42187.
Epub 2012 Aug 3.

# Imaging Lung Function in Mice Using SPECT/CT and Per-Voxel Analysis

Brian N. Jobse[1,2,3], Rod G. Rhem[1], Cory A. J. R. McCurry[1], Iris Q. Wang[1], N. Renée Labiris[1,3]*

AFFILIATIONS
1 Department of Medicine, Division of Respirology, McMaster University, Hamilton, Ontario, Canada, 2 Department of Pathology and Molecular Medicine, Division of Respiratory Diseases and Allergy, McMaster Immunology Research Centre, McMaster University, Hamilton, Canada, 3 Firestone Institute for Respiratory Health, St. Joseph's Healthcare, Hamilton, Canada

CORRESPONDENCE
N.R. Labiris
Department of Medicine
Health Sciences Centre rm. 1V11
McMaster University
1280 Main St. W.
Hamilton, ON
Canada L8S 4K1
Fax: 905-546-1125
E-mail: labir@mcmaster.ca

Editor: Chin-Tu Chen, The University of Chicago, United States of America

Received April 25, 2012; Accepted July 2, 2012; Published August 3, 2012



Funding: Funding provided by Firestone Institute of Respiratory Health–AstraZeneca Collaboration Unrestricted Grant; NRL holds an internal Department of Medicine Career Award. The funders had no role in study design, data collection and analysis, decision to publish, or preparation of the manuscript.

Competing Interests: This study was partially funded by an AstraZeneca Collaboration Unrestricted Grant. There are no patents, products in development or marketed products to declare. This does not alter the authors' adherence to all the PLoS ONE policies on sharing data and materials, as detailed online in the guide for authors.

## 3.1 – ABSTRACT

Chronic lung disease is a major worldwide health concern but better tools are required to understand the underlying pathologies. Ventilation/perfusion (V/Q) single photon emission computed tomography (SPECT) with per-voxel analysis allows for non-invasive measurement of regional lung function. A clinically adapted V/Q methodology was used in healthy mice to investigate V/Q relationships. Twelve week-old mice were imaged to describe normal lung function while 36 week-old mice were imaged to determine how age affects V/Q. Mice were ventilated with Technegas™ and injected with $^{99m}$Tc-macroaggregated albumin to trace ventilation and perfusion, respectively. For both processes, SPECT and CT images were acquired, co-registered, and quantitatively analyzed. On a per-voxel basis, ventilation and perfusion were moderately correlated (R = 0.58±0.03) in 12 week old animals and a mean log(V/Q) ratio of -0.07±0.01 and standard deviation of 0.36±0.02 were found, defining the extent of V/Q matching. In contrast, 36 week old animals had significantly increased levels of V/Q mismatching throughout the periphery of the lung. Measures of V/Q were consistent across healthy animals and differences were observed with age demonstrating the capability of this technique in quantifying lung function. Per-voxel analysis and the ability to non-invasively assess lung function will aid in the investigation of chronic lung disease models and drug efficacy studies.

## 3.2 – INTRODUCTION

Chronic respiratory diseases such as asthma and chronic obstructive pulmonary disease (COPD) are burdensome on healthcare systems and are associated with substantial morbidity and mortality worldwide [1]. Methodologies for three-dimensional imaging of the lung are important as they allow for better characterization and understanding of these obstructive diseases [2]. While volumetric CT densitometry is now widely used, it generally contributes only structural information while other imaging techniques can provide functional information such as the contribution of alveolar ventilation (V) and pulmonary capillary perfusion (Q) to gas exchange within the lung [3]. There are non-imaging methods of V/Q assessment [4], and the forced-expiration pulmonary function tests (PFTs) currently used for diagnosis of obstructive diseases are relatively simple to perform, but these methods cannot evaluate lung function in a regional manner. In addition, PFTs are unable to differentiate pathologies and are insensitive to early disease [5]. While imaging methods are technically more difficult than PFTs they can provide both global and regional functional information. Further, these volumetric techniques are necessary to address the heterogeneous underlying pathologies that make up diseases such as COPD [2,6,7].

In the field of clinical nuclear medicine, static V/Q imaging is routinely performed with single photon emission computed tomography (SPECT) along with Technegas™ and $^{99m}$Techetium-labelled macroaggregated albumin (MAA) to provide the distributions of V and Q, respectively. Images acquired by this

method depict the relative contributions of the core pulmonary processes of V and Q within any particular region in the lung. When V/Q images are co-registered to CT, regional analysis can be coupled to structural information. Clinical research examining the pathophysiology of COPD has been shown to benefit significantly from the use of radiologist-scored V/Q SPECT/CT [6] but investigation into the use of per-voxel volumetric analysis has only just begun in this area [8,9].

Pre-clinical models illustrating the utility of SPECT/CT as a tool in respiratory research are currently scarce [10]. Noninvasive assessment of small animal models offers an approach to address a natural link between discoveries at the molecular level and the application of clinically relevant diagnostics or therapeutics [10,11,12]. 3D imaging has now been used in various pulmonary disease models including asthma and emphysema, among others [10,13,14]. In regards to preclinical functional lung imaging, V/Q scanning has only seen service in rats through use of magnetic resonance imaging (MRI) and has so far lacked whole lung assessment [15,16]. Global lung measurements of V/Q have also been made in rats using the multiple inert gas elimination technique [17], but as this methodology does not employ any imaging modality it cannot offer regional analysis. Although rats offer better resolution of lung structure due to their size, the ability to test molecular hypotheses is greater in mice due to the relative abundance of knockout strains and commercially available tests. The mouse has yet to be investigated by any V/Q methodology and no extensive quantitative V/Q evaluation of lung function has been performed in a murine model.

Utilizing V/Q SPECT/CT to measure functional consequences of known pathologies in murine models could improve our understanding of the pathophysiology of respiratory disease and translate knowledge gained to the clinical setting, where similar imaging methodologies can be applied in most nuclear medicine departments. In this study we have successfully adapted a common clinical V/Q imaging protocol, employing Technegas$^{TM}$ and $^{99m}$Tc-MAA, to mice. In addition, we have applied a three-dimensional quantitative per-voxel analysis to characterize the naïve lung environment. Further, the sensitivity of this lung function measurement was tested by global and regional assessment of age-related changes. This work provides a foundation for further investigation of lung function in respiratory disease models.

## 3.3 – MATERIALS AND METHODS

**Animals**

Female BALB/c mice (Charles River, QC, Canada) were acclimatised to specific pathogen-free housing conditions for a period of 2–3 weeks, with a 12:12 hour light:dark cycle, prior to imaging. Experimentation was performed on 17 mice (12–16 weeks old, henceforth referred to as 12 w.o.) while another group of mice were housed for a further 24 weeks before imaging (henceforth referred to as 36

w.o.). The experiments described in this study were approved by the Animal Research Ethics Board of McMaster University (Animal Utilization Protocol #080514) in accordance with the guidelines of the Canadian Council on Animal Care.

**Imaging Protocol**

Healthy, untreated mice were tracheally intubated through the oral cavity with a 20-gauge catheter following anaesthetization with ketamine/xylazine (90 mg/kg, 6 mg/kg). Animals were then ventilated (0.02 L/min, 125 strokes/min) on a Rodent Ventilator (Model 683, Harvard Apparatus, Holliston, MA, USA) with Technegas™ (Cyclomedica, Lucas Heights, NSW, Australia) (0.04–0.12 MBq/mL) for 15 minutes, alternating between Technegas™ and room air in intervals of 15–30 seconds. Technegas™ is an ultrafine aerosol composed of carbon particles labeled with $^{99m}$Tc and suspended in argon, with a mean aerosol diameter between 30 and 60 nm [18]. Following ventilation mice were moved and strapped securely to a heated bed for animal welfare and consistency in body temperature between animals. SPECT scans were acquired on an X-SPECT system (Gamma Medica, Northridge, CA, USA) using dual sodium iodide crystals in combination with low energy pinhole collimators with 1 mm aperture and a radius of rotation of 3.5 cm. The ventilation SPECT scan consisted of thirty-two 50 second projections and was followed immediately by the collection of four rotations of 1024 X-ray projections for CT, also acquired on the X-SPECT system with x-ray tube characteristics of 75 kVp and 220 μA. Following ventilation SPECT and CT scans, mice were injected with 11–15 MBq of $^{99m}$Tc-MAA via the tail vein. Care was taken not to shift the position of the animal during the injection. Perfusion imaging entailed a 1024-projection CT scan and a SPECT scan of thirty-two 40 second projections. Supplemental gaseous anaesthesia was used (isoflurane (1%, 1 L/min)) to ensure sedation throughout the imaging procedure (approximately 1 hour 20 minutes).

Mice were recovered from the imaging procedure and monitored until radioactivity had decayed to background levels. All imaging work was completed at the McMaster Centre for Preclinical and Translational Imaging (MCPTI) at McMaster University (Hamilton, ON, Canada). A simplified protocol, detailing the sequence of imaging methodology, is shown in Figure 3.1.

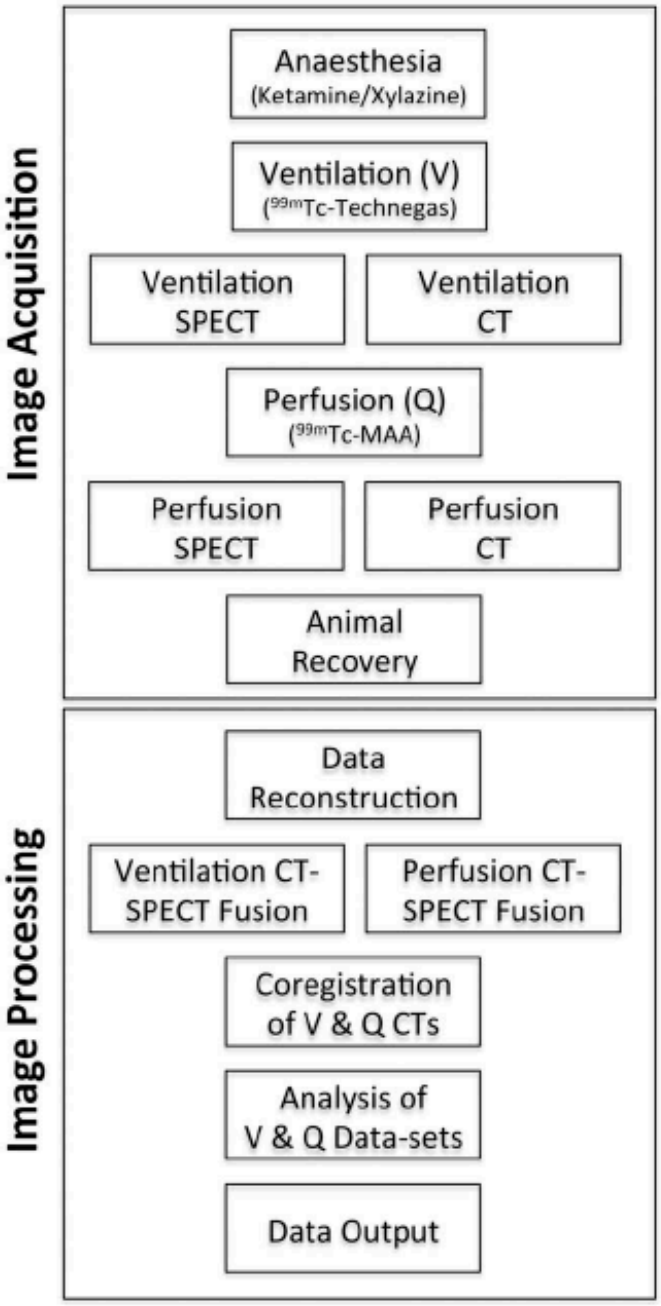


FIGURE 3.1
Simplified representation of the methodology used in image acquisition and processing to provide the final V/Q data sets.

**Reconstruction of 3D SPECT/CT Images**

SPECT images for both ventilation and perfusion scans were produced by iterative reconstruction of their respective projections using FLEX$^{TM}$-SPECT software (Gamma Medica) into 80x80x80 arrays (0.472 mm isotropic voxels). The projections from the four ventilation CT rotations were first summed, then images were reconstructed using a Feldkamp cone beam back-projection algorithm in COBRA (Exxim Sofware, Pleasanton, CA, USA) into 512x512x512 arrays (0.115 mm isotropic voxels). This high quality CT image was used in the processing and analysis of V/Q data to provide anatomical features for SPECT coregistration and to also allow for a density-based assessment of the lung environment. The perfusion CT projections were reconstructed under the same conditions. Calibration of each CT image for Hounsfield Unit (HU) scaling was performed using empty airspace within the field of view and a water-filled tube included in each scan.

**Fusion and Co-registration of Ventilation and Perfusion SPECT/CT Data**

Ventilation and perfusion CT images ($512^3$ matrix) were first subjected to a Gaussian filter ($\sigma$=0.8) using Matlab version 7.5 (Mathworks, Natick, MA, USA). A 'Lung' label was produced for the CT images as described previously for rats [13] using Amira 5.1 software (Visage Imaging, Andover, MA, USA), with the exception that the trachea and main bronchi (up to the point where they enter lung tissue) were removed from the ventilation lung label. Briefly, a 250HU threshold-limited growing algorithm was used to define the airspace. This selection was then subjected to a simple volume-growing algorithm and another threshold of 100HU applied to exclude tissues and structures not belonging to the lung. A hole-filling algorithm was also applied to include internal structures such as major blood vessels and, finally, the label was manually examined to ensure the process was consistent across animals. CT images and lung labels were then compressed to a matrix of $256^3$ for computational purposes. Representative axial, coronal, and sagittal images for the CT, lung label, ventilation, and perfusion scans can be seen in Figure 3.2 while a representative lung label is shown in Figure 3.3A.

The perfusion CT and SPECT were fused, with in-house software developed in Matlab, by a process that maximised mutual information (MI) within the lung region as defined by the label field [19]. Powell's multidimensional direction set method was used to maximise MI using a one dimensional search algorithm based on golden section search and parabolic interpolation [20]: SPECT images underwent rigid body transformation until a change of less than 0.01 mm (translation) or 0.01 degrees (rotation) was observed along or around each axis to obtain fusion parameters. During the process, the $80^3$ matrix of the SPECT image was interpolated for comparison to the CT image and was resampled to a $256^3$ matrix when the stop criteria were met; this corresponds to a change in voxel size from 0.40 $mm^3$ to 0.23 $mm^3$. When maximised MI was reached the result was visually inspected to confirm fusion quality. Parameters obtained from fusion of the perfusion SPECT and CT were then applied to the ventilation SPECT and CT

as the spatial relationship between these two data sets remains constant.

The ventilation and perfusion data sets were then co-registered by repeating the MI maximisation process through rigid body transformation of their respective CT images, again within the lung segmentation. Specifically, the perfusion CT was adjusted to fit the ventilation CT. These co-registration parameters were then applied to the perfusion SPECT data allowing for comparison of ventilation and perfusion SPECT images. A simplified representation of image processing is shown in Figure 3.1.

**Quantitative Per-Voxel Assessment**
Co-registration of images allows for analysis of SPECT and CT data on a per-voxel basis. Within the lung label all voxels had a HU, V, Q, and log(V/Q) value; presented data represent distributions of all voxels within the lung label averaged across all animals, unless otherwise stated. V and Q values were converted to relative frequencies by dividing the activity value of each voxel by the total activity in the lung label and then multiplying by 100. The relative frequency of both V and Q were used to calculate V/Q ratios and a base 10 logarithm was applied to provide a log-normal distribution. Analysis of the log(V/Q) data involved calculation of the mean, standard deviation, skewness, excess kurtosis, and percentage of total lung volume (TLV) greater than ±2 averaged standard deviations from the averaged mean log(V/Q), as a measure of V/Q mismatching. Any voxel where only V equalled zero was set to a log(V/Q) ratio of $-\infty$ and any voxel where only Q equalled zero was set to a log(V/Q) ratio of $+\infty$; these values were not included in the calculation of the log(V/Q) mean, standard deviation, skew or kurtosis. Any voxels where both V and Q equalled zero were noted and given a log(V/Q) value of zero.

**Regionalization of Images**
Two different methods of regionalization were performed on V, Q, and log(V/Q) data. Apex, middle, and base divisions were made by finding the axial slices closest to the 33 and 66 percentiles of volume. Inner and outer divisions were made by eroding the outer boundary of the lung label by 3 voxels, using a six-neighbour structuring element in a volumetric manner, and subtracting the new inner data from the original whole lung to produce the outer data. Standard deviations of log(V/Q) were calculated for all voxels in a region in the same manner as described above.

**Respiratory-gated CT Image Processing & Quantitation**
Inspiratory-and expiratory-gated CT images were produced by applying RespGate software (RespGate, Hamilton, ON, Canada) [21] to all ventilation CT projections. Respiratory-gated images were then reconstructed and calibrated as described for the ungated image used in the V/Q analysis. Air volume information from respiratory-gated CTs was extracted by a method previously described in rats [13]. Briefly, a segmentation was made encompassing the thoracic cavity using Amira 5.1 software and a histogram of the densities

(25HU/bin) within this region of interest was produced. The volume of air within the thoracic segmentation was calculated from the histogram by multiplying the number of voxels in a HU density bin against an air coefficient for that HU bin and converting the result into millilitres. The air coefficient was defined by the centre of the HU bin and represented the fraction of air in a voxel of that value; e.g., the air coefficient for -500 HU is 0.5. Summation of the air histogram from the end expiratory image allowed for quantitation of functional residual capacity (FRC) and tidal volume (TV) was calculated as the difference between air volume in the inspiratory and expiratory lung states.

**Data Analysis**

Images were analyzed and all measures were output with the aid of Matlab. Boxplots represent the lower quartile, median and upper quartile while whiskers represent the minimum and maximum values within the data set. Data are expressed as the mean±SEM and, where applicable, statistical significance was determined by unpaired two-tailed t-test in Graphpad Prism (Graphpad Software Inc, La Jolla, CA, USA); $p<0.05$ was considered statistically significant. Two of the seventeen 12 w.o. animals were excluded for the following reasons: one V/Q data set was a statistical outlier for the ratio of total perfusion activity to total ventilation activity, and another animal received an improper intravenous delivery of MAA, as noted at the time of injection. One 36 w.o. animal was also excluded as an outlier for increased FRC volume.

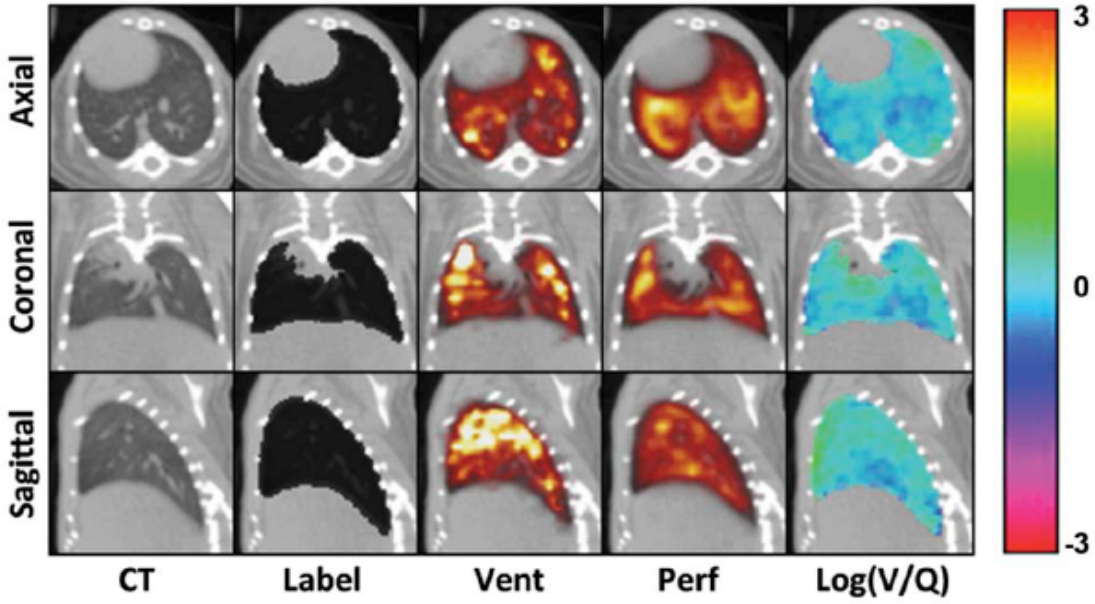


FIGURE 3.2

Representative CT and SPECT slice images in axial, coronal, and sagittal planes. The animal shown was chosen based on average mean and standard deviation values for the data set. CT refers to the ventilation-associated CT. Label refers to the lung segmentation seen as a black overlay on the CT. Vent and Perf refer to V and Q images with the colour scale increasing from red through yellow to white for both. Log(V/Q) refers to the final calculated data and the colour bar indicates the values seen in the associated log(V/Q) images.

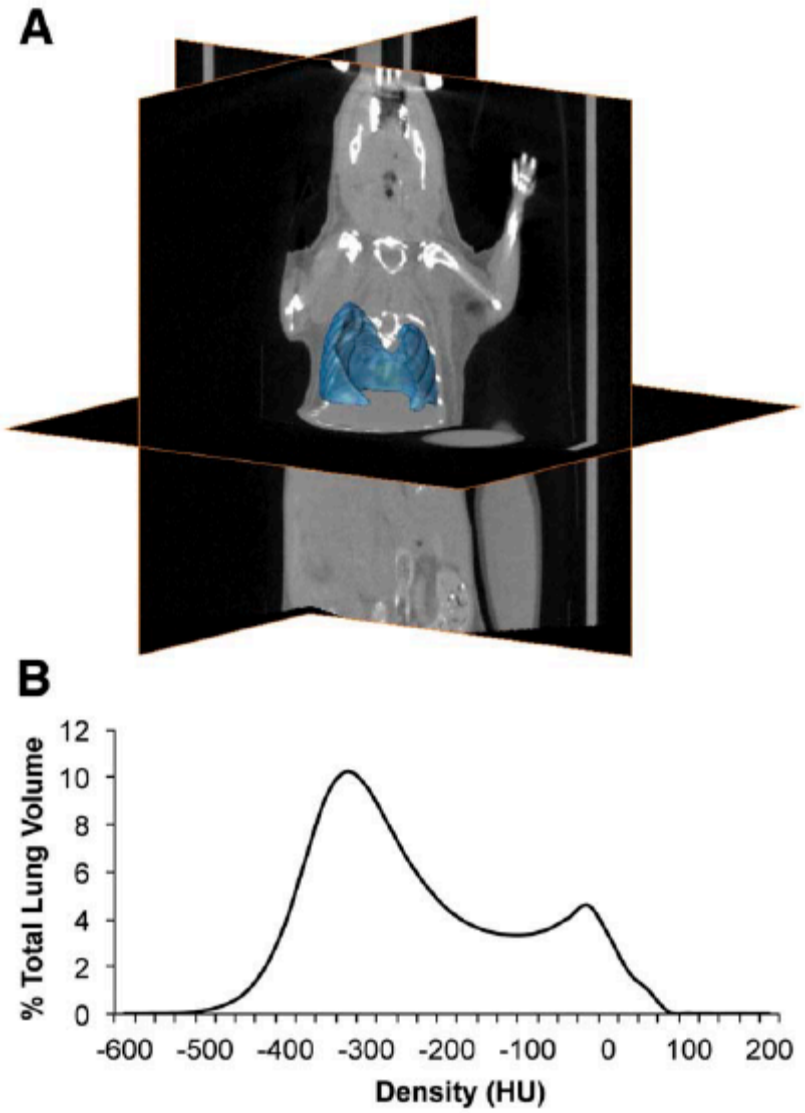


FIGURE 3.3
Lung segmentation used in the V/Q analysis. **A** Representative lung segmentation used in V/Q co-registration and analysis, with CT orthoslices for reference. **B** Average volume-standardised CT densitometry of ungated images in Hounsfield units (HU) depicting the distribution of densities within the label.

## 3.4 – RESULTS

Many lung function parameters can be measured from V/Q SPECT/CT: Ventilation and perfusion distribution within the lung can be determined; the relationship between these processes can be studied by measuring their correlation on a per-voxel basis; the degree of V/Q mismatching is illustrated in the log(V/Q) distribution and can be quantified using thresholds, such as two standard deviations from the mean; from the CT, tidal volume and FRC can be quantified in addition to changes in lung density. Investigating these parameters provides a detailed evaluation from which lung dysfunction can be assessed.

Typically, the distribution of deposition in the ventilation images was somewhat heterogeneous and typified by areas of increased intensities, predominately in apical regions, while decreased intensities were observed in basal regions (Figure 3.2). The lung perfusion distribution demonstrated greater uniformity of counts with less apparent skew towards the upper regions of the lung. Similarly, log(V/Q) images described a relatively homogeneous distribution with only small regions of obvious V/Q mismatch. The average total number of counts from ventilation with Technegas$^{TM}$, measured within the lung, was $1.96\pm0.33x10^5$ while the average total number of counts from perfusion with $^{99m}$Tc-MAA was $3.61\pm0.31x10^6$ (data not shown) creating a mean ratio of 24.2±3.7 to 1 between perfusion and ventilation total activity. This ratio was unaltered in the 36w.o. animals.

The degree of ventilation and perfusion matching in the lung was determined by plotting the distribution of log(V/Q) values (Figure 3.4A). The mean and standard deviation of log(V/Q) values were narrowly distributed with averages of -0.071±0.006 and 0.36±0.02, respectively (Figure 3.4A & B). In addition, the log(V/Q) distribution was not normal in nature as it was negatively skewed and positively kurtotic. Approximately 6.6% of TLV had a low log(V/Q) ratio mismatch while approximately 1.0% of TLV had a high log(V/Q) ratio mismatch (Figure 3.4A). Of the low log(V/Q) mismatched volume 3.23±0.75% of TLV was made up of voxels with a log(V/Q) value of -∞ but no significant proportion of voxels with values of +∞ were found (Figure 3.4C).

In the comparison of 12w.o. to 36w.o. animals, discrete histograms were generated for both ventilation and perfusion in order to assess any difference due to age in these physiological processes; 36w.o. animals demonstrated a shift towards lower relative count values for both ventilation and perfusion when compared to their younger counterparts (Figure 3.5A). The leftward shift of these distributions was not apparent when these processes were translated to a per-voxel log(V/Q) ratio, where the difference between 12w.o. and 36w.o. animals is much more subtle (Figure 3.5B). However, older animals had significant changes in standard deviation, skewness, and excess kurtosis of the log(V/Q) distribution (Figure 3.5C). Furthermore, values for positive and negative ∞ were significantly increased along with values for high log(V/Q) (Figure 3.5D); these changes were larger in magnitude for negative values than positive.

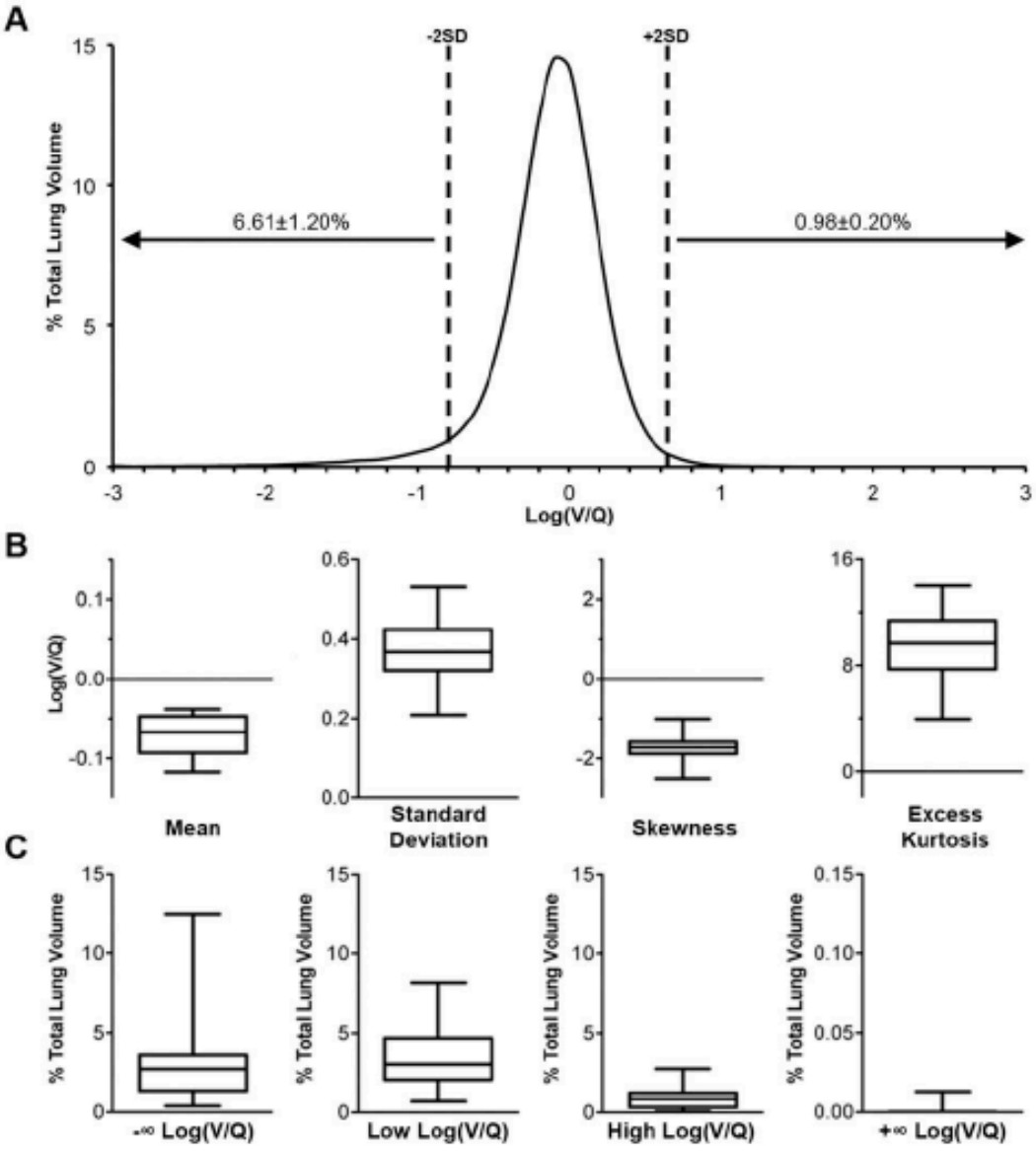


FIGURE 3.4
Distribution and measures of log(V/Q) data. **A** Average volume-standardised distribution of log(V/Q) values measured in percentage of total lung volume. Dashed lines indicate average ±2 standard deviations from the average mean. Values over arrows represent average±SEM percentage of lung volume beyond ±2 standard deviations, including log(V/Q) ±∞ values. **B** Descriptive analysis of log(V/Q) distribution central tendency and variation within the lung, calculated without ±∞ values. **C** Percentage of total lung volume with log(V/Q) mismatching. Mismatching is defined as values greater or less than 2 average standard deviations from the average mean. -∞ and +∞ refer to voxels where V = 0 and Q= 0, respectively. Box plots describe the data for all 12w.o. animals in terms of the median, interquartile range, and minimum/maximum values.

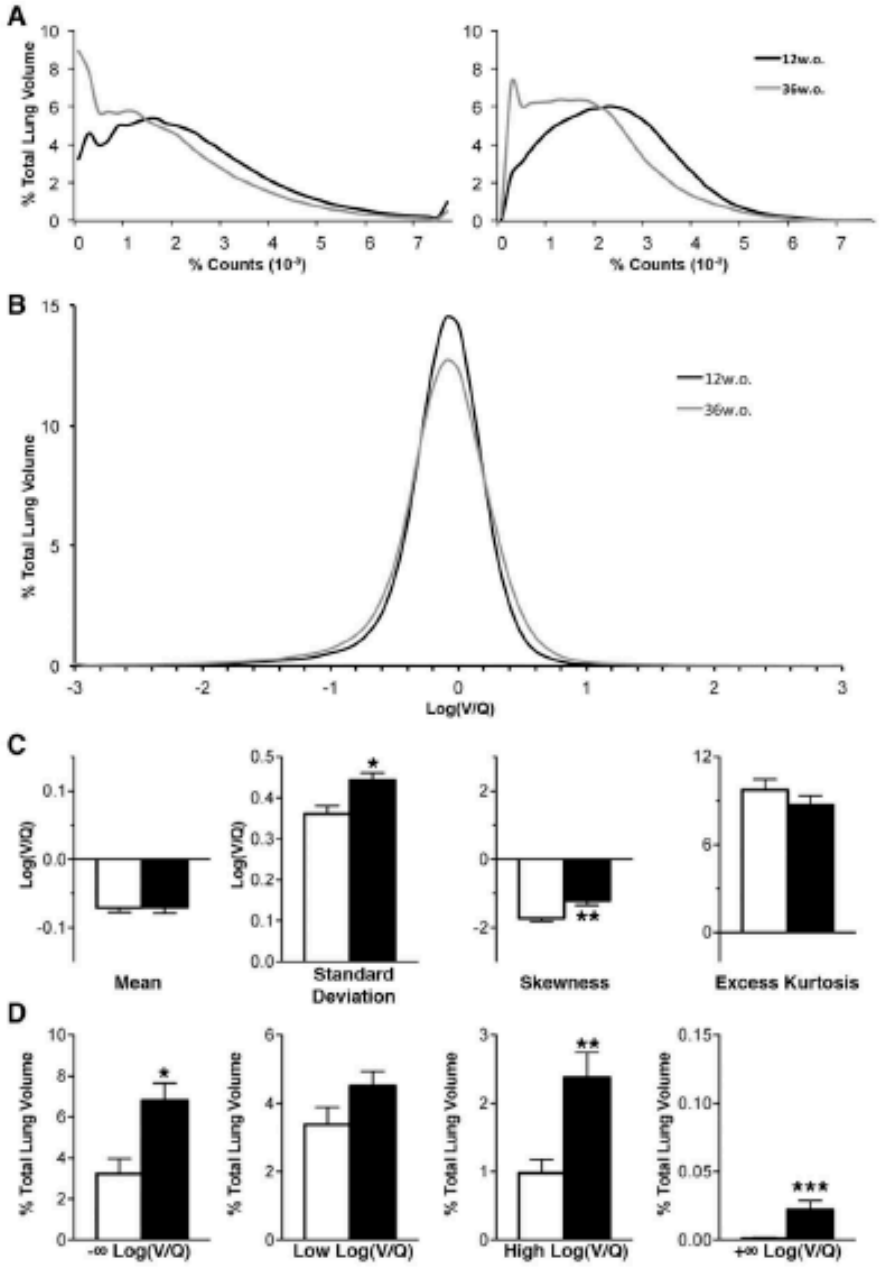


FIGURE 3.5

Effects of aging on lung function. **A** Average relative count distributions of ventilation (left) and perfusion (right) for 12w.o. (black) and 36w.o. (grey) animals in percent of total lung volume. **B** Average log(V/Q) distributions for 12w.o. (black) and 36w.o. (grey) animals. **C** Descriptive analysis of log(V/Q) distribution central tendency and variation within the lung, calculated without ±∞ values. **D** Percentage of total lung volume with log(V/Q) mismatching. Mismatching is defined as values greater or less than 2 average standard deviations from the average mean. -∞ and +∞ refer to voxels where V = 0 and Q= 0, respectively. White bars refer to averages and SEM for 12w.o. animals while black bars refer to averages and SEM 36w.o. animals. *p<0.05, **p<0.01 by two-tailed t-test.

Log(V/Q) images of 12 and 36w.o. animals indicated that V/Q mismatching was distributed throughout the lung (Figure 3.6A). Regionalization of lung volume into apex, middle, and base divisions (approximately 33.3% of volume per division) as well as inner and outer divisions (approximately 45 and 55% of volume per division, respectively) allowed for further analysis of the distribution of V/Q heterogeneity and mismatch; no change in regional volume proportion was observed with age. In 12w.o. animals, the standard deviation of log(V/Q) values was greater in the basal region of the lung compared to the apex or middle regions (Figure 3.6B). In 36w.o. animals increases in standard deviation over 12.w.o. values were observed in all three regions. Inner and outer regionalization demonstrated that the increase in standard deviation values with age was greater in the periphery of the lung (Figure 3.6B). This age-related difference in the outer region was associated with a significant decrease in the percentage of both ventilation and perfusion counts in that region (data not shown), indicating that the increase in V/Q heterogeneity is associated with alterations in the distribution of both processes. This regional distribution of increased log(V/Q) heterogeneity indicates that mismatching is present throughout the lung and is primarily associated with the periphery.

The CT density distribution of the lung was described by a bimodal curve with a primary peak at approximately -325 HU, describing the air volume, and a lesser peak at approximately -25 HU, describing tissue volumes within or surrounding the lung (Figure 3.3B). Post-acquisition respiratory gating produced CT images of end inspiratory and end expiratory lung states. These curves are unimodal in nature due to the calculation of air content based on HU. There were notable differences in density distributions between inspiratory and expiratory states including a broadening of the peak and a shift towards lower HU values during inspiration (Figure 3.7A). These curves were further shifted towards lower densities in older mice. For 12w.o. animals, FRC was determined to be 0.12±0.01 mL while TV was determined to be 0.048±0.004 mL. FRC was significantly increased in the 36w.o. group while TV remained constant (Figure 3.7B).

When FRC, denoting lung volume, was plotted against the median value for ventilation and perfusion distributions a high degree of correlation ($R^2$ of 0.77, $p<0.0001$ and 0.75, $p<0.0001$ respectively) was observed for all 12w.o. animals indicating that the leftward shift in these distributions in the 36w.o. animals was due to the increased FRC values in this group. However, no correlation was seen when FRC was plotted against the standard deviation of the log(V/Q) curve, as a general measure of V/Q heterogeneity, indicating that FRC is not a driving factor in the log(V/Q) mismatch observed in older animals. In addition to the increase in FRC, a small increase in body mass was observed in 36w.o. mice (Table 1).

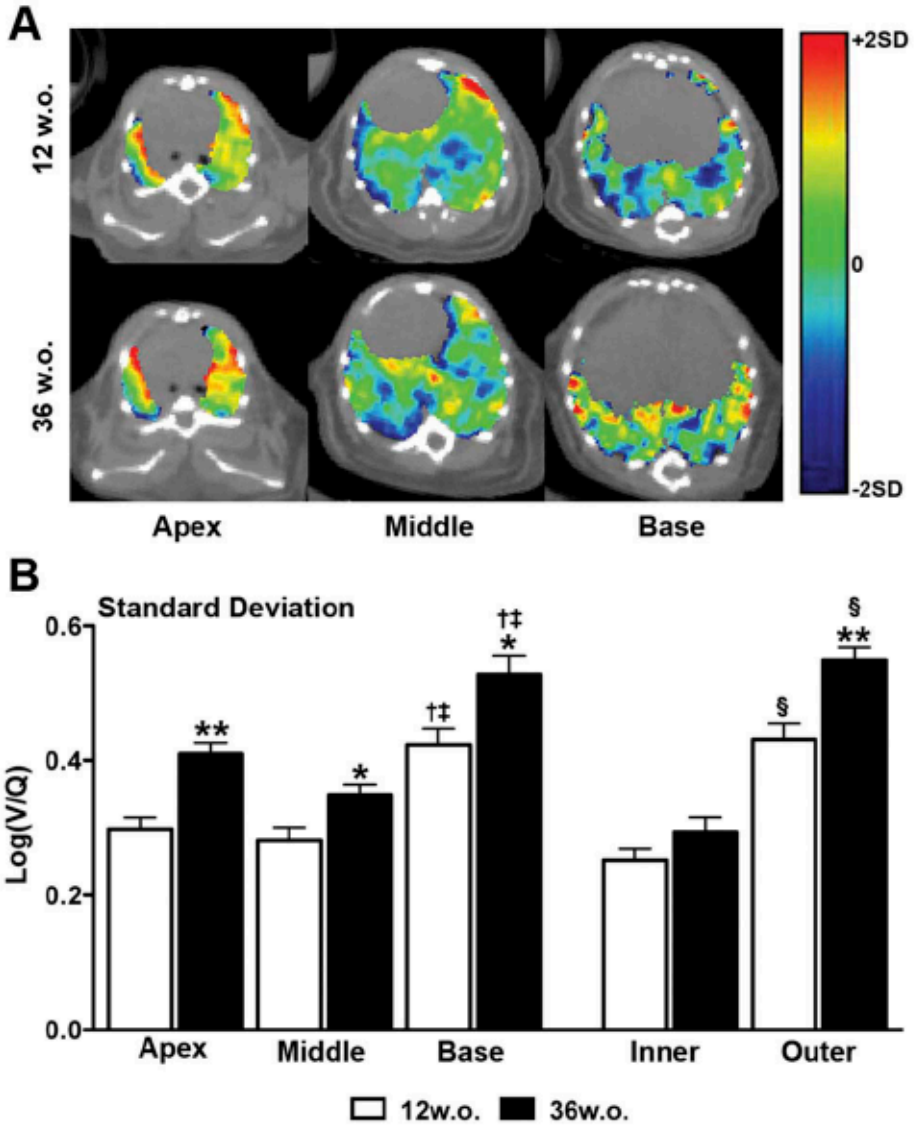


FIGURE 3.6
Regionalization of V/Q mismatching. **A** Representative axial log(V/Q) slices depicting changes with age in the apex, middle, and base of the lung. The colour scale represents 2 average standard deviations from the average mean of 12w.o. animals. **B** Regional analysis of averaged log(V/Q) standard deviation values in the apex, middle, and base of the lung as well as inner and outer regions. *p<0.05, **p<0.01 by two-tailed ttest between 12 and 36w.o. groups. †p<0.05 apex vs. base, ‡p<0.05 middle vs. base by one-way ANOVA with Tukey post-hoc. §p<0.05 by two-tailed t-test between inner and outer regions.

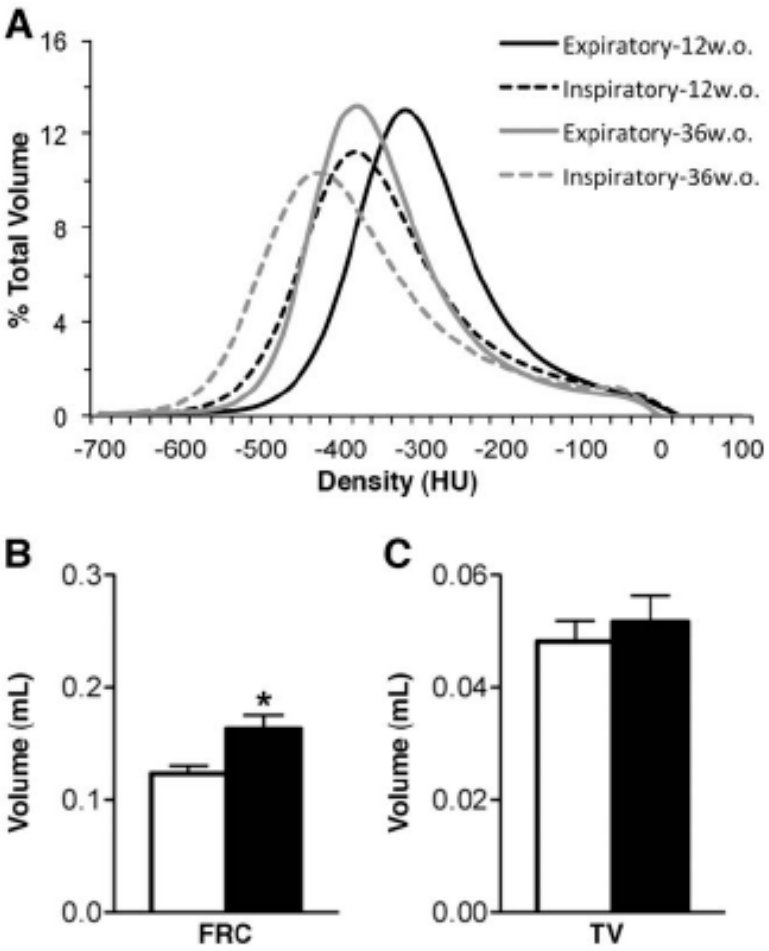


FIGURE 3.7

Respiratory-gated CT data for 12w.o. and 36w.o. groups. **A** Average volume standardised Hounsfield unit (HU) densitometry of expiratory (solid line) and inspiratory (dashed line) lung states for 12w.o. (black) and 36w.o. (grey) animals. **B** Average functional residual capacity (FRC) and tidal volume (TV), calculated from gated CT data. White bars refer to 12w.o. animals while black bars refer to 36w.o. animals. *$p<0.05$ by two-tailed t-test.

TABLE 3.1
Comparison of group characteristics between 12 week old and 36 weeks old mice.

| | 12 w.o. | 36 w.o. |
|---|---|---|
| Number | 15 | 6 |
| Mass (g) | 22±0.3 | 24±0.6* |
| Q:V Ratio | 24.2±3.7 | 14.2±1.7 |
| Log(V/Q) Mean | −0.071±0.007 | −0.071±0.008 |
| Log(V/Q) Standard Deviation | 0.361±0.020 | 0.442±0.018* |
| Log(V/Q) Skewness | −1.73±0.09 | −1.22±0.13** |
| Log(V/Q) Excess Kurtosis | 9.75±0.70 | 8.70±0.63 |
| Log(V/Q) −∞ values | 3.23±0.75 | 6.82±0.83* |
| Log(V/Q) +∞ values | 0.0012±0.0009 | 0.0223±0.0066*** |
| Log(V/Q) Low values | 3.38±0.50 | 4.52±0.42 |
| Log(V/Q) High values | 0.98±0.20 | 2.38±0.36** |
| Functional Residual Capacity (mL) | 0.124±0.007 | 0.163±0.013* |
| Tidal Volume (mL) | 0.048±0.004 | 0.052±0.005 |

*p<0.05, **p<0.01, ***p<0.001 by two-tailed t-test against 12 w.o. animals.
doi:10.1371/journal.pone.0042187.t001

## 3.5 – DISCUSSION

The capability to study the core processes of a vital organ, namely ventilation and perfusion in the lung, at a scale relevant to these processes represents an imperative step towards understanding lung function and how it changes in respiratory disease. This study demonstrates that we have successfully translated a common clinical V/Q imaging technique to the preclinical setting to measure lung function in mice. Using V/Q SPECT/CT as a biomarker of lung function will support preclinical investigations of the pathogenesis of respiratory diseases and screening of novel drug therapies, helping to bridge the gap to the clinical understanding of disease and drug efficacy. In addition, we have developed a preclinical method of image co-registration and data analysis to objectively evaluate V/Q at a per-voxel level so that regional assessments of lung function can be performed.

A V/Q ratio of 0.80, or a log(V/Q) of -0.097, is considered optimal for a healthy human lung [22]. We found a mean log(V/Q) of -0.071±0.006, corresponding to a V/Q ratio of 0.85, in our naïve mice indicating that healthy mammalian lungs have similar respiratory physiology. These values represent the gas exchange capability for the entire lung, but ventilation and perfusion, at a small scale, are somewhat heterogeneous processes. While early work suggested that gravity was a large determinant of heterogeneity in V/Q ratios [23], methodologies with better resolution describe greater variability at any particular axial height within the lung for both ventilation and perfusion [24]. It is now thought that the majority of this intrinsic variability can be attributed to factors related to the basic architecture of the lung [25]. To define the natural degree of heterogeneity in this

model V/Q mismatching was defined as the percentage of total lung volume (TLV) with log(V/Q) ratios ±2 standard deviations from the mean, as 95% of values should fall within this range for a normal distribution. For this purpose the average mean and standard deviation of the total data set was used with the notion that severely mismatched voxels would fall beyond the scope of this average ''normally functioning'' region. Only a small percentage of volume (~1%) was found above +2SD while a higher proportion (~7%) was found below -2SD. This population included voxels where ventilation values, but not perfusion values, equalled zero and thus had a log(V/Q) value of -∞. We found that approximately 3% of TLV had such a log(V/Q). Most of these zero ventilation values appear at the perimeter of the lung-label, especially around the caudal-most edges, and likely represent tissues not associated with alveolar regions or marginal errors in the co-registration process that were included in the lung label. Such voxels that are non-lung could contribute to the ±∞ categories; however, since the segmentation employed is a standardised process any sampling errors between animals should be consistent. Overall, the variability in V/Q distribution within the naïve animals studied was low, with a log(V/Q) standard deviation of 0.36±0.02, and therefore represents a typical degree of ventilation and perfusion heterogeneity in this system.

In humans, a decline in V/Q matching is known to occur with increased age [26,27,28] so we elected to study the effect of aging on lung function to determine the sensitivity of our methodology. To provide an experimental model to this effect a subset of mice were allowed to age for approximately 6 months, which is a considerable amount of time in the life of a mouse. Though the mice at 36 weeks of age had significantly more mass, and obesity is known to impact lung function [29], these mice were not considered obese and their weight would have little, if any, impact on V/Q matching (R=0.1426, p=0.79). However, we found that older animals had a significant increase in V/Q mismatching, as defined by the standard deviation of the log(V/Q) data, over their younger counterparts suggesting that this measure is sensitive to minor changes in lung function. The greater FRC observed in 36w.o. animals is likely associated with a reduction in lung elasticity, which is in turn due to a general loss of alveolar surface area [26]. This change in alveolar structure is potentially responsible for the increased V/Q heterogeneity demonstrated in older mice as similar mechanisms have been proposed clinically [30]. Regionalization of images further indicated that the increase in standard deviation of the log(V/Q) data is spread throughout the lung, but is also primarily associated with the peripheral volumes. The increase in standard deviation values in the outer region was associated with decreases in the percentages of both ventilation and perfusion associated with this volume. As greater than 30% of ventilation and perfusion counts were still present in this region at 36 weeks of age, and both ventilation and perfusion were decreased, it is unclear from this data what process is causing the increased V/Q mismatch observed. A decrease in perfusion with increasing distance toward the periphery has been noted previously by other methods [31] but the peripheral involvement of V/Q mismatch with age requires further research.

This study employed a per-voxel analysis in order to better depict the intrinsic V/Q heterogeneity in the lungs. Although the voxels used (0.23 $mm^3$) were larger than the alveolar structure, a great number of V/Q measurements were made within the lung label, forty-six thousand on average for a mouse lung. The strength of this approach is that measurements of the whole lung, such as mean and standard deviation, can be broken down into constituent parts. Small areas of mismatched V/Q will not necessarily stand out in global measurements but even these regions, in a voxel-by-voxel analysis, are likely made up of many voxels. The location and extent of mismatching could be quantified and a better understanding gained of how the lung functions on a regional level. We elected to use a segmentation defined from the ungated CT to ensure that all lung-associated voxels within the ungated SPECT images were included in the analysis. Suga et al. [8], in a clinical study, employed a threshold of 10% of maximum in their ventilation image data to define a region of interest for the lungs, but this method fails to address any regions of low ventilation activity and therefore could potentially exclude regions of lung, depending on the disease or model being used. Inclusion of all lung-associated volume is preferable and anatomical imaging, such as CT, is therefore not only desirable but also necessary.

Compared to clinical V/Q SPECT, the method used to deliver Technegas™ had to be modified for this preclinical work; while human patients are capable of inspiring an entire dose of activity in one to three breaths, mice require mechanical ventilation over the course of several minutes with Technegas™ at a relatively high level of radioactivity. Anaesthetic use is a further difference, though we intentionally kept the doses of these agents at a minimum to decrease any possible effect on respiration; respiratory gating confirmed that breathing patterns were similar between animals. Despite the differences between a clinical V/Q and the preclinical technique demonstrated here the results of this study represent a comparable methodology that achieves consistent results.

An important consideration for this methodology is the radiation dose to the subject animal. Work by Travis et al. suggests that the lethal dose for 50% (LD50) for BALB/c mice is above 5 Gy and that the dose rate required is well beyond that used in our study. Furthermore, no pathological changes were observed in the lungs or kidneys at a dose-rate of 100 mGy/min [32]. Based on previous whole body dosimetry measurements of mice using the same X-SPECT system, average CT radiation absorption dose can be approximated at 270 mGy [14], delivered over the course of approximately 25 minutes. Further, whole body dose from $^{99m}$Tc exposure can be approximated at 51 mGy [33]. Thus, we estimate that the total radiation dose to a mouse from V/Q SPECT/CT is 321 mGy, well below the radiation dose required to have a significant negative impact on biological processes in BALB/c mice. This total dose could be reduced substantially if basic CT scans were acquired for co-registration purposes only instead of the multiple rotations required for high quality respiratory-gated images.

The characterization of V/Q relationships in the lungs of healthy mice is a foundation upon which lung function can be studied under various physiological conditions and disease models. Respiratory diseases such as COPD would greatly benefit from V/Q imaging as our understanding of its progressive pathology and its impact on respiratory function could be considerably augmented by this lung function imaging methodology. We believe that the presented work demonstrates that we can reliably measure biomarkers of lung function using a clinically adapted method for performing V/Q SPECT in mice. The methodologies employed for delivery of radiolabelled tracer molecules, spatial alignment of images, and analysis of the resulting data provide a platform for investigations into the functional consequences of lung disease within experimental mouse models.

## 3.6 – ACKNOWLEDGEMENTS

The authors gratefully thank Dr. T.H. Farncombe and Ms. C. Saab for their expertise and contributions towards imaging; Dr. K. Taylor for dose estimates in mice; Dr. K. Gulenchyn and the McMaster Department of Nuclear Medicine, Hamilton Health Sciences (Hamilton, ON, CAN) for use of the TechnegasTM system; and the Firestone Institute for Respiratory Health (Hamilton, ON, CAN) for tuition support (BNJ).

## 3.7 – REFERENCES

1. Bousquet J, Khaltaev N (2007) Global surveillance, prevention and control of chronic respiratory diseases: a comprehensive approach.: World Health Organization.
2. Jones PW, Agusti AG (2006) Outcomes and markers in the assessment of chronic obstructive pulmonary disease. Eur Respir J 27: 822–832.
3. Petersson J, Glenny RW (2012) Imaging Regional PAO2 and Gas Exchange. J Appl Physiol. (In Press)
4. Wagner PD (2008) The multiple inert gas elimination technique (MIGET). Intensive Care Med 34: 994–1001.
5. Miller MR, Quanjer PH, Swanney MP, Ruppel G, Enright PL (2011) Interpreting lung function data using 80% predicted and fixed thresholds misclassifies more than 20% of patients. Chest 139: 52–59.
6. Jogi J, Ekberg M, Jonson B, Bozovic G, Bajc M (2011) Ventilation/perfusion SPECT in chronic obstructive pulmonary disease: an evaluation by reference to symptoms, spirometric lung function and emphysema, as assessed with HRCT. Eur J Nucl Med Mol Imaging 38: 1344–1352.
7. King GG, Harris B, Mahadev S (2010) V/Q SPECT: utility for investigation of pulmonary physiology. Semin Nucl Med 40: 467–473.
8. Suga K, Kawakami Y, Koike H, Iwanaga H, Tokuda O, et al. (2010) Lung ventilation-perfusion imbalance in pulmonary emphysema: assessment with automated V/Q quotient SPECT. Ann Nucl Med 24: 269–277.
9. Marsh S, Barnden L, O'Keeffe D (2011) Validation of co-registration of clinical

lung ventilation and perfusion SPECT. Australas Phys Eng Sci Med 34: 63–68.
10. Koba W, Kim K, Lipton ML, Jelicks L, Das B, et al. (2011) Imaging devices for use in small animals. Semin Nucl Med 41: 151–165.
11. Franc BL, Acton PD, Mari C, Hasegawa BH (2008) Small-animal SPECT and SPECT/CT: important tools for preclinical investigation. J Nucl Med 49: 1651–1663.
12. Dolovich M, Labiris R (2004) Imaging drug delivery and drug responses in the lung. Proc Am Thorac Soc 1: 329–337.
13. Jobse BN, Johnson JR, Farncombe TH, Labiris R, Walker TD, et al. (2009) Evaluation of allergic lung inflammation by computed tomography in a rat model in vivo. Eur Respir J 33: 1437–1447.
14. Froese AR, Ask K, Labiris R, Farncombe T, Warburton D, et al. (2007) Three-dimensional computed tomography imaging in an animal model of emphysema. Eur Respir J 30: 1082–1089.
15. Mistry NN, Qi Y, Hedlund LW, Johnson GA (2010) Ventilation/perfusion imaging in a rat model of airway obstruction. Magn Reson Med 63: 728–735.
16. Togao O, Ohno Y, Dimitrov I, Hsia CC, Takahashi M (2011) Ventilation/perfusion imaging of the lung using ultra-short echo time (UTE) MRI in an animal model of pulmonary embolism. J Magn Reson Imaging.
17. Alfaro V, Roca-Acin J, Palacios L, Guitart R (2001) Multiple inert gas elimination technique for determining ventilation/perfusion distributions in rat during normoxia, hypoxia and hyperoxia. Clin Exp Pharmacol Physiol 28: 419–424.
18. Senden TJ, Moock KH, Gerald JF, Burch WM, Browitt RJ, et al. (1997) The physical and chemical nature of technegas. J Nucl Med 38: 1327–1333.
19. Maes F, Collignon A, Vandermeulen D, Marchal G, Suetens P (1997) Multimodality image registration by maximization of mutual information. IEEE Trans Med Imaging 16: 187–198.
20. Press W, Teukolsky SA, Vetterling WT, Flannery BP (2007) (Powell's) Methods in Multidimensions. Numerical Recipes in C: The Art of Scientific Computing. 3rd ed. Cambridge: Cambridge University Press. 509–515.
21. Farncombe TH (2008) Software-based respiratory gating for small animal conebeam CT. Med Phys 35: 1785–1792.
22. Levitski MG (2007) Ventilation-Perfusion Relationships. In: Malley JEKG, editor. Pulmonary Physiology. 7th ed: McGraw-Hill. 113–129.
23. West JB, Dollery CT (1960) Distribution of blood flow and ventilation-perfusion ratio in the lung, measured with radioactive carbon dioxide. J Appl Physiol 15: 405–410.
24. Kreck TC, Krueger MA, Altemeier WA, Sinclair SE, Robertson HT, et al. (2001) Determination of regional ventilation and perfusion in the lung using xenon and computed tomography. J Appl Physiol 91: 1741–1749.
25. Galvin I, Drummond GB, Nirmalan M (2007) Distribution of blood flow and ventilation in the lung: gravity is not the only factor. Br J Anaesth 98: 420–428.
26. Sprung J, Gajic O, Warner DO (2006) Review article: age related alterations in respiratory function-anesthetic considerations. Can J Anaesth 53: 1244–1257.
27. Cardus J, Burgos F, Diaz O, Roca J, Barbera JA, et al. (1997) Increase in

pulmonary ventilation-perfusion inequality with age in healthy individuals. Am J Respir Crit Care Med 156: 648–653.
28. Holland J, Milic-Emili J, Macklem PT, Bates DV (1968) Regional distribution of pulmonary ventilation and perfusion in elderly subjects. J Clin Invest 47: 81–92.
29. Littleton SW (2012) Impact of obesity on respiratory function. Respirology 17:43–49.
30. Fain SB, Altes TA, Panth SR, Evans MD, Waters B, et al. (2005) Detection of age-dependent changes in healthy adult lungs with diffusion-weighted 3He MRI. Acad Radiol 12: 1385–1393.
31. Glenny RW, Lamm WJ, Albert RK, Robertson HT (1991) Gravity is a minor determinant of pulmonary blood flow distribution. J Appl Physiol 71: 620–629.
32. Travis EL, Peters LJ, McNeill J, Thames HD, Jr., Karolis C (1985) Effect of dose-rate on total body irradiation: lethality and pathologic findings. Radiother Oncol 4: 341–351.
33. Funk T, Sun M, Hasegawa BH (2004) Radiation dose estimate in small animal SPECT and PET. Med Phys 31: 2680–2686.

# CHAPTER 4
# Detection of Lung Dysfunction using Ventilation and Perfusion SPECT in a Mouse Model of Chronic Cigarette Smoke Exposure

## 4.0 – Overview of Chapter 4

The third article of this thesis is entitled "Detection of Lung Dysfunction using Ventilation and Perfusion SPECT in a Mouse Model of Chronic Cigarette Smoke Exposure". Using the V/Q methods established in Chapter 3, a characterization of prolonged cigarette smoke exposure demonstrated that the lung progressively loses the ability to match ventilation and perfusion, above and beyond the level of V/Q mismatching caused by aging alone. The data also indicate that V/Q imaging and quantification was sensitive to very minor changes in lung function. This was further illustrated by comparing V/Q results to those from CT in the same animals. While V/Q depicts lung dysfunction in this model, CT was not capable of discriminating between controls and cigarette smoke exposed mice, demonstrating that the functional measurements are much more sensitive to pathologies that are not necessarily obvious.

These pathologies were also investigated using cellular profiles from bronchoalveolar lavage and measurement of airspace enlargement from whole slice histological analysis. In conjunction with CT, these data describe the fact that, while present, the inflammatory and emphysematous pathologies are not large-scale in nature. However, as V/Q mismatching was present, these pathologies likely play a role in lung dysfunction. Importantly, V/Q imaging could detect early consequences of cigarette smoke exposure that could not be detected by other noninvasive measures such as CT.

This article adds to what has been published in the clinical literature and is further evidence that V/Q SPECT imaging has great value in the assessment of lung dysfunction. In addition, the quantification tools used in this article could be applied to future clinical studies; no current articles use a statistical analysis of per-voxel data. As the methodology used was clinically relevant, results from small animal models, such as the cigarette smoke exposure, will aid in the understanding of the pathogenesis of smoking related disease.

The Journal of Nuclear Medicine accepted this article for publication on the 10$^{th}$ of October, 2012 but it has yet to be published. Once in print, the copyright allows for this article to be reproduced in this thesis.

Accepted for Publication in the Journal of Nuclear Medicine
10/10/12

# Detection of Lung Dysfunction using Ventilation and Perfusion SPECT in a Mouse Model of Chronic Cigarette Smoke Exposure

Brian N. Jobse[1,2,3], Rod G. Rhem[1], Iris Q. Wang[1], William B. Counter[1,3], Martin R. Stämpfli [2,3], and N. Renée Labiris[1,3]

AFFILIATIONS
1 Department of Medicine, Division of Respirology, McMaster University, Hamilton, Ontario, Canada, 2 Department of Pathology and Molecular Medicine, Division of Respiratory Diseases and Allergy, McMaster Immunology Research Centre, McMaster University, Hamilton, Canada, 3 Firestone Institute for Respiratory Health, St. Joseph's Healthcare, Hamilton, Canada

CORRESPONDENCE
N.R. Labiris
Department of Medicine
Health Sciences Centre rm. 1V11
McMaster University
1280 Main St. W.
Hamilton, ON
Canada L8S 4K1
Fax: 905-546-1125
E-mail: labir@mcmaster.ca

Funding: Funding provided by Firestone Institute of Respiratory Health–AstraZeneca Collaboration Unrestricted Grant; NRL holds an internal Department of Medicine Career Award. The funders had no role in study design, data collection and analysis, decision to publish, or preparation of the manuscript.

Competing Interests: This study was partially funded by an AstraZeneca Collaboration Unrestricted Grant.

## 4.1 – ABSTRACT

Chronic obstructive pulmonary disease (COPD) is a leading cause of morbidity and mortality worldwide. Exposure to cigarette smoke (CS) is a major risk factor for developing this chronic airflow impairment but the early progression of disease is not well defined or understood. Ventilation/Perfusion (V/Q) single photon emission computed tomography (SPECT) provides a non-invasive assessment of lung function to further our current understanding of how CS affects the lung.

**Methods:** BALB/c mice were imaged with V/Q SPECT and computed tomography (CT) after 8 and 24 weeks of whole-body exposure to mainstream CS. Broncho-alveolar lavage (BAL) was collected and cell differentials produced to determine inflammatory patterns. Histological lung sections were collected and a semi-automated quantitative analysis of airspace enlargement applied to whole histology slices.

**Results**: Exposure to CS induced an inflammatory response that included increases in the numbers of both mononuclear cells and neutrophils. Airspace enlargement was also significantly increased at 8 weeks CS exposure and was still more pronounced at 24 weeks. V and Q correlation at the voxel level depicted a significant decrease in matching at 8 weeks CS exposure that was also apparent after 24 weeks. The standard deviation of the log(V/Q) curve, a basic measure of heterogeneity, was increased from 0.44±0.02 in age-matched controls to 0.62±0.05 with CS exposure at 24 weeks, indicating an increase in V/Q mismatching between 8 and 24 weeks CS exposure. CT, however, was not capable of discriminating control from CS exposed animals at either time-point, even with greater resolution and respiratory gating.

**Conclusion**: This study demonstrated that, prior to CT detection of structural changes, V/Q imaging detected changes in gas exchange potential. This functional impairment corresponded to increased lung inflammation and increased airspace enlargement. *In vivo* V/Q imaging can detect early changes to the lung caused by cigarette smoke exposure and thus provides a non-invasive method of longitudinally studying lung dysfunction in preclinical models. In the future, these measures could be applied clinically to study and diagnose the early stages of COPD.

## 4.2 – INTRODUCTION

Chronic obstructive pulmonary disease (COPD) is a worldwide health concern with high morbidity and mortality and an increasing burden on healthcare systems [1,2]. Exposure to cigarette smoke, which is a major risk factor in COPD pathogenesis, leads to various pathologies including, but not limited to, chronic inflammation, increased mucus production, small airway fibrosis, and airspace enlargement, otherwise known as emphysema [3]. Together, these pathologies, which are heterogeneously present in the small airways and periphery of the lung, lead to a reduction in overall gas exchange function that becomes debilitating over time [1]. Traditionally, COPD is diagnosed by spirometric measures such as forced vital capacity (FVC) and forced expiratory volume over

one second ($FEV_1$); these airflow-measurement techniques are also used in staging disease severity, monitoring disease progression, and measuring drug efficacy.

Although diagnosis of COPD by spirometry allows for a relatively simple measure of lung function and disease staging severity in afflicted individuals, the pathology of COPD tends to be in the smallest airways and these airways contribute little to airflow resistance under normal circumstances [4]; therefore, spirometry cannot detect the impact of small airway obstruction until it has developed considerably, making it insensitive to early disease. Further, spirometry doesn't differentiate the varying pathologies, such as small airway obstruction and emphysema, associated with COPD [5,6]. Because of the lack of early diagnoses, due in part to the insensitivity of spirometry and the heterogeneous nature of the disease, a thorough understanding of early pathogenesis is still required. Until this disease can be phenotyped and precise roles of the various pathologies determined in relation to air flow, blood flow, and gas exchange our inability to prevent lung dysfunction or provide patients with fully individualized treatment regimens will continue [7,8]. It is therefore necessary to develop tools that can be used to phenotype COPD, provide earlier diagnosis, and allow for greater understanding of this disease.

Clinical methods that measure ventilation/perfusion (V/Q) ratios in the lung have been shown to have high sensitivity to COPD pathologies, as demonstrated by Rodríguez-Roisin *et al.* using the multiple inert gas elimination technique (MIGET) [9]. While this methodology is well suited to understand respiratory disease mechanisms, due to the ability to describe the distribution of V/Q ratios in the lung, it lacks the ability to spatially distinguish underlying pathologies [10] and is not readily available in clinical practice. V/Q single photon emission computed tomography (SPECT) imaging, on the other hand, is a well-established nuclear medicine technique that provides spatial information regarding the two core processes of respiratory gas exchange, ventilation of alveolar units and perfusion of the pulmonary capillary beds [11], and the results of this technique correlate well with those derived from MIGET [12]. SPECT V/Q is commonly used in the diagnosis of pulmonary embolism but has been shown to be sensitive to early indicators of COPD in addition to being capable of identifying co-morbid disease and distinguishing pathophysiological changes [13,14]. Furthermore, co-registration of nuclear imaging data to computed tomography (CT) images allows for greater insight into the anatomical position of lung dysfunction as well as structural information such as the distribution of emphysema.

While V/Q imaging techniques hold great promise in providing a better understanding of chronic respiratory illnesses such as COPD, these techniques can also be used in preclinical research, to study disease pathogenesis and evaluate the efficacy of therapies. Preclinical models for investigating COPD include a host of different agents to elicit pathologies such as inflammation and

emphysema, but cigarette smoke exposure is likely the most relevant when modelling the pathogenesis of this disease [15].

We have applied V/Q imaging to a preclinical model of COPD to determine the impact of prolonged cigarette smoke exposure on the relationship between ventilation and perfusion in the lung. Inflammatory measures as well as histological assessment of airspace enlargement were collected to describe two of the major pathologies present in this model and to provide context for the V/Q measurements. In addition, anatomical data from CT images was compared to the functional measures obtained through V/Q imaging. While CT may not be sensitive to early changes in the lung associated with cigarette smoke exposure, V/Q imaging provides a method by which to study the functional consequences of the inflammation and airspace enlargement present under these conditions.

## 4.3 – MATERIALS AND METHODS

**Animals**

Female BALB/c mice (Charles River, QC, Canada) were acclimatized to specific pathogen-free housing conditions for a period of 2-3 weeks, with a 12:12 hour light:dark cycle, prior to experimentation. The studies described here were approved by the Animal Research Ethics Board of McMaster University (Hamilton, ON, Canada) in accordance with the guidelines of the Canadian Council on Animal Care. 'Baseline' and '24 week control' V/Q and CT imaging data were published previously in a related article [16].

**Cigarette smoke exposure protocol**

Mice were exposed to the smoke generated from 12 2R4F reference cigarettes (University of Kentucky, Lexington, KY, USA), with the filters removed, for 50 minutes twice daily, 5 days/week using a SIU48 whole body exposure system (Promech Lab, Vintrie, Sweden) for either 8 or 24 weeks. Details of the exposure protocol were reported previously [17]. Average total particulate matter during exposure was 786μg/L. Control animals were exposed to room air alone. Prior to cigarette smoke exposure animals were acclimatized to the system during a 3-day period. Smoke exposure in this system is well tolerated and results in increased levels of carboxyhaemoglobin and cotinine [17].

**Collection and measurement of specimens**

Mice were sacrificed and BAL was collected approximately 16 hours after the final cigarette smoke exposure. The lungs were removed and lavaged twice with PBS (0.25mL followed by 0.20mL). Total cell counts were determined using a haemocytometer. After centrifugation, cell pellets were resuspended in PBS and slides were prepared by cytocentrifugation (Shandon Inc., Pittsburgh, PA, USA) at 9.66g for 2 min. Hema3 (Fisher Scientific Co., Kalamazoo, MI, USA) was used to stain all slides. Differential counts of BAL cells were determined from at least 500 leukocytes using standard haemocytological procedures to classify the cells as neutrophils, eosinophils, or mononuclear cells. The number of animals in each

group for cellular outcomes was as follows: baseline (5); 8 weeks control (7); 8 weeks CS (8); 24 weeks control (4); 24 weeks CS (7). The left lung lobe was inflated to 30cm pressure using 10% formalin, fixed, sectioned into 4 pieces, and embedded in paraffin; 3-mm thick sections were stained with haematoxylin and eosin (H&E). Images of whole H&E stained lung slices were acquired at 16x magnification and an image resolution of 2560 x 1920 pixels, producing pixels 6.098μm in length, on a Leica DMRA microscope (Leica Microsystems, Wetzlar, Germany). Airspace enlargement was quantified using Pneumometrics (Pneumometrics software V.1, Hamilton, Ontario, Canada); each data-point for an animal represents the average of 4 whole histological slices obtained for the left lung lobe with major airways and blood vessels identified by the user and removed. Briefly, the program converted the histological image to a binary image and separated contiguous airspaces using a step-wise morphological closing operation. The program then automatically measured the dimensions and perimeters of airspaces and provided the total area within a range of airspace sizes. The number of animals in each group for histological outcomes was as follows: baseline (5); 8 weeks control (7); 8 weeks CS (7); 24 weeks control (4); 24 weeks CS (6).

**Imaging protocol**

Imaging was performed as previously described [16]. In brief, mice were tracheally intubated through the oral cavity following anaesthetization with ketamine/xylazine (90mg/kg, 6mg/kg). Animals were then ventilated (0.02L/min, 125 strokes/min) on a Rodent Ventilator (Model 683, Harvard Apparatus, Holliston, MA, USA) with Technegas™ (Cyclomedica, Lucas Heights, NSW, Australia) (0.04-0.12MBq/mL) for 15 minutes. After Technegas™ delivery animals were removed from the ventilator and allowed to breathe freely. SPECT scans were acquired on an X-SPECT system (Gamma Medica, Northridge, CA, USA) using pinhole collimators and a radius of rotation of 3.5cm. A high quality ventilation CT was collected immediately after the SPECT scan, also acquired on the X-SPECT system with x-ray tube characteristics of 75kVp and 220μA. Following ventilation SPECT and CT scans, mice were injected with 11-15MBq of $^{99m}$Tc-MAA via the tail vein. Perfusion imaging entailed a CT and SPECT scan. Supplemental gaseous anaesthesia was used (isoflurane (1%, 1L/min)) to ensure sedation throughout the imaging procedure.

SPECT and CT images were reconstructed, fused, and co-registered as previously described [16]. Calibration of each CT image for Hounsfield Unit (HU) scaling was performed using a water-filled tube included in each scan and air within the field of view but external to the animal. A 'Lung' region of interest (ROI) was produced for the ventilation CT images, as described previously, using Amira 5.1 software (Visage Imaging, Andover, MA, USA). An example of an axial slice of the lung ROI is shown in Figure 4.1A. The perfusion CT and SPECT were fused, with in-house software, by a process that maximized mutual information (MI) by rigid body transformation within the lung region as defined by the lung ROI, as previously described. MI-derived parameters obtained from fusion of the

perfusion SPECT and CT were then applied to the ventilation SPECT and CT. The ventilation and perfusion data sets were then co-registered by repeating the MI maximization process through rigid body transformation of their respective CT images, again within the lung segmentation.

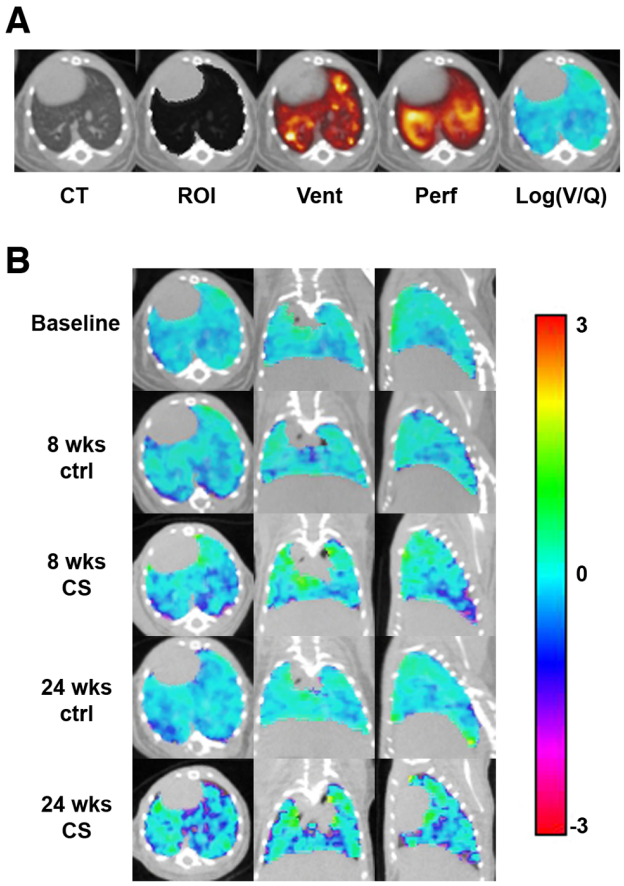


FIGURE 4.1
Representative SPECT and CT images. **A** CT and SPECT axial slice images for an animal at Baseline. **CT** refers to the ventilation-associated CT. **ROI** refers to the lung segmentation seen as a black overlay on the CT. **Vent** and **Perf** refer to V and Q SPECT images with the colour scale increasing from red through yellow to white for both. **Log(V/Q)** refers to the final calculated data. **B** Log(V/Q) images in axial, coronal, and sagittal planes for all experimental time points. The animals shown were chosen based on average standard deviation, mean, and V vs. Q correlation values for the data set. The colour bar indicates the values seen in the associated log(V/Q) images. **CS** denotes cigarette smoke exposed while **Ctrl** denotes age-matched controls.

**Respiratory-gated CT Image Processing & Quantitation**
Inspiratory- and expiratory-gated CT images were produced by applying RespGate software (RespGate, Hamilton, ON, Canada) to all ventilation CT projections [18]. Respiratory-gated images were then reconstructed and calibrated as described for the ungated image used in the V/Q analysis. Lung-associated air volume from respiratory-gated CTs was extracted by a method previously described based on a segmentation of the entire thoracic cavity [16,19]. Functional residual capacity (FRC) and tidal volume (TV) were calculated from these data. To detect emphysematous changes thresholds of -450 and -550HU were employed as these values are indicative of severe alveolar destruction in mouse models with the CT system used in this study [20].

**Quantitative Per-Voxel Image Data Analysis**
Co-registration of images allows for analysis of SPECT and CT data on a per-voxel basis. Within the lung ROI all voxels have a density value (HU), relative ventilation (V) and perfusion (Q) counts, V/Q and a log(V/Q) value (Figure 4.1A); presented data represent mean distributions of all voxels within the lung ROI for each experimental group, unless otherwise stated. V and Q values were converted to relative frequencies by dividing the activity value of each voxel by the total activity in the lung ROI. The relationship between V and Q data was determined by finding Pearson's correlation coefficient for the plot of the relative ventilation vs. perfusion values in each voxel. V/Q ratios were calculated using the relative frequency of both V and Q and a base 10 logarithm was applied to provide a log-normal distribution. Analysis of the log(V/Q) data involved calculation of the mean, standard deviation, and percentage of total lung volume (TLV) greater than ±2 averaged standard deviations from the averaged baseline mean log(V/Q), as a measure of V/Q mismatching; 'low' log(V/Q) henceforth refers to negative values greater than 2 standard deviations from the baseline mean while 'high' log(V/Q) refers to positive values found by the same process. Because of the use of the logarithmic scale any voxel where only V equalled zero was set to a log(V/Q) ratio of $-\infty$ and any voxel where only Q equalled zero was set to a log(V/Q) ratio of $+\infty$; these values were not included in the calculation of the log(V/Q) mean and standard deviation but were included in measures of high and low log(V/Q). Any voxels where both V and Q equalled zero were noted and given a log(V/Q) value of zero. The number of animals in each group for imaging outcomes was as follows: baseline (15); 8 weeks control (4); 8 weeks CS (7); 24 weeks control (6); 24 weeks CS (7).

**Data Analysis**
Data were expressed as the mean±SEM. When comparing age-matched experimental groups statistical significance was determined by unpaired, two-tailed t-test (Graphpad Software Inc, La Jolla, CA, USA). Within an experimental group results were compared between exposure time-points and baseline using a one-way ANOVA with Tukey post-hoc analysis. In addition, two-way ANOVAs were applied to all measurements to test for interaction between smoke exposure and time. $p<0.05$ was considered statistically significant for all tests.

## 4.4 – RESULTS

BALB/c mice were exposed to cigarette smoke, or room air to provide age-matched controls, for a period of 24 weeks. V/Q SPECT/CT images were acquired after 8 and 24 weeks of CS exposure. Visual inspection of log(V/Q) data indicated increased heterogeneity and mismatching over time in the CS exposed groups as compared to their age-matched controls (Figure 4.1B). This mismatching was obvious after 24 weeks, however, no specific patterns of mismatching were observed between animals within the CS exposed groups.

To further evaluate V and Q distributions, their association on a per-voxel basis was examined (Figure 4.2A). Of note, the average V vs. Q distribution at baseline had a proportion of voxels falling on the line of unity, indicating perfectly matched V and Q values. While this situation was largely unchanged in age-matched controls, CS exposed animals eventually lost this feature. As a quantification of these data, the correlation between V and Q, measured by Pearson's coefficient, did not change over time in control groups but was significantly less in CS-exposed groups compared to their age-matched controls at both 8 and 24 weeks (Figure 4.2B). These data indicate that V/Q mismatching caused by CS exposure was present as early as 8 weeks.

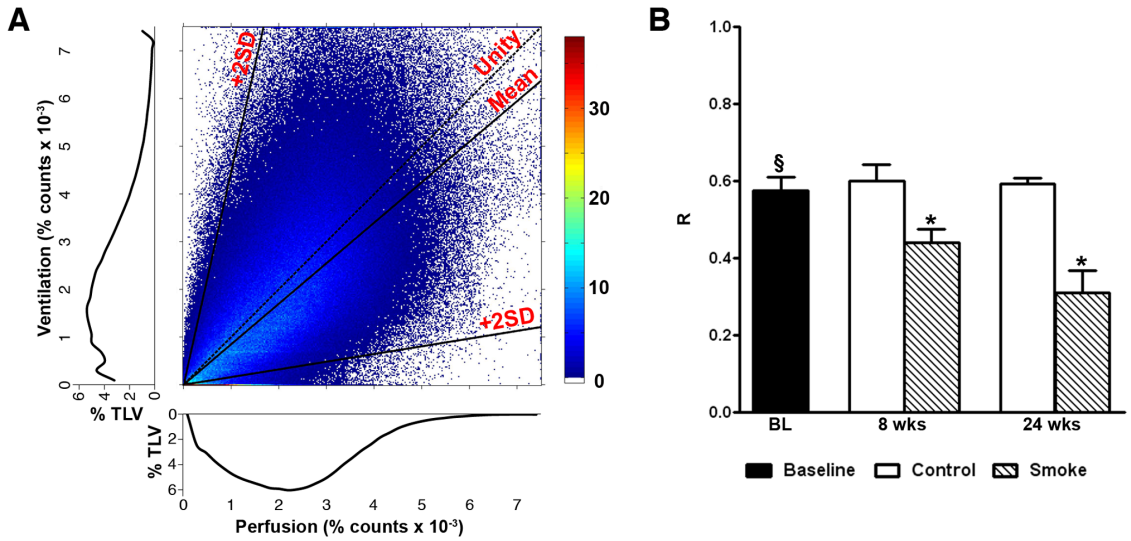


FIGURE 4.2

Relationship of ventilation and perfusion distributions. **A** Baseline V vs. Q scatter plot representing averaged data. The x- and y-axes represent perfusion (Q) and ventilation (V), respectively; each point represents the V and Q value of a single voxel while the scale bar represents the number of stacked voxels. Average baseline distributions for V and Q are shown separately in the axis-associated graphs. A line for V=Q (**Unity**) as well as lines for the mean log(V/Q) (**Mean)** and two standard deviations from the mean (**+2SD)** are shown. **B** Pearson's correlation coefficient (**R**) for assessing the relationship between ventilation and perfusion counts. *p<0.05 vs. age-matched control by two-tailed unpaired t-test. §p<0.05 baseline vs. 24 weeks CS by one-way ANOVA with Tukey post-hoc.

V/Q relationships were further qualified through the distribution of log(V/Q) values where a decrease in the peak and a widening of the curve was apparent with increasing CS exposure (Figure 4.3A). The mean log(V/Q) value of the 24 week CS exposure group was significantly more negative than that at baseline, 8 weeks CS exposure, and age-matched controls at 24 weeks (Figure 4.3B); significant interaction in the mean log(V/Q) was found between time and CS exposure through two-way ANOVA. The standard deviation (SD) of the log(V/Q) distribution, a measure of heterogeneity, demonstrated no significant difference after 8 weeks of CS exposure when compared to baseline and age-matched controls. After 24 weeks of CS exposure, however, a significant increase in SD was found compared to age-matched controls as well as in comparison to baseline and 8 weeks CS exposure. As reported previously [16], the age-matched control group at 24 weeks also demonstrated a significant increase in the SD of log(V/Q) over that of baseline animals (Figure 4.3B). Therefore, while V/Q mismatch is progressive with age there is still a significant increase in mismatching in CS exposed mice over controls at 24 weeks.

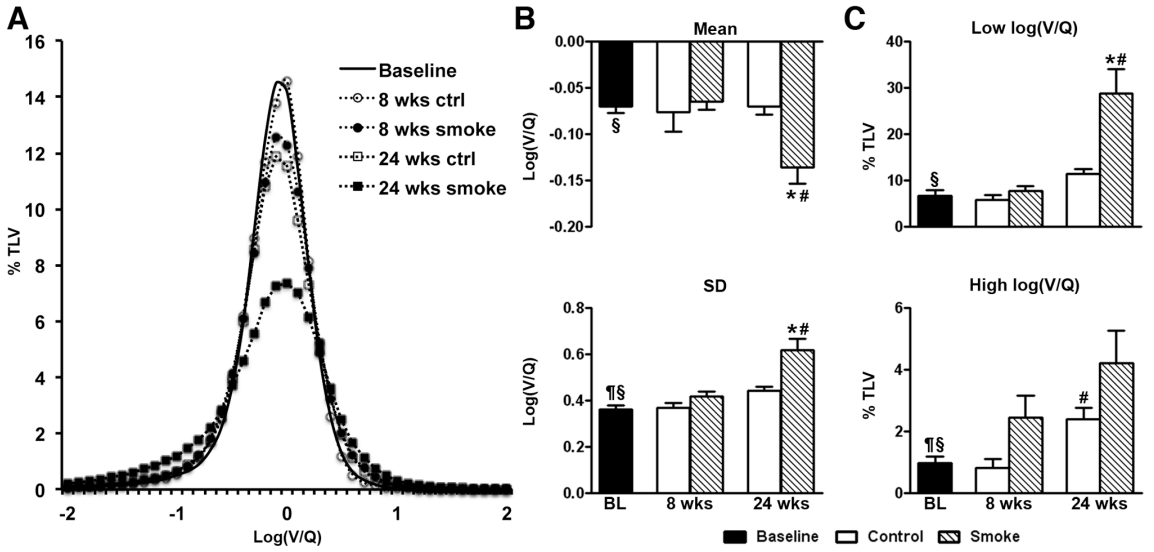


FIGURE 4.3

Log(V/Q) distribution. **A** Volume-standardized distribution of log(V/Q) values measured in percentage of total lung volume (%TLV). Baseline (black), 8 week control (open circles) 8 week CS-exposed (closed circles), 24 week control (open squares), and 24 week CS-exposed (closed squares) are shown. **B** Mean (top) and standard deviation (bottom) of log(V/Q) distributions for all experimental groups, calculated without ±∞ values. **C** Percentage of total lung volume with log(V/Q) mismatching. Mismatching was defined as values greater or less than 2 average standard deviations from the average mean and include voxels where V=0 (-∞) and Q=0 (+∞). *p<0.05 vs. age-matched control by two-tailed unpaired t-test. #p<0.05 vs. 8 weeks by one-way ANOVA with Tukey post-hoc. ¶p<0.05 baseline vs. 24 weeks control by one-way ANOVA with Tukey post-hoc. §p<0.05 baseline vs. 24 weeks CS by one-way ANOVA with Tukey post-hoc.

The percentage of lung volume with low log(V/Q) values, that is reduced ventilation in comparison to perfusion, was substantially increased with 24 weeks of CS exposure over the age-matched control, baseline, and the 8 week CS exposure groups (Figure 4.3C). Further, there was a significant interaction between time and CS exposure in these low log(V/Q) values. The proportion of high log(V/Q) values, or voxels with greater ventilation than perfusion, was increased in both CS exposed mice and the controls at 24 weeks compared to baseline. In this model, the proportion of low log(V/Q) values was much greater than that seen for high log(V/Q) values.

BAL samples were collected to provide insight into the inflammatory environment associated with the V/Q mismatching observed. A significant increase in total leukocyte number in the BAL was found at 8 weeks for mice exposed to CS, compared to controls, and this inflammatory burden remained elevated up to 24 weeks (Figure 4.4). The absolute number of neutrophils was also significantly increased by 8 weeks of CS exposure, compared to age-matched controls, and a further increase in neutrophils was seen after 24 weeks of exposure compared to levels at 8 weeks. The difference between 8 and 24 weeks also reflects a significant interaction between time and CS exposure.

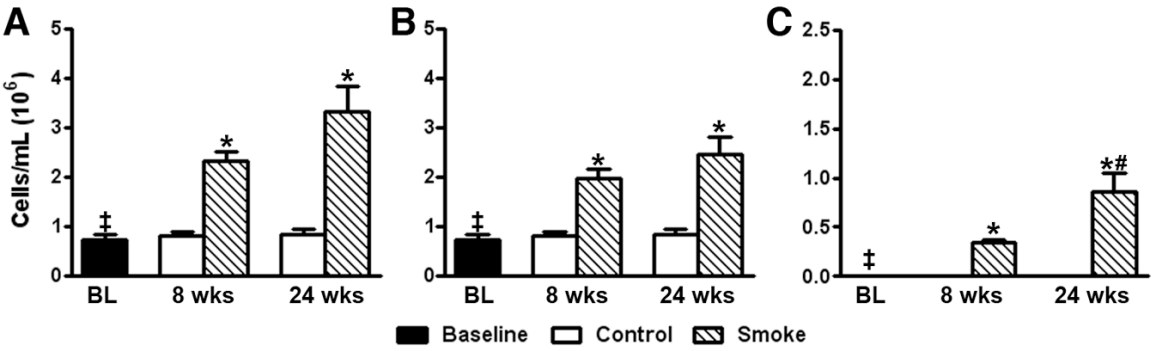


FIGURE 4.4
Inflammatory cell counts from broncho-alveolar lavage (BAL). **A** Total cell number, **B** mononuclear cells, and **C** neutrophils (right) are shown. *p<0.05 vs. age-matched control by two-tailed unpaired t-test. ‡p<0.05 baseline vs. 8 and 24 weeks CS by one-way ANOVA with Tukey post-hoc.

Airspace enlargement was measured in whole histological H&E stained lung slices to determine the structural consequences of CS exposure. Representative histology slices from control and CS exposed groups at 24 weeks depict the overall extent of airspace enlargement (Figure 4.5A). Quantification of all airspaces within the histological images revealed that their size distribution was not Gaussian in nature. Therefore, airspace enlargement was analyzed by plotting the percentage of total airspace area against logarithmic ranges of airspace size to produce a simplified distribution. In animals exposed to 8 weeks of CS the area associated with larger airspaces, between $10^4$ and $10^5 \mu m^2$, was

significantly increased over that of the age-matched controls. Animals exposed to 24 weeks of CS demonstrated a similar increase between $10^4$ and $10^5\mu m^2$ and also showed a significant reciprocal decrease in airspaces between $10^3$ and $10^4\mu m^2$ (Figure 4.5B). Increases in airspace enlargement were also observed in control animals in an age-dependent manner. Therefore, while a degree of airspace enlargement was observed with age alone, exposure to cigarette smoke lead to a significant increase in this pathology at both 8 and 24 weeks.

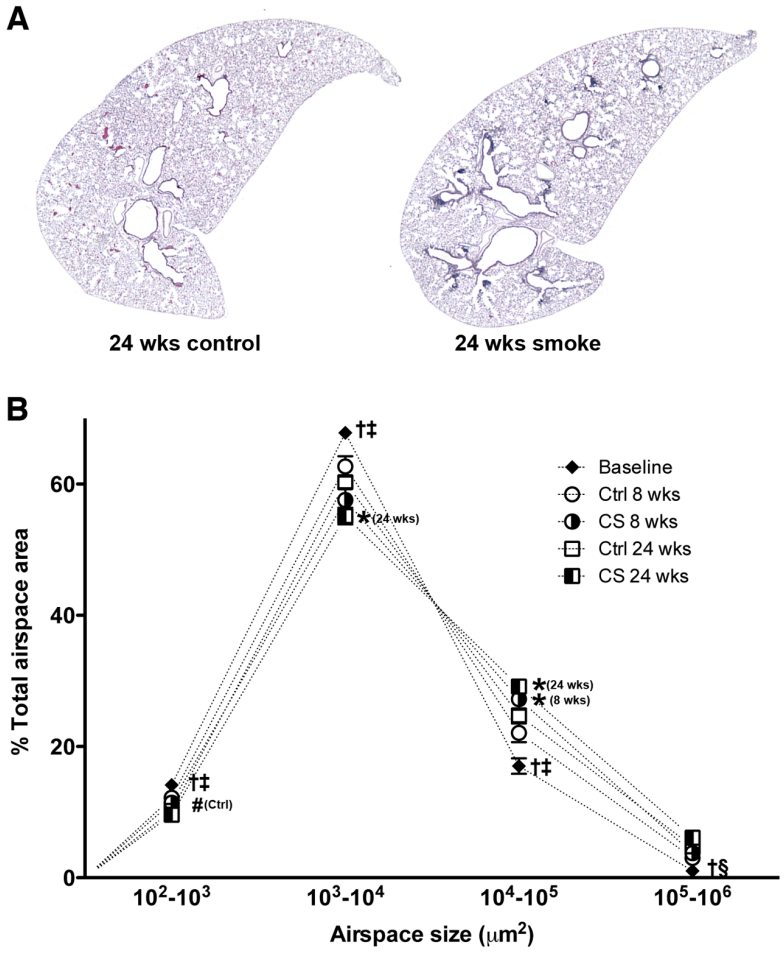


FIGURE 4.5

Assessment of airspace enlargement using quantitative histological analysis. **A** Representative whole lung slices, stained with H&E, for control (left) and CS exposed (right) mice at 24 weeks. **B** Comparison of total airspace area associated with logarithmic airspace size ranges; connected points represent the distribution of airspace area derived from whole-slice histological quantification and averaged across animals. *$p<0.05$ vs. age-matched control by two-tailed unpaired t-test. #$p<0.05$ vs. 8 weeks by one-way ANOVA with Tukey post-hoc. §$p<0.05$ baseline vs. 24 weeks control by one-way ANOVA with Tukey post-hoc. †$p<0.05$ baseline vs. 8 and 24 weeks control by one-way ANOVA with Tukey post-hoc. ‡$p<0.05$ baseline vs. 8 and 24 weeks CS by one-way ANOVA with Tukey post-hoc. Statistical analyses were confined to airspace size ranges. Bracketed terms denote the group to which the statistical mark belongs. Note: Major airways and vessels are removed prior to quantitation.

In contrast, CT densitometry was not different between the 24 week CS exposure and the age-matched control groups (Figure 4.6). Summation of air volumes in the lung yielded no significant differences in FRC or TV between CS exposure groups and their age-matched controls (data not shown); however, a significant increase in FRC was observed between baseline and both controls and CS-exposed mice at 24 weeks. Further, no difference was observed in the frequency of voxels less than -550HU or -400HU (data not shown) between CS exposure groups and their controls indicating no major volumes of emphysema were present.

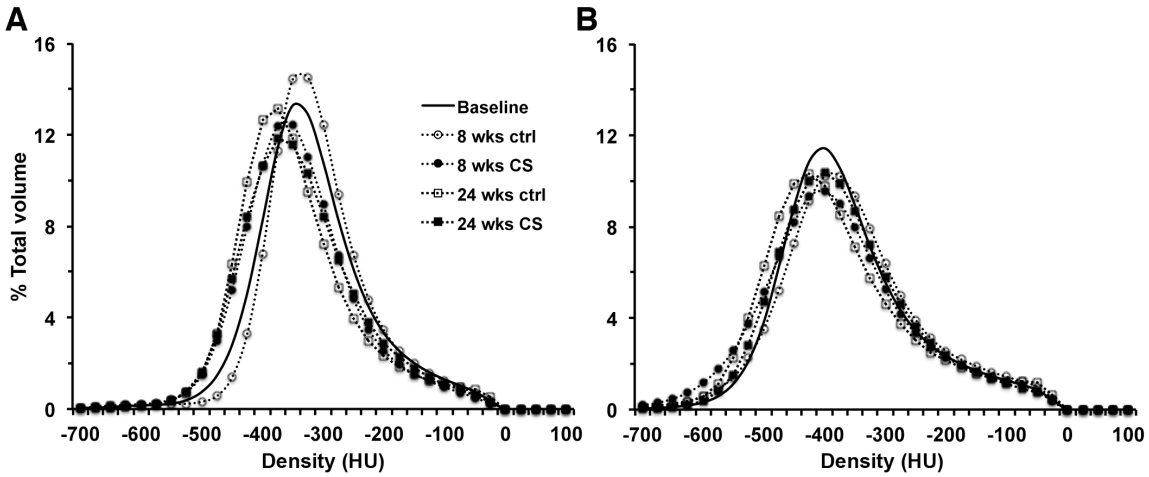


FIGURE 4.6
Respiratory-gated CT Densitometry. Hounsfield unit (HU) density distributions in percent of total volume are shown for **A** end expiratory and **B** end inspiratory breathing states. Baseline (black), 8 week control (open circles), 8 week CS-exposed (closed circles), 24 week control (open squares), and 24 week CS-exposed (closed squares) are shown.

## 4.5 – DISCUSSION

Continuing exposure to cigarette smoke is known to have immunological and structural consequences [6] that eventually lead to a reduction in gas exchange capability. The progression of this lung dysfunction and how the core pulmonary processes of ventilation and perfusion are affected are issues that are not well defined. The ability of this methodology, and other similar 3D methods, to spatially examine the impact of varying pathologies on gas exchange in the lung provides the necessary tools to study complex and chronic diseases such as COPD. Preclinical investigation of ventilation and perfusion in models of COPD will allow for a better understanding of clinical disease progression by providing a translational approach to measurement of these core lung processes.

The approach taken in this study was to determine the impact of sustained cigarette smoke exposure on the lung and the ability to match ventilation to perfusion in this context. Previously in clinical studies, Jogi *et al.* have

demonstrated that V/Q SPECT is sensitive to COPD-related pathologies [13] and Suga *et al.* have quantified the V/Q mismatch due to emphysema in a per-voxel manner [14]. Our results affirm that V/Q methodologies, being functional measurements, are sensitive to early pathological changes leading to COPD that may not be apparent, even at a higher resolution, in anatomical imaging systems such as CT. Since V/Q imaging is a common nuclear medicine technique and SPECT/CT systems are increasingly used [21], V/Q measurement could play an important role in the diagnosis, treatment, and further understanding of COPD [13,22,23].

We have demonstrated that V/Q mismatching progressively increased during cigarette smoke exposure in mice. The SPECT results presented here indicated that low V/Q mismatch predominated over high V/Q mismatch in the lungs of mice exposed to 24 weeks of CS. The CS exposure model caused significant neutrophilia and monocyte infiltration while only a slight increase in airspace enlargement was observed after 24 weeks. The V/Q profile observed in this context is consistent with clinical MIGET data where V/Q mismatch was observed in GOLD stage I [9]. MIGET studies have also provided evidence that high V/Q values tend to be present in patients with emphysematous pathology while low V/Q values tend to be present in patients with greater inflammatory indices and small airway pathology [24,25]. Lower V/Q values have also been observed through positron emission tomography after acute exposure to CS in sheep [26]. The dominance of low V/Q mismatching in our model is therefore most likely associated with airway narrowing and obstruction caused by the increase in lung inflammation.

While the effects of airspace enlargement in this model were small, a significant increase in airspace area was found in the size range between $10^4$ and $10^5 \mu m^2$, indicating that the effect was predominantly associated with larger airspaces in the acinar complex. The impact of age on the lung structure was also apparent between baseline and the control groups at either time-point, as shown in Figure 4.5B. This result lends strength to findings derived from CT images where an increase in volume was observed over baseline values in both CS exposed and control mice but no difference was found between these age-matched groups. Airspace enlargement, as observed in control animals through both CT and histology, was potentially involved in the increase in V/Q heterogeneity, as measured by the standard deviation of the log(V/Q), as these results increased with increasing age in the absence of aberrant immunological processes [16,27].

In addition to airspace enlargement and inflammation, other pathologies associated with COPD likely contribute to V/Q mismatching seen clinically. Inflammatory exudate, small airway remodelling, increased mucus production, and loss of tethering forces could lead to an altered ventilation profile through the closure of small airways. While inflammation and airspace enlargement likely have a role in lung dysfunction, the levels of these pathologies observed in this study may not adequately account for all of the V/Q mismatching detected.

A healthy pulmonary vasculature could adapt blood flow, predominantly through hypoxic vasoconstriction, to provide matched V/Q [28]. This system is impaired in COPD patients [29] and vascular abnormalities have been identified in other models of CS exposure in small animals [30,31].

While murine models may not reflect all of the pathologies associated with COPD at once, they allow the study of individual aspects of disease. Our results indicate that inflammation is likely responsible for some of the V/Q abnormalities observed and that airspace enlargement may have a limited role in this model. Further work in several models of COPD pathologies will be necessary to determine the relative contributions of these pathologies to V/Q mismatching. Since smoking cessation has been shown to reduce some inflammatory parameters [32], the study of smoking cessation in this controlled system will be a necessary step towards confirming the roles of the pathologies observed towards V/Q mismatching, and also to demonstrate the ability of this methodology to investigate therapeutic approaches.

Through a per-voxel analysis of V/Q, this study has demonstrated that chronic exposure to the noxious and particulate components of cigarette smoke is enough to elicit alterations in gas exchange capacity. V/Q mismatching is a sensitive, non-invasive measure of lung dysfunction that can provide insight into many of the pathologies and obstructions that cause COPD. In COPD, and preclinical models thereof, the ability to detect incipient disease is necessary to allow for the investigation of the underlying biological mechanisms. Further, the ability to track progression provides a system in which interventions can be tested. Within this cigarette smoke exposure model V/Q SPECT imaging has proven useful to establish both detection and progression and can be used further in the investigation of treatment options.

## 4.6 – ACKNOWLEDGEMENTS

The authors gratefully thank Dr. Troy H. Farncombe and Chantal Saab for their expertise and contributions towards imaging and Joanna Kasinska for expert technical support; Dr. Karen Gulenchyn and the McMaster Department of Nuclear Medicine, Hamilton Health Sciences (Hamilton, ON, CAN) for use of the Technegas™ system; and the Firestone Institute for Respiratory Health (Hamilton, ON, CAN) for tuition support (BNJ).

## 4.7 – REFERENCES

1. Rabe KF, Hurd S, Anzueto A, Barnes PJ, Buist SA, et al. (2007) Global strategy for the diagnosis, management, and prevention of chronic obstructive pulmonary disease: GOLD executive summary. Am J Respir Crit Care Med 176: 532-555.
2. Lopez AD, Shibuya K, Rao C, Mathers CD, Hansell AL, et al. (2006) Chronic obstructive pulmonary disease: current burden and future projections. Eur Respir J 27: 397-412.

3. Barnes PJ (2008) Immunology of asthma and chronic obstructive pulmonary disease. Nat Rev Immunol 8: 183-192.
4. Hogg JC (2004) Pathophysiology of airflow limitation in chronic obstructive pulmonary disease. Lancet 364: 709-721.
5. Han MK, Agusti A, Calverley PM, Celli BR, Criner G, et al. (2010) Chronic obstructive pulmonary disease phenotypes: the future of COPD. Am J Respir Crit Care Med 182: 598-604.
6. Hogg JC, Timens W (2009) The pathology of chronic obstructive pulmonary disease. Annu Rev Pathol 4: 435-459.
7. Yoon HI, Sin DD (2011) Biomarkers of therapeutic response in patients with chronic obstructive pulmonary disease: a critical review of the literature. Drugs 71: 1821-1837.
8. Rabe KF, Wedzicha JA (2011) Controversies in treatment of chronic obstructive pulmonary disease. Lancet 378: 1038-1047.
9. Rodriguez-Roisin R, Drakulovic M, Rodriguez DA, Roca J, Barbera JA, et al. (2009) Ventilation-perfusion imbalance and chronic obstructive pulmonary disease staging severity. J Appl Physiol 106: 1902-1908.
10. Wagner PD (2008) The multiple inert gas elimination technique (MIGET). Intensive Care Med 34: 994-1001.
11. Roach PJ, Bailey DL, Harris BE (2008) Enhancing lung scintigraphy with single-photon emission computed tomography. Semin Nucl Med 38: 441-449.
12. Petersson J, Sanchez-Crespo A, Rohdin M, Montmerle S, Nyren S, et al. (2004) Physiological evaluation of a new quantitative SPECT method measuring regional ventilation and perfusion. J Appl Physiol 96: 1127-1136.
13. Jogi J, Ekberg M, Jonson B, Bozovic G, Bajc M (2011) Ventilation/perfusion SPECT in chronic obstructive pulmonary disease: an evaluation by reference to symptoms, spirometric lung function and emphysema, as assessed with HRCT. Eur J Nucl Med Mol Imaging 38: 1344-1352.
14. Suga K, Kawakami Y, Koike H, Iwanaga H, Tokuda O, et al. (2010) Lung ventilation-perfusion imbalance in pulmonary emphysema: assessment with automated V/Q quotient SPECT. Ann Nucl Med 24: 269-277.
15. Stevenson CS, Birrell MA (2011) Moving towards a new generation of animal models for asthma and COPD with improved clinical relevance. Pharmacol Ther 130: 93-105.
16. Jobse BN, Rhem RG, McCurry CA, Wang IQ, Labiris NR (2012) Imaging Lung Function in Mice Using SPECT/CT and Per-Voxel Analysis. PLoS One 7: e42187.
17. Botelho FM, Gaschler GJ, Kianpour S, Zavitz CC, Trimble NJ, et al. (2010) Innate immune processes are sufficient for driving cigarette smoke-induced inflammation in mice. Am J Respir Cell Mol Biol 42: 394-403.
18. Farncombe TH (2008) Software-based respiratory gating for small animal conebeam CT. Med Phys 35: 1785-1792.
19. Jobse BN, Johnson JR, Farncombe TH, Labiris R, Walker TD, et al. (2009) Evaluation of allergic lung inflammation by computed tomography in a rat model in vivo. Eur Respir J 33: 1437-1447.

20. Froese AR, Ask K, Labiris R, Farncombe T, Warburton D, et al. (2007) Three-dimensional computed tomography imaging in an animal model of emphysema. Eur Respir J 30: 1082-1089.
21. Mariani G, Bruselli L, Kuwert T, Kim EE, Flotats A, et al. (2010) A review on the clinical uses of SPECT/CT. Eur J Nucl Med Mol Imaging 37: 1959-1985.
22. Bajc M, Neilly JB, Miniati M, Schuemichen C, Meignan M, et al. (2009) EANM guidelines for ventilation/perfusion scintigraphy : Part 1. Pulmonary imaging with ventilation/perfusion single photon emission tomography. Eur J Nucl Med Mol Imaging 36: 1356-1370.
23. King GG, Harris B, Mahadev S (2010) V/Q SPECT: utility for investigation of pulmonary physiology. Semin Nucl Med 40: 467-473.
24. Wagner PD, Dantzker DR, Dueck R, Clausen JL, West JB (1977) Ventilation-perfusion inequality in chronic obstructive pulmonary disease. J Clin Invest 59: 203-216.
25. Barbera JA, Ramirez J, Roca J, Wagner PD, Sanchez-Lloret J, et al. (1990) Lung structure and gas exchange in mild chronic obstructive pulmonary disease. Am Rev Respir Dis 141: 895-901.
26. Schroeder T, Vidal Melo MF, Musch G, Harris RS, Winkler T, et al. (2007) PET imaging of regional 18F-FDG uptake and lung function after cigarette smoke inhalation. J Nucl Med 48: 413-419.
27. Sprung J, Gajic O, Warner DO (2006) Review article: age related alterations in respiratory function - anesthetic considerations. Can J Anaesth 53: 1244-1257.
28. Glenny RW (2009) Determinants of regional ventilation and blood flow in the lung. Intensive Care Med 35: 1833-1842.
29. Vidal Melo MF, Winkler T, Harris RS, Musch G, Greene RE, et al. (2010) Spatial heterogeneity of lung perfusion assessed with (13)N PET as a vascular biomarker in chronic obstructive pulmonary disease. J Nucl Med 51: 57-65.
30. Wright JL, Churg A (2008) Short-term exposure to cigarette smoke induces endothelial dysfunction in small intrapulmonary arteries: analysis using guinea pig precision cut lung slices. J Appl Physiol 104: 1462-1469.
31. Ferrer E, Peinado VI, Diez M, Carrasco JL, Musri MM, et al. (2009) Effects of cigarette smoke on endothelial function of pulmonary arteries in the guinea pig. Respir Res 10: 76.
32. Wen Y, Reid DW, Zhang D, Ward C, Wood-Baker R, et al. (2010) Assessment of airway inflammation using sputum, BAL, and endobronchial biopsies in current and ex-smokers with established COPD. Int J Chron Obstruct Pulmon Dis 5: 327-334.

# CHAPTER 5
# Impact of Inflammation, Emphysema, and Smoking Cessation on V/Q Mismatching in Mouse Models of COPD

## 5.0 – Overview of Chapter 5

The fourth article of this thesis is entitled "Impact of Inflammation, Emphysema, and Smoking Cessation on V/Q Mismatching in Mouse Models of COPD". This work endeavoured to determine how COPD-associated pathologies could impact V/Q and, further, described the effect of smoking cessation. In addition, the data presented in this article represent a refinement of V/Q methodology where mice breathe the ventilation tracer freely instead of the direct ventilation used previously, resulting in a simpler and more efficient delivery.

Inflammation and airspace enlargement were investigated by using severe models of these pathologies. Emphysema was shown to affect V/Q, but only at levels beyond those observed in mice exposed to cigarette smoke. Inflammation also had a role to play in V/Q mismatch, though the distribution may be more important than the overall quantity. Finally, cessation lead to a return of most V/Q measurements to that of controls, providing evidence that the cigarette smoke itself, in addition to the inflammation, are likely important to the V/Q mismatching seen in this model.

These findings demonstrate that V/Q measurements are sensitive to various models, and that the relative role of each type of pathology to lung function could be ascertained with more experimentation. In addition, the data suggest that if lung dysfunction can be detected while it is still reversible, then irreversible structural damage and the associated gas exchange limitation could be avoided. This article also demonstrated how the V/Q SPECT methodology could be used in small animal models to aid in the process of determining the specifics behind gas exchange abnormalities in COPD.

This article has been submitted previously in an alternate format but has yet to be accepted for peer review.

To be submitted for peer review

# Impact of Inflammation, Emphysema, and Smoking Cessation on V/Q Mismatching in Mouse Models of COPD

Brian N. Jobse[1], Cory A.J.R. McCurry[1], Mathieu C. Morrisette[2], Rod G. Rhem[3], Martin R. Stämpfli[2,4], and N. Renée Labiris[3,4]

AFFILIATIONS
[1]Medical Sciences Graduate Program, McMaster University, Hamilton, Canada. [2]Department of Pathology and Molecular Medicine, McMaster Immunology Research Centre, McMaster University; [3]Department of Medicine, Division of Respirology, McMaster University; [4]Firestone Institute for Respiratory Health at St. Joseph's Healthcare, Hamilton, Canada.

CORRESPONDENCE
N.R. Labiris
Department of Medicine
Health Sciences Centre rm. 1V11
McMaster University
1280 Main St. W.
Hamilton, ON
Canada L8S 4K1
Fax: 905-546-1125
E-mail: labir@mcmaster.ca

FINANCIAL SUPPORT
Firestone Institute of Respiratory Health – AstraZeneca Collaboration Unrestricted Grant; The Canadian Institutes of Health Research; N.R. Labiris holds an internal Department of Medicine Career Award.

## 5.1 – ABSTRACT

Chronic obstructive pulmonary disease (COPD) greatly affects ventilation (V) and perfusion (Q) of the lung. Inflammation and emphysema are two predominant COPD-related pathologies that likely impact V/Q. However, there is little direct evidence regarding the roles that these pathologies play in the V/Q mismatch observed in COPD. The impact of cigarette smoking cessation on V/Q mismatching, in the context of established pathology, is also not well understood and requires investigation. Three distinct murine models of COPD were used to investigate the impact of different pathologies on V/Q, as measured by single photon emission computed tomography (SPECT) and computed tomography (CT). Lipopolysaccharide (LPS) was used to produce neutrophilic inflammation, porcine pancreatic elastase (PPE) was used to produce emphysema, and long-term cigarette smoke (CS) exposure and cessation were used to investigate the combination of these pathologies. CS exposure caused significant V/Q mismatch in the context of inflammation and mild airspace enlargement. LPS-induced inflammation also caused V/Q mismatch. Following cessation of CS exposure, inflammatory cell levels returned to those of controls. Similarly, V/Q measures returned to normal after smoking cessation, despite evidence of mild airspace enlargement. However, PPE administration induced robust airspace enlargement that was associated with V/Q mismatching. Both inflammation and airspace enlargement may contribute to V/Q mismatch in COPD. While inflammation-associated V/Q mismatch resolves following smoking cessation, robust emphysematous damage may cause persistent impairment. Early smoking cessation is therefore critical before emphysema progresses to the point where it significantly and irreversibly impacts gas exchange.

## 5.2 – INTRODUCTION

Ventilation (V) and perfusion (Q) are two of the fundamental physiological processes within the lung contributing to gas exchange, and the relationship between these processes is dysfunctional in patients with chronic obstructive pulmonary disease (COPD) [1]. Cigarette smoke (CS) is a primary risk factor for the disease, prolonged exposure to which can lead to airway inflammation, airspace enlargement, and several other pathologies [2]. These pathologies are generally slow to develop and heterogeneous in nature, but ultimately lead to the irreversible airflow limitation that is the hallmark of COPD [3, 4]. Cessation of cigarette smoking is currently one of the only therapies capable of slowing the progression of COPD. Unfortunately, years of cessation are often necessary before improvements to airflow limitation, inflammatory state, infection risk, and cardiovascular comorbidities are seen [5, 6]. To better understand the benefits and limitations of smoking cessation, the impact on ventilation and perfusion requires investigation in the context of the pathologies associated with cigarette smoke exposure.

V/Q relationships in the lung can be measured by several non-invasive methods but, unfortunately, these techniques are not commonly used in clinical practice, aside from the diagnosis of pulmonary embolism; quantification of results, even in clinical research, is rare. Rodríguez-Roisin *et al.* made use of the multiple inert gas elimination technique (MIGET) to quantitatively demonstrate that V/Q is a sensitive measure of the earliest stages of COPD [7]. A more widely available methodology for V/Q can be performed in nuclear medicine departments utilizing single photon emission computed tomography (SPECT) to provide three-dimensional maps of ventilation and perfusion [8, 9]. Jogi *et al.* have shown the ability of this technique to identify early disease, stage disease severity, and even identify comorbid disease [10]. Further, Suga *et al.* have quantified the impact of emphysema on V/Q in the lungs of COPD patients [11].

Modelling aspects of COPD in mice provides the means by which to investigate the individual pathologies that make up this heterogeneous disease [12]. Using a methodology adapted from clinical V/Q SPECT, our laboratory has confirmed the utility of this technique in measuring changes in V/Q with age [13] and in the context of prolonged cigarette smoke exposure (Jobse *et al*., J Nucl Med, accepted for publication 10/10/12). Notably, these results indicated that smoke-induced changes to V/Q are present after 8 weeks of exposure, that V/Q mismatching increases with length of exposure, and that inflammation and minor airspace enlargement are prominent features associated with exposure to cigarette smoke.

Understanding the progression of cigarette smoke-induced pathology and the mechanisms behind V/Q mismatch in COPD-associated pathologies are important steps in furthering the ability to diagnose and treat this widespread and burdensome disease. In the current study, the impact of smoking cessation on V/Q mismatching has been investigated. In addition, the contributions of inflammation and airspace enlargement have been examined, by employing simple models for these pathologies, to provide insight into the dysfunction associated with cigarette smoke exposure. Assessment of the cellular and structural aspects of these pathologies, using both traditional and non-invasive methods, provides a more thorough comprehension of V/Q relationships under disease conditions. Together, these data explore the V/Q relationships associated with COPD.

## 5.3 – MATERIALS AND METHODS

**Animals**

Specific pathogen-free 10-12 week old female BALB/c mice were purchased from Charles River Laboratories (Senneville, QC, Canada). Mice were acclimatized to housing conditions for a period of 2 weeks prior to experimentation. Housing conditions consisted of a 12:12 hour light:dark cycle and unrestricted food and water. The studies described were approved by the Animal Research Ethics Board of McMaster University (Hamilton, ON, Canada) in accordance with the guidelines of the Canadian Council on Animal Care.

**Cigarette smoke exposure protocol**

Mice were exposed to the smoke generated from 12 2R4F reference cigarettes (University of Kentucky, Lexington, KY, USA), with the filters removed, for 50 minutes twice daily, 5 days/week using a SIU48 whole body exposure system (Promech Lab, Vintrie, Sweden). Details of the exposure protocol have been reported previously [14]. Control animals were exposed to room air only. Following 24 weeks of smoke exposure, mice were divided into two groups: one subset continued smoke exposure, while another ceased smoke exposure and was exposed to room air only. Controls continued to receive room air. This treatment continued for 16 weeks beyond the original 24 week exposure for a total protocol length of 40 weeks. Average total particulate matter during exposure was 653μg/L. Smoke exposure in this system is well tolerated and results in increased levels of carboxyhaemoglobin and cotinine [14].

**Lipopolysaccharide exposure protocol**

To model neutrophilic lung inflammation, naïve 26 week old mice were anaesthetized with isoflurane (Baxter, Mississauga, ON, Canada) and 10.5μg of LPS (Sigma-Aldrich, Oakville, ON, Canada) in 35μL of sterile phosphate-buffered saline (PBS) was administered intranasally. Controls received 35μL PBS alone. Animals were imaged 24 hours post LPS exposure and sacrifice occurred immediately after imaging was performed.

**Porcine pancreatic elastase exposure protocol**

Mice were anaesthetized with isoflurane and 4 units of PPE (EPC Inc., Owensville, MO, USA) in 30μL of sterile PBS was administered intranasally. Controls received 30μL PBS alone. After exposure mice were left for a period of 45 days prior to acquisition of data.

**Imaging protocol**

Imaging was performed as previously described [13] with minor modifications. Ketamine/Xylazine (90mg/kg, 6mg/kg) anaesthetized mice freely breathed Technegas™ (Cyclomedica, Lucas Heights, NSW, Australia) (0.04-0.12MBq/mL), from a nose cone within a sealed and HEPA filtered (PALL corp., Missisauga, ON, Canada) acrylic chamber for a period of 15 minutes. Prior to ventilation, oxygen was mixed into the Technegas™ to a level of approximately 20% $O_2$. A

Rodent Ventilator (Model 683, Harvard Apparatus, Holliston, MA, USA) provided flow to the nose cone (0.02L/min, 125 strokes/min). SPECT scans were acquired on an X-SPECT system (Gamma Medica, Northridge, CA, USA) using pinhole collimators and a radius of rotation of 3.5cm. A high quality ventilation CT was collected immediately after the SPECT scan, also acquired on the X-SPECT system with x-ray tube characteristics of 75kVp and 220μA. Following ventilation SPECT and CT scans, mice were injected with 11-15MBq of $^{99m}$Tc-MAA via the tail vein. Perfusion imaging entailed a CT and SPECT scan. Supplemental gaseous anaesthesia was used (isoflurane 1%, 1L/min) to ensure sedation throughout the imaging procedure.

SPECT and CT images were reconstructed, fused, and co-registered as previously described [13]. Calibration of each CT image for Hounsfield Unit (HU) scaling was performed using a water-filled tube included in each scan and air within the field of view but external to the animal. A 'Lung' region of interest (ROI) was produced for the ventilation CT images, as described previously, using Amira 5.1 software (Visage Imaging, Andover, MA, USA). Fusion parameters between SPECT and CT were found for an experimental time-point by use of a phantom of $^{99m}$Tc-pertechnetate in capillary tubes at varying angles to each other. CT and SPECT images were acquired for phantoms, reconstructed as described, and fused by in-house, mutual information (MI) maximizing software. These parameters were then used for both ventilation and perfusion data sets. The V and Q data sets were then co-registered by repeating the MI maximization process through rigid body transformation of their respective CT images within the lung ROI.

**Quantitative Per-Voxel Image Data Analysis**

V and Q values were converted to relative frequencies by dividing the activity value of each voxel by the total activity in the lung ROI and then multiplying by 100. V/Q ratios were calculated using the relative frequency of both V and Q and a base 10 logarithm was applied to provide a log-normal distribution. Analysis of the log(V/Q) data involved calculation of the mean and standard deviation of the distribution. Because of the use of the logarithmic scale any voxel where only V equalled zero was set to a log(V/Q) ratio of $-\infty$ and any voxel where only Q equalled zero was set to a log(V/Q) ratio of $+\infty$; these values were not included in the calculation of the log(V/Q) mean and standard deviation. Any voxels where both V and Q equalled zero were noted and given a log(V/Q) value of zero. To assess emphysema in CT images, volumes of low attenuation (VLA) were calculated by summing the percentage of lung volume less than -400HU, as control animals for the PPE study had less than 1% of volume associated with values beyond this Hounsfield unit threshold.

**Collection and measurement of specimens**

Mice were sacrificed at the experimental endpoints indicated in the results section and bronchoalveolar lavage (BAL) was collected by a method detailed previously (Jobse *et al*., J Nucl Med, accepted for publication 10/10/12). Briefly,

the lungs were removed and lavaged twice with PBS (0.45mL total). Total cell counts were determined by haemocytometer and differential cell counts were determined after cytocentrifugation and staining from at least 500 leukocytes using standard haemocytological procedures to classify the cells as neutrophils, eosinophils, or mononuclear cells.

Measures of airspace enlargement, including airspace area distributions, airspaces per unit area, and the mean area to perimeter ratio, were made by use of Pneumometrics software (Pneumometrics software V.1, Hamilton, Ontario, Canada) from haemotoxylin and eosin (H&E) stained lung histology sections, also by a method described previously (Jobse *et al*., J Nucl Med, accepted for publication 10/10/12); each result for an animal represents the average of 4 histological slices obtained for the left lung lobe with major airways and blood vessels identified by the user and removed. To statistically analyze the distribution of airspace area, the average 75$^{th}$ percentile of control animals at 24 weeks was found (~15000 $\mu m^2$) and used as a threshold to calculate the total percentage of area beyond that value. Bronchoalveolar lavage (BAL) cell counts and the histological airspace area distributions for animals at 24 weeks have been reported previously (Jobse *et al*., J Nucl Med, accepted for publication 10/10/12).

**Data Analysis**

Data were expressed as the mean±SEM. Statistical significance was determined by an unpaired, two-tailed t-test in Prism (Graphpad Software Inc, La Jolla, CA, USA) when comparing age-matched experimental groups. For cessation-related data, a one-way ANOVA with Tukey post-hoc test was performed. $p<0.05$ was considered statistically significant for all statistical tests. The number of mice used in the various outcomes are described in Table 1.

## 5.4 – RESULTS

**Smoke exposure caused V/Q mismatch, inflammation, and airspace enlargement.**

Mice were exposed to CS for 24 weeks to establish the degree of V/Q mismatching and the lung conditions in which mismatching takes place. Exposure to cigarette smoke for a period of 24 weeks elicited significant V/Q mismatching (Figure 5.1A & B) but no density changes were observed in CT images compared to controls (Figure 5.1A). Quantification of log(V/Q) curves yielded a significant decrease in the mean and a significant increase in the standard deviation of the data (Figure 5.1C&D). Analysis of BAL fluid demonstrated that 24 weeks of smoke exposure caused robust inflammation, with a total cell count of 3.3±0.5 $x10^6$ compared to 0.8±0.1 $x10^6$ for controls. Similarly, increases were observed for both mononuclear cells and neutrophils (Figure 5.2A). A shift towards greater airspace size was observed histologically in the distribution of airspace area (Figure 5.2B) and statistically confirmed by quantification of the airspace area beyond the control 75$^{th}$ percentile (data not shown). In addition, a decrease of the number of airspaces per unit area (Figure 5.2C) was seen. Thus, CS exposure caused V/Q mismatch in the context of both inflammation and a small but significant degree of airspace enlargement.

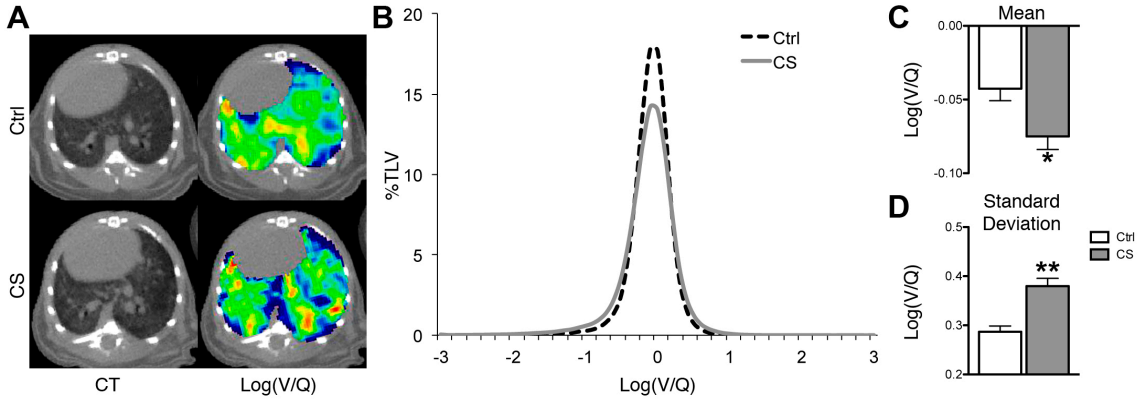


FIGURE 5.1

Impact of 24 weeks smoke exposure on lung function. **A** Representative axial CT (left) and log(V/Q) (right) images for control (top) and cigarette smoke exposed (bottom) animals after 24 weeks. **B** Log(V/Q) distributions for animals at 24 weeks. **E** Average mean log(V/Q) values. **F** Average log(V/Q) standard deviation values. *p<0.05, **p<0.01 by two-tailed t-test compared to age-matched controls.

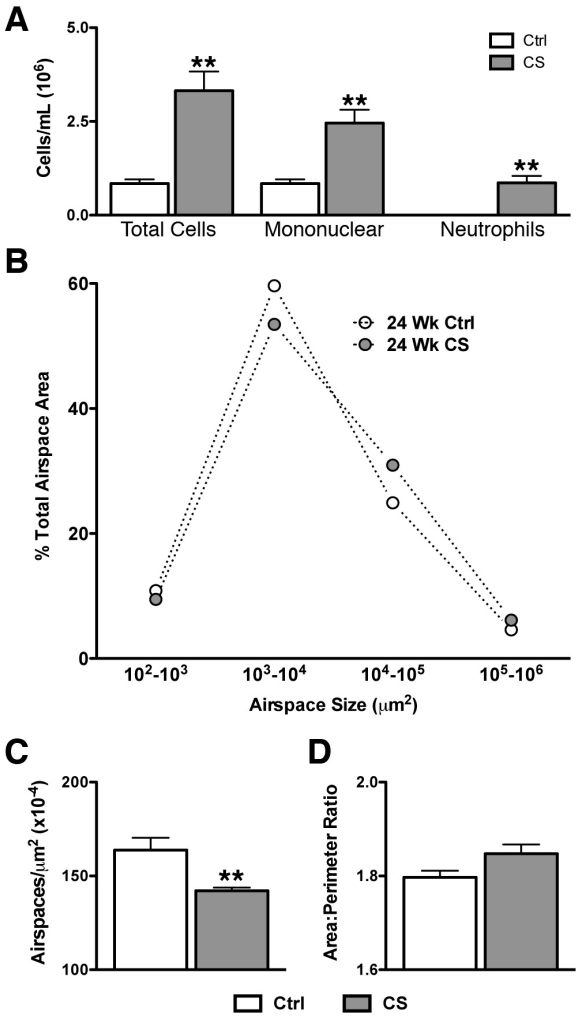


FIGURE 5.2

Inflammation and airspace enlargement after 24 weeks smoke exposure. **A** BAL total cells, mononuclear cells, and neutrophils at 24 weeks. **B** Average airspace area distributions by logarithmic bins of airspace size for 24 weeks, describing whole slice histology. **C** Average airspaces per unit area. **D** Average area to perimeter ratio produced from analysis of whole slice histology at 24. **p<0.01 by two-tailed t-test compared to age-matched controls.

**Inflammation alone caused V/Q mismatch**

The effect of inflammation on V/Q mismatch was investigated by exposing mice to LPS. LPS exposure produced a total cell count of 5.3±0.4 x$10^6$ compared to 0.7±0.1x$10^6$ for control animals; this increase was almost entirely neutrophilic (Figure 5.3). The increased inflammation associated with LPS was also apparent in CT images, as depicted by peribronchial increases in density (Figure 5.4A). The log(V/Q) distribution demonstrated that this inflammation was capable of altering lung function (Figure 5.4B) and significant changes were observed in both the mean and standard deviation of these data (Figure 5.4C&D). Thus, neutrophilic inflammation alone was capable of causing V/Q mismatch.

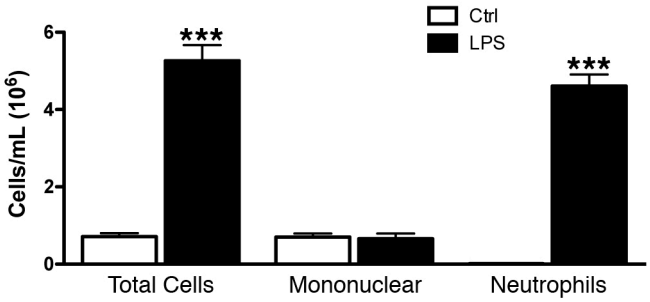


FIGURE 5.3

BAL cell counts for LPS and cigarette smoke exposed groups at 14 weeks. Total cells and the associated number of mononuclear cells and neutrophils are shown. ***p<0.001 by two-tailed t-test compared to age-matched controls.

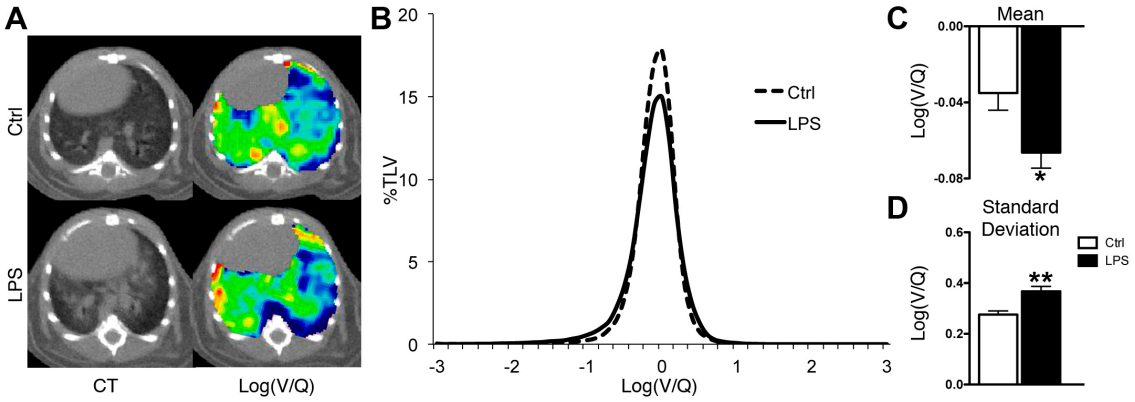


FIGURE 5.4

Functional impact of LPS exposure. **A** Representative axial CT (left) and log(V/Q) (right) images for control (top) and LPS exposed animals. **B** Log(V/Q) distributions. **C** Average mean log(V/Q) values. **D** Average log(V/Q) standard deviation. *p<0.05, **p<0.01 by two-tailed t-test compared to age-matched controls.

**Airspace enlargement alone caused V/Q mismatch**

The role of airspace enlargement in V/Q mismatching was next investigated as a major pathology associated with COPD. To produce airspace enlargement greater than the levels observed after exposure to cigarette smoke, mice were exposed to PPE. Emphysema-like lesions were readily apparent in the CT images (Figure 5.5A). While the control group was described by a bimodal distribution representing air- and tissue-filled regions within the lung segmentation, the PPE group showed a large leftward shift towards lower density values, indicating a greater extent of air within the lung (Figure 5.5B). The lung ROI volume analyzed was significantly greater in PPE-exposed animals than in controls (Figure 5.5C). When the percentage of volume below -400HU was calculated, a threshold describing emphysematous lesions, a significant increase was found in PPE animals (Figure 5.5C) with 21.9±2.4% of the lung volume below -400HU compared to 0.6±0.1% in controls.

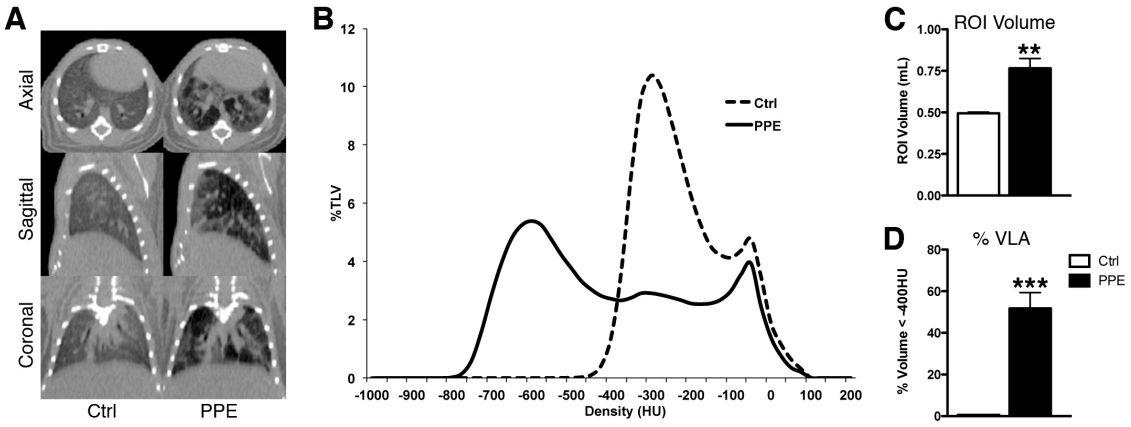


FIGURE 5.5

Density-based analysis of PPE imaging data. **A** Representative axial, sagittal, and coronal CT slices from PPE-exposed and age-matched controls. **B** Average Hounsfield unit (HU) density distributions for control and PPE-exposed groups. **C** Volume of the lung region of interest (ROI). **D** Quantification of percentage of volume with density values less than -400HU, A.K.A. percentage volume of low attenuation (%VLA), signifying severe airspace enlargement. **p<0.01, ***p<0.001 by two-tailed t-test compared to age-matched controls.

Log(V/Q) measurements were affected by the altered lung structure produced by PPE exposure, though no consistent pattern was observed relating emphysematous lesions to mismatched V/Q (Figure 5.6A). A broadening of the log(V/Q) distribution was seen (Figure 5.6B) and was further described by a significant decrease in the mean and an increase in the standard deviation (Figure 5.6C&D). No difference was observed in BAL inflammatory levels between control and PPE exposed mice at the experimental endpoint (data not shown). Therefore, emphysematous lesions were capable of producing V/Q mismatch, which appeared to be distributed throughout the lung.

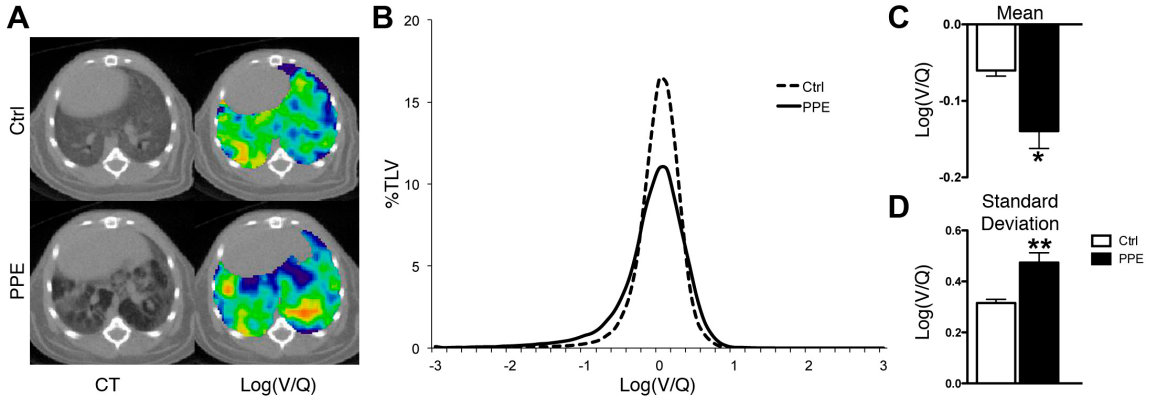


FIGURE 5.6
PPE-induced damage and V/Q mismatch. **A** Representative axial CT (top) and log(V/Q) (bottom) images for control (left) and PPE exposed (right) animals. **B** Log(V/Q) distributions for animals 45 days after PPE exposure. **C** Average mean log(V/Q) values. **D** Average log(V/Q) standard deviation values following PPE exposure. *p<0.05, **p<0.01, by two-tailed t-test compared to age-matched controls.

**Cigarette smoke cessation resolved V/Q mismatch**

Cessation of cigarette smoke exposure was next examined to determine the relative roles of inflammation and airspace enlargement to the V/Q mismatching observed after 24 weeks of exposure. Following 16 weeks of cessation, significant decreases were observed in the BAL total cell count, as well as within the mononuclear and neutrophil compartments, bringing these levels back to those observed in controls (Figure 5.7A). However, the lungs of smoking cessation animals still showed evidence of bronchial associated lymphoid tissue (Figure 5.7B); these immune structures were present after 24 weeks of smoke exposure and did not resolve over this period of cessation. Histological analysis of airspace enlargement demonstrated that continuing smoke and cessation groups had similar airspace area distribution profiles (Figure 5.7C). The percentage of area above the control 75$^{th}$ percentile was significantly increased in both of these groups compared to controls (data not shown). Similarly, the decrease in the number of airspaces per unit area (Figure 5.7D), and an increase in the area to perimeter ratio (Figure 5.7E), confirmed that the airspace enlargement seen at 24 weeks was still apparent after 16 weeks of cessation.

There was no discernible difference in log(V/Q) distributions between control animals and those that stopped smoking after 24 weeks of cigarette smoke exposure while continuing smokers maintained the altered log(V/Q) distribution (Figure 5.8A&B). With smoking cessation a significant increase of the mean log(V/Q) value, from -0.08±0.01 after 24 weeks smoke exposure to -0.03±0.01 after 16 weeks of smoking cessation, and a significant decrease of the standard deviation of these data, from 0.38±0.02 to 0.33±0.02 after cessation, was observed. Thus, cessation for 16 weeks returned V/Q mismatching back to control values.

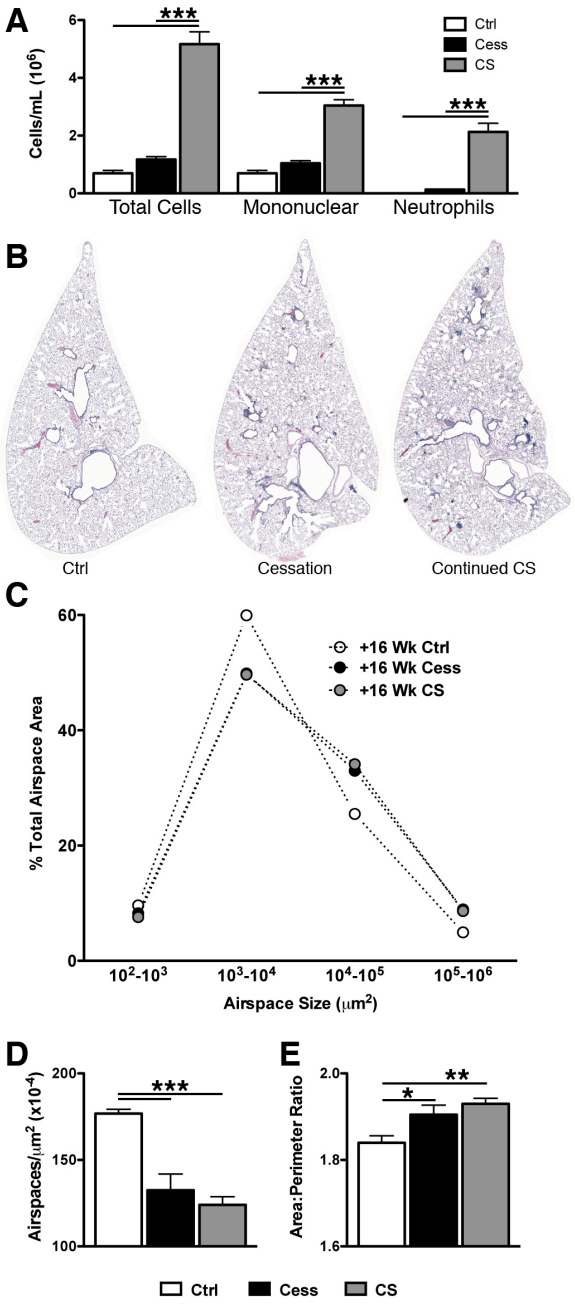


FIGURE 5.7
Inflammation and airspace enlargement after 16 weeks cessation. **A** BAL total cells, mononuclear cells, and neutrophils at 16 weeks post 24 week smoke exposure. ***p<0.001 by one-way ANOVA with Tukey post-hoc. **B** Representative, H&E stained, whole slice histology from a control (left), cessation (middle), and continuing smokers at the +16 week time-point. **C** Average airspace area distributions by logarithmic bins of airspace, describing whole slice histology. **D** Average airspaces per unit area and **E** average area to perimeter ratio produced from analysis of whole slice histology. *p<0.05, **p<0.01, ***p<0.001 by one-way ANOVA with Tukey post-hoc.

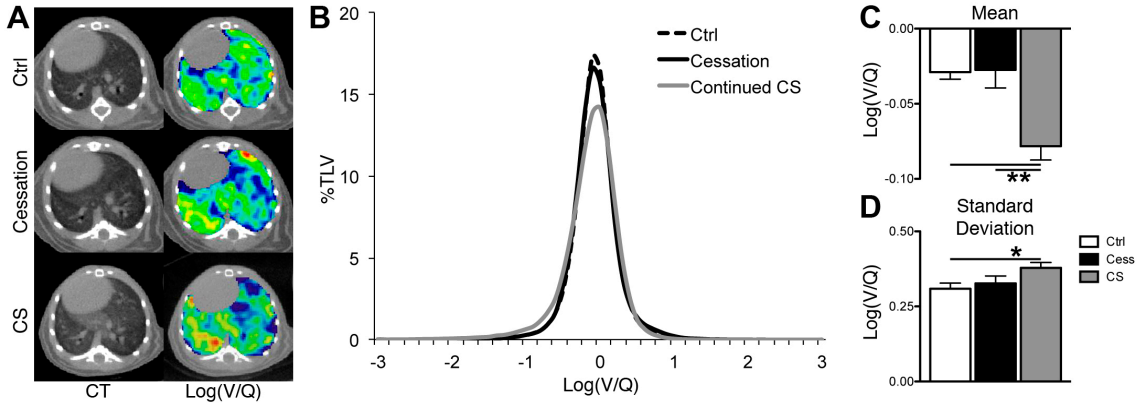


FIGURE 5.8
Impact of 16 weeks cessation on lung function. **A** Representative axial CT (left) and log(V/Q) (right) images for control (top), cessation (middle), and continuing cigarette smoke exposed (bottom) animals after 24 weeks. **B** Log(V/Q) distributions for animals at +16 weeks. **E** Average mean log(V/Q) values. **F** Average log(V/Q) standard deviation values. *p<0.05, **p<0.01 by one-way ANOVA with Tukey post-hoc.

TABLE 5.1
Subject numbers used in experimentation

| Experiment | Group | Imaging | BAL | Histology |
|---|---|---|---|---|
| 24 weeks smoke exposure | Control | 5 | 4 | 4 |
| | Smoke | 12 | 7 | 6 |
| 40 weeks smoke exposure | Control | 4 | 7 | 7 |
| | Cessation | 4 | 4 | 4 |
| | Smoke | 7 | 7 | 7 |
| LPS exposure | Control | 4 | 5 | n/a |
| | LPS | 5 | 4 | n/a |
| PPE exposure | Control | 4 | n/a | n/a |
| | PPE | 4 | n/a | n/a |

## 5.5 – DISCUSSION

Ventilation and perfusion of the lung can both be compromised in COPD, and the capability of matching these processes dysregulated. The objective of the current study was to investigate the V/Q perturbations associated with two of the major pathologies associated with COPD using mouse models of neutrophilic inflammation and emphysema. Further, the impact of smoking cessation was described and evidence gathered regarding the relative roles of inflammation and airspace enlargement in V/Q mismatching.

The mouse models employed in the studies presented were relatively simple in nature to allow for effective interpretation of results. These models, utilizing LPS, PPE, and cigarette smoke, are all well-established and the impact of these exposures on resistance to airflow, the immune system, and other aspects of the lung have been reviewed previously [12]. Investigation of V/Q relationships in these models adds to the understanding of the consequences of pathological disruption on the potential for gas exchange. The LPS and PPE models, causing inflammation and airspace enlargement, respectively, were used as examples of severe pathology, so the V/Q mismatching observed was not surprising. Cigarette smoke, on the other hand, caused less pronounced inflammation and only subtle airspace enlargement but nevertheless caused V/Q mismatching similar to that observed in the other models employed.

We found that smoking cessation resulted in a return to normal lung function, as measured by V/Q relationships, and decreased inflammation. However, it has been established that other pathological markers, such as bronchial-associated lymphoid tissue, remain after smoking cessation [15]. Likewise, the airspace enlargement present after 24 weeks of cigarette smoke exposure persisted after smoking cessation, but these emphysematous lesions caused by cigarette smoke exposure were mild compared to elastase induced airspace enlargement and likely did not contribute to V/Q mismatch. However, if airspace enlargement were to continue, V/Q mismatch and impaired gas exchange would eventually ensue, indicating that smoking cessation in human patients is critical before emphysematous lesions are present; at this stage the V/Q mismatch from inflammation could resolve leaving the gas exchange capabilities of the lung largely intact.

Work by Suga *et al.* has begun to explore the V/Q relationships in COPD patients with advanced emphysema [11] but our results suggest that changes in V/Q may not be apparent, due to airspace enlargement alone, until this pathology has progressed substantially. The relationship between volumes of low x-ray attenuation and V/Q was not apparent in the comparison of log(V/Q) images to CT images in PPE-exposed animals. This warrants further investigation and V/Q SPECT/CT provides the necessary tools to address this concern. It is now understood that emphysema progression continues after smoking cessation [16, 17], so development of methods that can be used clinically to track and understand this pathology are paramount.

The impact of inflammation on V/Q status is also an important topic that is not yet well understood. While LPS caused a greater inflammatory reaction than cigarette smoke, as observed in both BAL measurements and CT images, it did not elicit a V/Q disturbance greater than that of cigarette smoke. It is likely that the distribution of this inflammation is an important factor, especially as it pertains to the small airways. As airflow resistance is inversely proportionate to the radius of the airway to the fourth power, as described by Poiseuille's equation, even slight changes in the lumen of small airways could alter the distribution of ventilation and impact V/Q relationships. Investigations by Gaschler *et al.* into this topic demonstrated that mucus secretion is not present within the small airways after 8 weeks of cigarette smoke exposure [18], but there is thickening of the epithelial layer [19]. V/Q mismatching is present after 8 weeks smoke exposure in this model (Jobse *et al.*, J Nucl Med, accepted for publication 10/10/12), but further investigation into the mechanisms by which inflammation could affect airflow in this manner is required. While LPS-derived inflammation caused V/Q mismatch, likely through airflow obstruction, it is important to note that cigarette smoke contains additional components, such as nitric oxide, that could interfere with vascular mechanisms, such as hypoxic vasoconstriction, leading to inadequate matching of perfusion to ventilation [20, 21]. Thus, the V/Q mismatch observed in this model of cigarette smoke exposure is likely dependent on both inflammation and an alteration in perfusion, though greater investigation is still necessary.

In comparison to clinical findings, our data are consistent with those previously reported by Rodríguez-Roisin *et al.* where V/Q was shown to be sensitive to GOLD stage I and that mismatching increased with GOLD staging severity (77). The authors also provided evidence that the V/Q abnormalities seen in GOLD stage I were associated with smaller airways, alveolar airspaces, and small blood vessels. Our data suggests that inflammation could play a large role in the V/Q mismatching observed in early COPD, while other pathologies, such as emphysema and small airway fibrosis, become a principal cause of V/Q mismatching in the later stages of COPD.

The pulmonary processes of ventilation and perfusion are both affected by long-term exposure to cigarette smoke. Cessation of cigarette smoking results in a return of V/Q assessed lung function to normal, but the pathological consequences of continued exposure eventually lead to structural damage and functional impairment. It is possible that these pathologies could be detected early with the aid of V/Q methods and cessation initiated before major damage permanently alters pulmonary lung function. While models of COPD cannot reproduce the disease itself in entirety, they allow research to address both the pathogenesis of the disease and the constituent pathologies therein. Spatial methodologies utilizing V/Q, especially those coupled to anatomical imaging methods, can provide information not accessible by other means. The ability to translate knowledge of lung structure and function garnered in preclinical

models to that seen in clinical disease could provide better diagnosis, treatment, and understanding of chronic respiratory diseases such as COPD.

## 5.6 – ACKNOWLEDGEMENTS

The authors gratefully thank Dr. T.H. Farncombe and C. Saab for their expertise and contributions towards imaging and J. Kasinska for expert technical support; Dr. K. Gulenchyn and the McMaster Department of Nuclear Medicine, Hamilton Health Sciences (Hamilton, ON, CAN) for use of the Technegas™ system; and the Firestone Institute for Respiratory Health (St. Joseph's Healthcare, Hamilton, ON, CAN) for tuition support (BNJ).

## 5.7 – REFERENCES

1. Wagner PD, Dantzker DR, Dueck R, Clausen JL, West JB (1977) Ventilation-perfusion inequality in chronic obstructive pulmonary disease. J Clin Invest 59: 203-216.
2. Rabe KF, Hurd S, Anzueto A, Barnes PJ, Buist SA, et al. (2007) Global strategy for the diagnosis, management, and prevention of chronic obstructive pulmonary disease: GOLD executive summary. Am J Respir Crit Care Med 176: 532-555.
3. Hogg JC, Timens W (2009) The pathology of chronic obstructive pulmonary disease. Annu Rev Pathol 4: 435-459.
4. Han MK, Agusti A, Calverley PM, Celli BR, Criner G, et al. (2010) Chronic obstructive pulmonary disease phenotypes: the future of COPD. Am J Respir Crit Care Med 182: 598-604.
5. Godtfredsen NS, Prescott E (2011) Benefits of smoking cessation with focus on cardiovascular and respiratory comorbidities. Clin Respir J 5: 187-194.
6. Decramer M, Janssens W, Miravitlles M (2012) Chronic obstructive pulmonary disease. Lancet 379: 1341-1351.
7. Rodriguez-Roisin R, Drakulovic M, Rodriguez DA, Roca J, Barbera JA, et al. (2009) Ventilation-perfusion imbalance and chronic obstructive pulmonary disease staging severity. J Appl Physiol 106: 1902-1908.
8. Roach PJ, Bailey DL, Harris BE (2008) Enhancing lung scintigraphy with single-photon emission computed tomography. Semin Nucl Med 38: 441-449.
9. King GG, Harris B, Mahadev S (2010) V/Q SPECT: utility for investigation of pulmonary physiology. Semin Nucl Med 40: 467-473.
10. Jogi J, Ekberg M, Jonson B, Bozovic G, Bajc M (2011) Ventilation/perfusion SPECT in chronic obstructive pulmonary disease: an evaluation by reference to symptoms, spirometric lung function and emphysema, as assessed with HRCT. Eur J Nucl Med Mol Imaging 38: 1344-1352.
11. Suga K, Kawakami Y, Koike H, Iwanaga H, Tokuda O, et al. (2010) Lung ventilation-perfusion imbalance in pulmonary emphysema: assessment with automated V/Q quotient SPECT. Ann Nucl Med 24: 269-277.
12. Stevenson CS, Birrell MA (2011) Moving towards a new generation of animal models for asthma and COPD with improved clinical relevance. Pharmacol Ther 130: 93-105.

13. Jobse BN, Rhem RG, McCurry CA, Wang IQ, Labiris NR (2012) Imaging Lung Function in Mice Using SPECT/CT and Per-Voxel Analysis. PLoS One 7: e42187.
14. Botelho FM, Gaschler GJ, Kianpour S, Zavitz CC, Trimble NJ, et al. (2010) Innate immune processes are sufficient for driving cigarette smoke-induced inflammation in mice. Am J Respir Cell Mol Biol 42: 394-403.
15. Braber S, Henricks PA, Nijkamp FP, Kraneveld AD, Folkerts G (2010) Inflammatory changes in the airways of mice caused by cigarette smoke exposure are only partially reversed after smoking cessation. Respir Res 11: 99.
16. Miller M, Cho JY, Pham A, Friedman PJ, Ramsdell J, et al. (2011) Persistent airway inflammation and emphysema progression on CT scan in ex-smokers observed for 4 years. Chest 139: 1380-1387.
17. Kirby M, Mathew L, Wheatley A, Santyr GE, McCormack DG, et al. (2010) Chronic obstructive pulmonary disease: longitudinal hyperpolarized (3)He MR imaging. Radiology 256: 280-289.
18. Gaschler GJ, Zavitz CC, Bauer CM, Stampfli MR (2010) Mechanisms of clearance of nontypeable Haemophilus influenzae from cigarette smoke-exposed mouse lungs. Eur Respir J 36: 1131-1142.
19. Gaschler GJ, Skrtic M, Zavitz CC, Lindahl M, Onnervik PO, et al. (2009) Bacteria challenge in smoke-exposed mice exacerbates inflammation and skews the inflammatory profile. Am J Respir Crit Care Med 179: 666-675.
20. Wright JL, Churg A (2008) Short-term exposure to cigarette smoke induces endothelial dysfunction in small intrapulmonary arteries: analysis using guinea pig precision cut lung slices. J Appl Physiol 104: 1462-1469.
21. Ferrer E, Peinado VI, Diez M, Carrasco JL, Musri MM, et al. (2009) Effects of cigarette smoke on endothelial function of pulmonary arteries in the guinea pig. Respir Res 10: 76.

# Chapter 6
# Discussion and Conclusion

### 6.00 – Overview of Work Completed

The collected works of this thesis represent novel advances in, or uses of non-invasive imaging methodologies to characterize and investigate the lung in the context of chronic disease pathologies. Progress in the understanding of lung densitometry, as presented in Chapter 2, provided a better understanding of the distribution and severity of allergic inflammation. Importantly, this research also required the development and validation of segmentation procedures, to produce lung or thoracic regions of interest, that were of further use in later experimentation. The V/Q methodology, as described in Chapter 3, provided all of the necessary techniques and many measurement options to allow investigation into the functional consequences of disease pathologies in the lung. The information in Chapter 4 then described the functional consequences of prolonged smoke exposure and compared these functional measurements to both CT densitometry and standard biological sampling approaches. Finally, the mechanisms underlying the V/Q mismatching observed after cigarette smoke exposure was investigated using two models of COPD pathologies and smoking cessation as a treatment. These data, as described in Chapter 5, demonstrated that different pathologies can cause V/Q mismatching and suggested possible mechanisms for the lung dysfunction observed after exposure to cigarette smoke. In addition to insight gained for the specific pathologies under investigation, these works are examples of the steps necessary to bring quantitative imaging to the forefront of disease research. The research described demonstrates that V/Q imaging is a sensitive tool that could be used both clinically and preclinically to study how obstructive lung disease impacts gas exchange capability in the lung.

## Section 6.1 – Contributions to Academic Research

### 6.10 – Summary of Technical Advances

While the primary goal of this work was to gain insight into diseases such as asthma and COPD using noninvasive functional and anatomical imaging, technical advances were necessary and represent a large part of the work completed. One of these advances was the development of protocols to appropriately segment CT images so that the lung tissue could be analyzed appropriately. In the case of a healthy lung environment this is not especially difficult due to the density differences between the largely air-filled alveolar tissues and the surrounding tissues. However, in heavily inflamed lungs, such as those seen after HDM exposure, these density differences may not be apparent. Using a standardized approach to segmentation, with specific thresholds applied across an experimental data set, a protocol was found that defined the lungs well with as little user intervention as possible. The first topic introduced in Chapter 2 was a validation of this protocol against a simpler thoracic segmentation.

Because the thoracic segment includes many tissues not directly associated with the lung, high-density regions cannot be analyzed from this region of interest. By experimental design, baseline data gathered for the HDM exposed animals allowed for comparison of thoracic-derived data to lung-derived data, thus validating the approach used and allowing for the rest of the measurements described in Chapter 2.

Thoracic segmentations were also used to analyze respiratory-gated images. Because the respiratory gating was applied post-acquisition, these images were not always of as high a quality as non-gated images due to the loss of projections not associated with either inspiratory or expiratory lung states. These images still contained valuable information, so thoracic segments were made and a relatively simple calculation applied to the resultant histograms to extract the volume of air contained in the thoracic region of interest. Both end expiratory air volume, or functional residual capacity, and the tidal volume of the breathing pattern can be accurately approximated using this technique. The results of this method were reported at the end of Chapter 2, and continued to be an important measure of lung function for subsequent work.

A major technical advance is the V/Q methodology described in Chapter 3. As this work describes the first quantitative application of both ventilation and perfusion imaging in a murine model, all of the underlying aspects of the methodology had to be developed. Much of the technique itself had already been established in the laboratory when I began work on the project, though practical limits of Technegas$^{TM}$ and $^{99m}$TC-MAA activities were introduced, as well as development of standardized operating procedures and quality assurance criteria allowing for better interpretation of data and so that technical difficulties could be overcome. Collection of the V/Q data, however, represents only the beginning of the methodology necessary to quantitatively assess the resultant images. The fusion of SPECT to CT images required refinement, the co-registration of CT images was made more streamlined and accurate, and protocols to ensure all data were appropriately handled were developed.

Importantly, the per-voxel measurement outcomes of the V/Q analysis needed to be developed and validated. Many measurements were introduced, some being more useful than others, and a core set of measurements that described the V/Q data established. These included, but were not limited to, the mean and standard deviation of the log(V/Q) data, the correlation of ventilation to perfusion, and the summation of mismatched voxels. These measurements are each important for different reasons. The mean and standard deviation of the log(V/Q) data describe the centre and heterogeneity of the distribution while the summation of mismatched voxels describes the amount of lung volume outside of what is considered normal in controls. The graphical plotting of ventilation values to their associated perfusion values, for which the Pearson's correlation coefficient is a simple measure, is a distinct method of describing the data that provides the opportunity to discriminate between the combinations of values that lead to the

V/Q ratios observed in the log(V/Q) distribution. Each measurement investigated required the development of program code, which was unfailingly written by Rodney Rhem. This program would then be used in the testing of the measure on a single data set, the application to an entire experimental data-set, and the statistical analysis necessary to interpret the results. For some measurements, this procedure was reiterated numerous times to provide the most efficient and accurate results possible. In addition, processing and analysis of the ventilation data produced by oral cannulation of the trachea and direct ventilation hinted that this technique might have limits dependent on the pathological state of the lung. For example, a trend toward fewer radioactive counts was found with increased length of cigarette smoke exposure. While this issue was not a problem for the experimental systems employed up to that point in time, it was necessary to evaluate other possibilities for ventilation so that investigation of severe lung pathologies would be possible. As such, equipment was adapted so that animals could freely breathe the Technegas™ from a nose cone. Fortunately, this change in technique was simpler than intubation and resulted in better delivery of Technegas™ to the lung, even under severe pathological conditions.

All of these methodological developments represent steps that were required to allow for the appropriate collection and interpretation of data from disease models. Without this work, none of the insight into pathological processes would be possible. As such, the time and effort involved in producing the more technical advances was integral to all results described.

Other developments were small but necessary to interpret V/Q data. For example, it was found that tracheal deposition of Technegas™ occurred in some images, and so the protocol for CT-derived lung segmentation was altered to exclude the major airways situated outside of the lung tissue itself. Other small alterations were made as well, though they mainly functioned to ensure data were consistent and standardized. For example, voxels with no ventilation or no perfusion, or both, had to be addressed separately from the rest of the data, due to the quotient involved and the need to logarithmically transform data.

## 6.11 – Knowledge of Allergic Inflammation

The work presented in Chapter 2 was primarily concerned with characterizing and understanding the distribution and temporal qualities of allergic inflammation. The previous understanding of HDM-induced inflammatory models was based on BAL and histological sections of the lung. BAL cell counting is useful in that it provides measures pertaining to the extent of inflammation and the types of inflammatory cells present. Histological sections provide some cellular information, if desired, but are most useful in describing the distribution of inflammation. As both of these methods are invasive and terminal, it was unknown if the *ex vivo* data reflected the inflammatory state *in vivo*.

CT imaging, on its own, is not capable of distinguishing cell types, or the difference between cellular and oedematous inflammatory infiltrates, but it is capable of describing the distribution and extent of inflammation *in vivo*. These characteristics of the inflammatory response to repeated HDM exposures were observed *in vivo*. In addition, the same animals were imaged at multiple time-points, providing information regarding the timing of allergic inflammatory events. This was especially useful because of the experimental design, which included an allergen dose-response, thus providing a better understanding of the temporal reaction to different levels of allergenic insult. Also, it was found that cellular findings from BAL do not accurately represent the overall inflammatory state of the lung, at least as BAL pertains to inflammation measured by CT in this model. While good accordance was found between the inflammatory distribution in histological sections and density changes in CT images, the CT methodology complements the biological sampling, and in some ways goes beyond it, due to its noninvasive nature and the ability to easily quantify the entire lung.

This work demonstrated that CT was well suited to quantify allergic inflammatory changes within the lungs of small animals. This method of noninvasively assessing the inflammatory status of the lung provided information not accessible by standard biological sampling procedures and has provided a better understanding of the model employed and the abilities of CT to detect and characterize inflammation. Imaging methods such as CT are now being used more often to study allergic airway disease clinically [52]. Murine models of allergic airway inflammation and remodelling, and their assessment by imaging methodologies, provide a translational tool to investigate disease processes and interventions.

### 6.12 – Understanding of V/Q in Aging

The proof-of-concept contained within the V/Q methodology, described in Chapter 3, aimed to evaluate the effects of aging on lung function. Mice that were six months apart in age were evaluated with V/Q imaging to determine if the preclinical techniques developed were sensitive to the aging process. This decline in V/Q matching is well established in humans [146,147] so the study of its effect on small animals was novel from a modelling perspective. The decline in lung function observed was small, but statistically significant.

To further highlight the abilities of volumetric imaging, the data were regionalized to demonstrate that three-dimensional V/Q images offer greater analysis opportunities than other, more standard lung function tests such as those measuring airway resistance. Lung function measured by airway resistance and lung function measured by V/Q are not comparable, but as airway resistance measures are the gold standard in human clinical practice and research it was necessary to demonstrate that additional insight could be gained from imaging methods. Of particular note, the regionalization of aged mice demonstrated that the V/Q mismatch was greater toward the peripheral edges of the lung. The gradient distribution of perfusion was known previously [148], but

the impact of aging on both ventilation and perfusion on this gradient was a novel finding. V/Q imaging, therefore, provided a functional assessment of the lung that was not possible by spirometric means. Overall, this proof-of-concept study utilized the research opportunities intrinsic to volumetric imaging to provide novel findings and confirmed that the murine lung is physiologically similar to the human lung, and as such makes a good model for further investigations of perturbations to the physiological systems therein.

### 6.13 – Characterization of V/Q during Cigarette Smoke Exposure

The study of lung function during long-term cigarette smoke exposure was undertaken so as to establish the effects of smoke on ventilation and perfusion in a controlled system. Other V/Q methods, namely the $^{13}N_2$ PET washout technique, had been used in larger animal models of acute smoke exposure [48], but no assessment had been made in murine models and no long-term characterization of V/Q under the influence of cigarette smoke existed.

As such, the work presented in Chapter 4 filled a void in small animal imaging, as this was the first assessment of V/Q in a murine cigarette smoke exposure model, and provided an in depth look into the effects of prolonged smoke exposure on lung function. In addition, this study was one of only a few published studies in small animals taken out to 6 months of smoke exposure. These long-term models are relevant to the study of cigarette smoke as it takes time for some smoke-related pathologies to begin. To complement the V/Q findings, cellular and morphometric histological analyses were conducted to better depict the environment in which V/Q mismatching was occurring. The histological analysis of airspace enlargement requires specific note as a novel program was produced within our laboratory and validated, in part, with the long-term smoke exposure data. This means of airspace quantification provided much more information than standard mean linear intercept measurements, and demonstrated that airspace enlargement is present after smoke exposure, albeit to a low degree. In addition to the small degree of airspace enlargement and inflammation observed, this research demonstrated that V/Q mismatching takes time to develop, but is present after 8 weeks of smoke exposure and progresses with greater length of exposure up to the 24 weeks studied.

While the work presented in Chapter 3 is primarily a characterization, it added to a field scarce in studies, both in regards to length of cigarette smoke exposure and to V/Q analysis thereof. This research has shown that cigarette smoke exposure causes V/Q mismatching and that quantification of this mismatch is potentially a valuable tool for investigating the pathogenesis of COPD-related pathologies. Further, the multiple experimental time-points included and the inclusion of multiple biological outcomes provided a large amount of information on this important model of COPD, and as such acted as a foundation for further investigation into this complex disease. As Rodríguez-Roisin *et al.*, using MIGET [149], and Jogi *et al.*, using SPECT [101], have already shown that V/Q methodologies are sensitive to COPD it stands to reason that further

volumetric V/Q studies, performed with methodologies such as SPECT, will add considerably to our understanding of the pathogenesis and progression of COPD. The use of murine V/Q studies to complement those performed clinically could add substantially to this better understanding of COPD.

### 6.14 – V/Q Investigation into COPD-associated Pathologies and Cessation

With the characterization of long-term smoke exposure complete and the associated V/Q related dysfunction established, effort was made to better understand the pathologies present in this model and how these pathologies could affect V/Q. To accomplish this, three separate models were employed. PPE was used to produce emphysema, LPS was used to produce robust neutrophilic inflammation, and smoking cessation was used to determine how these pathologies affected V/Q within the lung in the absence of cigarette smoke. Furthermore, the cessation model has clinical relevance in regards to the expected outcome of cessation on V/Q mismatching, a topic that has not yet been well studied. This research also begins the work of explaining how V/Q relates to different pathologies in the lung, information that has yet to be definitively established.

The results of the research presented in Chapter 5 demonstrated that both inflammation and emphysema, when present in sufficient quantity, cause V/Q mismatch. However, the mismatching observed after cigarette smoke exposure is likely reliant on the inflammation present, but not on the small degree of airspace enlargement. Cessation of smoke exposure allowed V/Q values to return to normal in the presence of mild pathological changes, indicating that it is crucial for those smokers predisposed to development of pathology to stop smoking prior to the lung dysfunction diagnosed by standard spirometric means. The study of V/Q relationships in each of the three experimental models used was a novel aspect of this research, but the results, when taken together, provide a better understanding of what causes V/Q mismatching during cigarette smoke exposure. Also, this work represents the first step towards understanding the complex interplay between pathologies in human patients. Volumetric quantification of V/Q in COPD patients has only just begun [102], but much more effort will be required before a full understanding of these clinical measurements can be attained. In particular, the study of these models established that both inflammation and emphysema could cause V/Q mismatch, but also that the relative levels of these pathologies and their distribution had an effect.

Importantly, the results of the PPE and LPS experiments provide insight into the results of the cessation data. As cessation is currently one of the only reliable treatments for COPD patients, an understanding of the core pulmonary processes of ventilation and perfusion in this context is required so that the benefits and limitations of this intervention are fully delineated. Cessation is of great clinical benefit to COPD patients as it reduces symptoms and limits the progression of lung function impairment. Our results indicate that much of the improvement in

gas exchange capability would be attributable to the resolution of inflammation. While further work is necessary to elucidate the specific details, the study presented provided valuable information and demonstrated the usefulness of pre-clinical V/Q measurement in understanding lung function in COPD.

## Section 6.2 – Limitations

### 6.20 – Methodological Limitations

The methods employed in the experimentation described are subject to various limitations that must be considered. Resolution is perhaps the most important consideration in all of the studies conducted. While resolution is commonly thought of as the pixel (or voxel) size of an image, it actually denotes the ability to distinguish two objects as being separate. In our research, this ability is important in differentiating between airways, parenchyma, blood vessels, and inflammation. The data for the HDM studies in BN rats was only slightly limited by resolution because the CT equipment employed produced high-resolution images and rats have relatively large lungs. Even here, however, it should be noted that these images do not have the resolution necessary to image alveolar structure. As such, most voxels represent an average of the tissue contained within; this is known as a partial volume effect [57]. Mice have alveolar structure that is comparable in size to rats, so the same considerations apply and are made more limiting by the relative size of the mouse lung. Effectively, this means that a threshold of altered densities in a particular volume must be met before a discernible difference appears between treatment and control animals. It is therefore not possible to detect low-level pathologies within the CT images acquired in the experiments described. For example, CT was not able to detect the mild airspace enlargement found histologically in Chapter 4.

Resolution is also a consideration, and likely a limitation, of the data derived from V/Q imaging. The intrinsic resolution of SPECT systems is less than that of CT systems due to the number of photons collected, the presence of scatter, and the reconstruction algorithms employed. This situation means that greater SPECT resolution could potentially lead to even greater V/Q sensitivity to pathology. It should be noted, however, that the SPECT machinery used, including the pinhole collimators, has spatial resolution only slightly less than other models currently available [150,151,152] and that our techniques already appear to be quite sensitive to pathology. In addition, due to the different resolutions of CT and SPECT it is difficult to infer the density of a particular V/Q value without robust density differences. For example, the voxel sizes for SPECT and CT commonly used in Chapters 2 through 5 differ by a factor of two: CT voxels were 0.115mm per side while SPECT voxels were 0.23mm per side. In a three-dimensional matrix this difference translates into a factor of eight, meaning each SPECT voxel has 8 associated CT voxels. While comparison of SPECT and CT data on the voxel level was not a primary goal of this work, and this

limitation is present in the clinical arena as well, it was a limitation that restrained the findings possible.

Another complication to the resolution of images is the presence of motion artifacts produced in live animals. In anaesthetized animals motion artifacts are due to heart movement, and, more importantly, movement associated with breathing. Images can be gated on the respiratory cycle, either during acquisition or post-acquisition to help limit the effects of respiratory motion. A post-acquisition respiratory gating procedure was used routinely in the analysis of CT data, but V/Q SPECT images could not be gated without greater numbers of projections or an acquisition-based gating system [153]. Both of these solutions would have lead to much longer imaging times that would potentially be detrimental to animal health and would lower the throughput of imaging studies. As such, the V/Q data presented represent the average V/Q over the respiratory cycle.

A difference between clinical and preclinical V/Q imaging that should be discussed was the delivery of Technegas™. Technegas™ is delivered to human patients in one to three breath holds [154], but this is obviously not possible in mice. Instead, mice were ventilated with Technegas™ while tracheally intubated and directly attached to a small animal ventilator that mimicked normal breathing rate and volume. Later, this technique was refined, as described briefly in Chapter 5, by having animals inhale Technegas™ freely from a nose cone. This change was beneficial to animal welfare, experimental complexity, and to the amount of radioactivity delivered to the lungs. However, with either of these delivery techniques ventilation scans do not represent breath-hold delivery as performed in human patients but are the average distribution of the ventilation tracer over the delivery period.

A further limitation in the V/Q methodology employed that must be noted is the fact that ventilation and perfusion data are gathered in series. This is also true in clinical V/Q scans utilizing Technegas™ and $^{99m}$Tc-MAA as the ventilation image must be acquired before administration of the same radioisotope during the perfusion phase. As such, these scans are sequential and do not reflect the precise state of V/Q at any one time. While the perfusion distribution itself represents a single pass of the pulmonary structure, it is acquired at a different point in time from the ventilation distribution. However, it is unlikely that large changes in perfusion take place between the acquisitions of the two SPECT scans while the animal is anaesthetized, a period of approximately 20 minutes. In addition, any changes that do occur are not likely to be larger in scale than the resolution of the SPECT system, meaning these changes will not be detected in the final product.

The rigid-body transformation used in the co-registration of ventilation and perfusion data is another technical issue. Because animals were only lightly sedated and the injection of $^{99m}$Tc-MAA was required between V and Q data

acquisition, a small amount of movement in the position of the animal is almost certain. This was not a problem in the majority of cases, but the relatively non-rigid nature of a biological organism such as a mouse caused instances where rigid transformation of data was not sufficient to properly align the data sets. This was only a limitation insofar as the exclusion of data sets that could not be acceptably co-registered lessened the number of animals in study groups and potentially impacted the results of the statistical analysis. While a non-rigid transformation would be ideal in this situation, more research and development in needed to add this aspect to the V/Q methodology.

Finally, radiation dose is an important aspect of both CT and SPECT imaging. Considerations and arguments regarding radiation dose were made for CT in chapter 2 and for SPECT/CT in chapter 3. While the absorbed dose the animals is minimal, it is possible that low-dose ionizing radiation has some immune modulatory effects, even at levels that do not cause observable damage [155,156,157]. Ultimately, the experimental control groups must act as controls for radiation exposure as well. Controls in all of the described studies were imaged in parallel to experimental animals allowing for interpretation of results. Furthermore, no pathological outcomes were observed in any control animals, indicating the radiation doses employed had no effect or, more likely, effects small enough not to impact the experimental design.

### 6.21 – Experimental Limitations

The experimental data described within the chapters of this thesis contain various limitations, though interpretation of results was always conducted with these limitations in mind. The limitations encountered were either due to experimental design or extenuating circumstances.

Noninvasive methods, such as those described in this thesis, allow for the potential of repeated measures from animals. Unfortunately, a worldwide medical radioisotope shortage resulted in an inability to gather data easily, in turn resulting in a lack of baseline data for many of the V/Q experiments. This situation is only a limitation in that greater insight could have been achieved if the same subjects could have been studied throughout the protocols.

It is also important to note that experimental readouts have differing sensitivity and comparison of these readouts in this context is not necessarily simple. Generally, additional experiments were run for a particular outcome and results added when statistical confirmation was required but, nevertheless, caution in the comparison of vastly different outcomes, E.G., BAL cell counts and density measurements by CT, is required.

## Section 6.3 – Future Directions

### 6.30 – Overview of Possibilities

Due to the variety of models used in pulmonary research and the general lack of pulmonary imaging research that has been conducted preclinically to date, the possibilities for further research are numerous. Both asthma and COPD research would benefit from further studies using the tools and methods developed for the articles described in Chapters 2 through 5. The V/Q method could be employed in the HDM model, the link between V/Q and pathology could be further explored, bacterial or viral induced exacerbations of the smoke-exposed lung could be investigated, and data could be described on a regional basis. Each of these situations will be discussed further and are likely the best options for continued research in this field with the tools now available. In several of these cases, preliminary data has been gathered in our laboratory but further research would add considerably to the understanding of lung function in disease. In addition, certain technical advances would serve to make the V/Q methodology even more robust. Further work in this field has the potential to determine the short- and long-term functional impact of inflammatory episodes on the lung and provide additional tools and information on the use of V/Q methodologies both preclinically and clinically.

### 6.31 – Comparison of V/Q data to other functional outcomes

It is an important consideration to compare V/Q measures to other functional outcomes, and these comparisons have yet to be well characterized. To date, preliminary work measuring blood oxygenation in smoke, influenza, and LPS models has been completed and pressure-volume relationships in the lung have been briefly investigated in a subset of smoking V/Q mice. Ideally, however, collection of V/Q, blood oxygen saturation, and mechanical airway resistance measures would take place in the same animals. A model of emphysema, such as that produced by administration of PPE, would be advantageous for this purpose as CT can easily quantify this pathology throughout the lung. A study of this nature would allow for direct comparison of the mechanical airway resistance, gas exchange potential as measured by V/Q, and gas exchange success as measured by oxygen saturation within the same animals with the same pathological conditions. This work would also help to relate V/Q measures to the more standard clinical readout of spirometry. Relationships between spirometric readings and V/Q do appear in the clinical literature [101], and V/Q SPECT measurements have been previously validated against the multiple inert gas elimination technique [97], but no V/Q comparison to similar measures has been accomplished preclinically. Therefore, the addition of alternate lung function readouts could add substantially to the understanding and interpretation of future work.

### 6.32 – Further Research in the HDM-induced allergic airway model

Further research in the HDM model, using either BN rats or BALB/c mice, would likely involve the collection of V/Q data. There is clinical evidence that the chronic inflammation and exacerbations of asthma lead to increased V/Q mismatching and decreased gas exchange. This could be confirmed in the HDM model and the mechanisms of V/Q mismatch, such as inflammation and airway remodelling, could be investigated in detail. While a preliminary experiment has taken place in an inflammatory setting using the HDM model in BN rats, further investigation is required before any conclusions can be drawn. The experimental design would favour an exacerbatory setting, wherein the animals would be sensitized to HDM, then allowed to rest for a period of time to allow inflammation to subside, and finally re-exposed to the allergen to create the exacerbation. Additionally, the same type of setting could be employed after the initiation of airway remodelling, possible with a 5 week HDM exposure protocol, to determine what impact this pathology has on V/Q mismatching.

Of note, the V/Q values associated with regions of robust inflammation should be elucidated. These volumes containing dense inflammation should either have matched V/Q as perfusion will be reduced to match the ventilation, or these volumes of inflammation could have a low V/Q value due to a lack of ventilation but normal or increased levels of perfusion to allow faster trafficking of immune cells. Either way, this relationship is not currently known and requires investigation.

Further, the impact of therapeutic intervention could be investigated once the models of HDM exacerbation have been characterized by V/Q. This research should determine the impact of a corticosteroid, a bronchodilator, and the combination thereof to provide data on the current gold standard therapies. Characterization of novel therapeutics could then commence.

### 6.33 – Further Research into COPD-related Pathologies

Similar to the characterization of the V/Q values associated with allergic inflammation, research into the values associated with neutrophilic inflammation and emphysema is needed to determine the impact of these pathologies on gas exchange capability. The distribution of inflammation is likely a key aspect of how inflammation affects V/Q in the lung, so various methods of eliciting inflammation, should be investigated. Dose responses of these options would likely be necessary to understand the overall impact on gas exchange. The actual V/Q values associated with regions of inflammation could also be investigated in these models, again, likely resulting in normal or low V/Q scores due to the aforementioned reasons. On the other hand, V/Q values associated with regions of emphysema should be normal or high. These volumes would have little perfusion capacity due to the destruction of the capillary beds, but if they have any ventilation capacity then a high V/Q would result. If both ventilation and perfusion capacities are destroyed then a V/Q of 1 would be obtained. A preliminary look at this characterization is possible through the PPE data

presented in Chapter 5, but the sample size is too small to determine these relationships with confidence. A dose response with PPE would be useful in confirming the results described in Chapter 5, and would also allow for a determination of V/Q score in relation to lesion size and equipment resolution.

Pathologies related to COPD, other than inflammation and emphysema, could be investigated by developing models or borrowing expertise from other laboratories. However, it is possible that some pathology cannot be appropriately reproduced or can only be reproduced with longer exposure to cigarette smoke. Whether small airway fibrosis occurs in a mouse model of cigarette smoke exposure is currently unknown, though profibrotic mediators have been shown to be present in the small airways of mice after 6 months [126]. Longer protocols may be required and could be introduced to determine if this pathology develops with time. After development of this fibrosis, cessation could be instituted to determine the relative impact of the fibrosis in the absence of inflammation, so long as the impact of emphysema was well understood. Unfortunately, protocols longer than those employed in the articles contained in this thesis are not generally feasible in a small animal research environment, so options capable of inducing pathology similar to smoke-induced small airway fibrosis should be investigated.

### 6.34 – Viral or Bacterial-induced Exacerbations of the Smoke Exposed Lung

Pathogens such as viruses and bacteria are known to cause exacerbations in COPD patients that lead to reduced lung function and hospitalization [26,158]. There is also evidence to suggest that these infections could play a role in the progression of the disease [159]. The cigarette smoke exposure model could be used in conjunction with a repeated infection scenario to investigate whether lower respiratory tract infections are capable of impacting the progression of disease. To accomplish this, mice could be cigarette smoke exposed and infectious agents delivered. V/Q scanning would take place at baseline and after every subsequent infection has resolved to determine the total impact of these infections on the progression of cigarette smoke-related disease. An experiment of this nature has been carried out in our laboratory, but further refinement of the experimental approach would be of benefit to the understanding of the interaction between cigarette smoke exposure and bacterial exacerbation on lung function and gas exchange.

Another investigation regarding the combination of smoke exposure and infection would involve influenza virus. Preliminary data in our laboratory indicated that while influenza infection alone caused only minor V/Q mismatching, influenza infection in the context of cigarette smoke causes severe V/Q mismatching. One option would be to investigate this relationship after only a short period of cigarette smoke exposure to determine if the increased inflammation, caused by the synergy between the responses to virus and cigarette smoke, is the driving force behind the V/Q mismatched observed at the later time-point used in the earlier study. However, it is also clear, as described

briefly in Chapter 5, that several pathologies associated with cigarette smoke exposure do not resolve following cessation, indicating that the immune response in the lung has been fundamentally altered. As such, the impact of influenza infection on V/Q mismatching could also be investigated after a period of cessation to determine whether it is the skewed immune response that is responsible for the gas exchange dysfunction observed previously.

### 6.35 – Regionalization of V/Q Data

In Chapters 2 and 3, several methods were used to describe the location of inflammation or V/Q mismatch, respectively. In Chapter 2, the amount of inflammation was described for each slice of the lung from apex to base and density thresholds applied to aid in the visual localization of inflammation. In Chapter 3, the V/Q mismatch associated with aging was localized to the periphery of the lung as compared to the core volume. Further regionalization techniques are a likely avenue of future work as they allow for analysis of data in ways that contribute significantly to the understanding of the disease processes being studied. The simplest concept for furthering our understanding of V/Q is to assess regions of intense inflammation or emphysema to determine their contribution towards V/Q in the whole lung.

A much more elaborate regionalization would be able to determine the path that air takes from trachea to alveoli, and similar information for the pulmonary vasculature but from heart to capillary bed and back again. With this information the data acquired could be analyzed in any manner desired. For example, the effects of inflammation along an airway on V/Q could be described for the alveolar units subsidiary to that airway. Alternately, with the ability to divide the lung into distinct lobes, an exposure or treatment such as PPE could be administered to a single lobe. This would likely require a rat model and the use of a bronchoscope to allow direction of exposure to be known. Once the model is established, regionalization could determine the effect of the pathology on the lobe in question as well as its neighbours to help determine the structure/function relationships at play.

### 6.36 – Potential Technical Advances in the V/Q Methodology

Within Chapter 5, a technical advance was made wherein Technegas™ was delivered by nose cone instead of direct intubation, increasing the levels of radioactivity delivered and causing fewer complications in the animals. Other technical advances are possible to increase the sensitivity of the data acquired and to aid in the processing and analysis of the data. Some of these options include the respiratory gating of SPECT data, utilizing non-rigid transformation in the co-registration of data sets, and utilizing different radioisotopes so as to scan for ventilation and perfusion simultaneously.

Similar to respiratory gating employed for anatomical images, gating of SPECT images provides a more accurate picture of gas radioisotope deposition. Unlike the post-acquisition respiratory gating utilized within this thesis, SPECT gating

would need to be performed during image acquisition due to the limited number of projections acquired. This technique has been argued as being of benefit to clinical research and would allow for collection of V/Q data without a respiratory motion artifact [160]. Furthermore, co-registration with respiratory-gated CT images would provide a greater ability to compare voxel densities with V/Q values to better understand how the structure of the lung affects its function.

Currently, a non-rigid transformation of CT data sets is employed to co-register ventilation and perfusion data sets. While this process was generally successful in aligning the V and Q data, it would sometimes fail due to even slight movements of an animal or a different breathing pattern between scans. Non-rigid transformation could overcome these issues by allowing one data set to be manipulated so as to fit the other. This process would first be performed on the CT images, where anatomical features are in great supply and the program has many landmarks. Once aligned, the fused SPECT data would be manipulated with the same parameters to provide a final co-registered data set. While computationally more complex and resource intensive than rigid transformation, this advance could increase accuracy of the data analyzed and reduce the number of V/Q scans acquired where quantitative analysis is impossible due to lack of proper co-registration.

Another method by which to improve the V/Q methodology would be dual isotope acquisition. Currently, $^{99m}$Technetium is used for both ventilation and perfusion scans, and therefore these processes must be imaged consecutively in series. If a different radioisotope was used for each process they could be scanned for simultaneously, cutting down on the length of the procedure and effectively eliminating the need for a separate co-registration process. As Technegas™ requires $^{99m}$Tc and this ventilation tracer is particularly useful for delivery to mice, a previously described option for a different perfusion radioisotope is $^{113m}$Indium [161]. It is possible to accomplish dual isotope scanning as different radioisotopes emit photons with distinct energy patterns. By choosing two isotopes with differing photon energies and with software to allow for discrimination of these different energies the SPECT system could allow for dual isotope scanning of V/Q. This advance would also mean that ventilation and perfusion distributions would be traced much closer in time to one another than is currently possible. However, it is unlikely that the benefits of dual isotope V/Q imaging in mice, in comparison to the current single isotope version, outweigh the costs of implementing this procedure.

Some of the possible advances to the V/Q methodology, such as non-rigid transformation, should be adopted simply to improve the current data acquisition abilities. Others, such as dual isotope scanning or respiratory gating of SPECT images, would be highly advantageous but would require significant time and resources to institute. Overall, the current techniques employed to acquire V/Q data are quite adequate, but there is always room for improvement.

## Section 6.4 – Conclusions

### 6.40 – Relevance of work completed

Investigation of chronic respiratory diseases is necessary to better understand the pathogenesis of pulmonary impairment and to provide therapeutic strategies for their management. Three-dimensional imaging modalities hold great potential for the continued characterization of these diseases in the spatial manner in which they form. However, qualitative assessments of diagnostic images, the current standard practice in this field, are not adequate in resolving small heterogeneous changes. Even large changes could benefit from quantitative analysis to allow for accurate assessment and the ability to determine the degree of disease without the aid of a radiologist or nuclear medicine physician.

Quantitative measurement of the lung by 3D imaging methods is therefore an extremely important future goal for medical science. While quantitation of images is becoming more frequent, little has been done to standardize data appropriately, likely due to a general lack of expertise in the field. If nothing else, the work completed for this thesis demonstrates that well standardized data can be interpreted readily and that a significant amount of diligence is necessary to ensure that this is the case. As the use of imaging methods to diagnose and investigate the lungs continues to grow, the methods of standardization employed will need to be addressed, and consensus reached in the scientific and medical communities regarding the best practices to ensure reliable interpretation of data. Some of the approaches put forward in this thesis will hopefully be included in these discussions.

Another aspect of this thesis relevant to medical science is the greater understanding of the chronic respiratory pathologies investigated. The spatial attributes of immune reactions and their impact on lung function will require much in the way of further investigation, a process that the articles included in this thesis directly relate to. Eventually, the knowledge gained by this process, coupled to greater computing power, will allow for assessment of the entire lung so as to provide better diagnosis than is currently possible.

### 6.41 – Final Thoughts

The improved diagnosis and treatment of chronic respiratory disease is an objective that will better the lives of patients and reduce the burden of disease on society. To accomplish this, steps forward in both technology and scientific understanding are necessary, ultimately leading to effective management of disease symptoms or intervention prior to the development of pathology. Both asthma and COPD can have a severe impact on the lives of patients, and together represent a major expense to the healthcare system [5,6].

There are many avenues to a better understanding of these diseases, including those investigating genetics and epigenetics, cellular processes and dysfunctions, immune function and dysregulation, neural involvement, and many other

aspects. It is of great importance, however, to understand how the final effects of these processes lead to pathology and lung function impairment. To properly understand how the lung is affected in disease, three-dimensional assessments are of great value, as the lung, in particular, is an organ wherein function is intimately tied to the three-dimensional structure and status. The noninvasive nature of imaging modalities is advantageous, as the lung can be characterized *in vivo* and the data obtained compared across time for the entire lung or any volume therein. Imaging modalities such as CT and SPECT provide information on the lung that cannot be gathered by alternate methods; the heterogeneous nature of COPD, for example, cannot be fully assessed without volumetric measures [162]. The use of imaging techniques will therefore be of great future importance in the clinical diagnosis, management, and study of obstructive lung diseases. The potential to proactively screen for lung disease, instead of attempting to control pathologies that have already been established, will likely be key in addressing the morbidity and mortality of these diseases and may help to alleviate the massive strain these disorders currently impose upon the healthcare system.

While further investigations into these diseases needs to take place in human patients, small animal modelling provides tools to address the constituent pathologies in a manner not possible in humans. For example, single pathologies can be modelled and addressed in mice while it is often impossible to separate pathologies in humans. In addition, therapeutic interventions can be screened once the models have been characterized. Because of the advantages imaging offers when researching the lung, such as the ability to perform longitudinal studies and the volumetric identification of biological and physiological processes, future work with imaging methods in small animal models will further our understanding of these lung diseases so that better diagnostics and therapeutics are available for human patients. This thesis represents several methodological improvements and valuable information regarding the state of the lung in health and disease.

Research utilizing CT is relatively common, both clinically and preclinically, but research utilizing V/Q methods is quite scarce. V/Q imaging is an important tool that appears to be sensitive to even minor alterations in the core processes of lung function and could therefore be used in early disease detection, when other outcomes, even those from other imaging methods like CT, fail to detect pathological changes. Furthermore, this methodology has a role to play in drug efficacy studies and has been proposed as an important biomarker of drug safety [163]. Medical science has been utilizing non-invasive imaging modalities for half a century, but only now stands on the cusp of utilizing the data contained within each image. Quantitative analyses of these data to their full potential will be complicated but extremely worthwhile, allowing for medical advancement within the lung and the body as a whole.

# REFERENCES FOR INTRODUCTION AND DISCUSSION

1. Mathers C. BT, Ma Fat D. (2008) The global burden of disease: 2004 update. Geneva: World Health Organization.
2. From the Global Strategy for Asthma Management and Prevention, Global Initiative for Asthma (GINA) 2011.
3. Lopez AD, Shibuya K, Rao C, Mathers CD, Hansell AL, et al. (2006) Chronic obstructive pulmonary disease: current burden and future projections. Eur Respir J 27: 397-412.
4. Rabe KF, Hurd S, Anzueto A, Barnes PJ, Buist SA, et al. (2007) Global strategy for the diagnosis, management, and prevention of chronic obstructive pulmonary disease: GOLD executive summary. Am J Respir Crit Care Med 176: 532-555.
5. Bahadori K, Doyle-Waters MM, Marra C, Lynd L, Alasaly K, et al. (2009) Economic burden of asthma: a systematic review. BMC Pulm Med 9: 24.
6. Najafzadeh M, Marra CA, Lynd LD, Sadatsafavi M, Fitzgerald JM, et al. (2012) Future Impact of Various Interventions on the Burden of COPD in Canada: A Dynamic Population Model. PLoS One 7: e46746.
7. Nair P, Dasgupta A, Brightling CE, Chung KF (2012) How to diagnose and phenotype asthma. Clin Chest Med 33: 445-457.
8. Han MK, Agusti A, Calverley PM, Celli BR, Criner G, et al. (2010) Chronic obstructive pulmonary disease phenotypes: the future of COPD. Am J Respir Crit Care Med 182: 598-604.
9. Paulus MJ, Gleason SS, Easterly ME, Foltz CJ (2001) A review of high-resolution X-ray computed tomography and other imaging modalities for small animal research. Lab Anim (NY) 30: 36-45.
10. Beckmann N, Kneuer R, Gremlich HU, Karmouty-Quintana H, Ble FX, et al. (2007) In vivo mouse imaging and spectroscopy in drug discovery. NMR Biomed 20: 154-185.
11. Schofield PN, Hoehndorf R, Gkoutos GV (2012) Mouse genetic and phenotypic resources for human genetics. Hum Mutat 33: 826-836.
12. Boron WF, Boulpaep EL (2003) Medical physiology : a cellular and molecular approach. Philadelphia, PA: W.B. Saunders. xiii, 1319 p. p.
13. Voet D, Voet JG (1995) Biochemistry. New York: J. Wiley & Sons. xvii, 1361 p. p.
14. Levitzky MG (2003) Pulmonary physiology. New York ; London: McGraw-Hill. 278 p. p.
15. Al-Muhsen S, Johnson JR, Hamid Q (2011) Remodeling in asthma. J Allergy Clin Immunol 128: 451-462; quiz 463-454.
16. Janeway C (2005) Immunobiology : the immune system in health and disease. New York: Garland Science. xxiii, 823 p. p.
17. Public Health Agency of Canada. Life and Breath: Respiratory Disease in Canada, 2007. Ottawa: Public Health Agency of Canada.
18. Zhang Y, Moffatt MF, Cookson WO (2012) Genetic and genomic approaches to asthma: new insights for the origins. Curr Opin Pulm Med 18: 6-13.
19. Holt PG, Sly PD (2012) Viral infections and atopy in asthma pathogenesis: new rationales for asthma prevention and treatment. Nat Med 18: 726-735.

20. Crinnion WJ (2012) Do environmental toxicants contribute to allergy and asthma? Altern Med Rev 17: 6-18.
21. Barnes PJ (2008) Immunology of asthma and chronic obstructive pulmonary disease. Nat Rev Immunol 8: 183-192.
22. Busse WW, Lemanske RF, Jr. (2001) Asthma. N Engl J Med 344: 350-362.
23. Hogg JC (2004) Pathophysiology of airflow limitation in chronic obstructive pulmonary disease. Lancet 364: 709-721.
24. Lee J, Sandford A, Man P, Sin DD (2011) Is the aging process accelerated in chronic obstructive pulmonary disease? Curr Opin Pulm Med 17: 90-97.
25. Arcavi L, Benowitz NL (2004) Cigarette smoking and infection. Arch Intern Med 164: 2206-2216.
26. Bahadori K, FitzGerald JM, Levy RD, Fera T, Swiston J (2009) Risk factors and outcomes associated with chronic obstructive pulmonary disease exacerbations requiring hospitalization. Can Respir J 16: e43-49.
27. Lundback B, Lindberg A, Lindstrom M, Ronmark E, Jonsson AC, et al. (2003) Not 15 but 50% of smokers develop COPD?--Report from the Obstructive Lung Disease in Northern Sweden Studies. Respir Med 97: 115-122.
28. Marwick JA, Chung KF (2010) Glucocorticoid insensitivity as a future target of therapy for chronic obstructive pulmonary disease. Int J Chron Obstruct Pulmon Dis 5: 297-309.
29. Gregory LG, Lloyd CM (2011) Orchestrating house dust mite-associated allergy in the lung. Trends Immunol 32: 402-411.
30. Kelly FJ, Fussell JC (2011) Air pollution and airway disease. Clin Exp Allergy 41: 1059-1071.
31. Ebert CS, Jr., Pillsbury HC, 3rd (2011) Epidemiology of allergy. Otolaryngol Clin North Am 44: 537-548, vii.
32. Dowson LJ, Guest PJ, Stockley RA (2001) Longitudinal changes in physiological, radiological, and health status measurements in alpha(1)-antitrypsin deficiency and factors associated with decline. Am J Respir Crit Care Med 164: 1805-1809.
33. Borgerding M, Klus H (2005) Analysis of complex mixtures--cigarette smoke. Exp Toxicol Pathol 57 Suppl 1: 43-73.
34. Aranda M, Pearl RG (2000) Inhaled nitric oxide and pulmonary vasoreactivity. J Clin Monit Comput 16: 393-401.
35. Hogg JC, Timens W (2009) The pathology of chronic obstructive pulmonary disease. Annu Rev Pathol 4: 435-459.
36. Doz E, Noulin N, Boichot E, Guenon I, Fick L, et al. (2008) Cigarette smoke-induced pulmonary inflammation is TLR4/MyD88 and IL-1R1/MyD88 signaling dependent. J Immunol 180: 1169-1178.
37. Larsson L, Szponar B, Ridha B, Pehrson C, Dutkiewicz J, et al. (2008) Identification of bacterial and fungal components in tobacco and tobacco smoke. Tob Induc Dis 4: 4.
38. Richmond I, Pritchard GE, Ashcroft T, Avery A, Corris PA, et al. (1993) Bronchus associated lymphoid tissue (BALT) in human lung: its distribution in smokers and non-smokers. Thorax 48: 1130-1134.

39. Brusselle GG, Joos GF, Bracke KR (2011) New insights into the immunology of chronic obstructive pulmonary disease. Lancet 378: 1015-1026.
40. Wen Y, Reid DW, Zhang D, Ward C, Wood-Baker R, et al. (2010) Assessment of airway inflammation using sputum, BAL, and endobronchial biopsies in current and ex-smokers with established COPD. Int J Chron Obstruct Pulmon Dis 5: 327-334.
41. Churg A, Zhou S, Wright JL (2012) Series "matrix metalloproteinases in lung health and disease": Matrix metalloproteinases in COPD. Eur Respir J 39: 197-209.
42. Owen CA (2008) Roles for proteinases in the pathogenesis of chronic obstructive pulmonary disease. Int J Chron Obstruct Pulmon Dis 3: 253-268.
43. Lederman M (1981) The early history of radiotherapy: 1895,Äì1939. International Journal of Radiation Oncology*Biology*Physics 7: 639-648.
44. Chandra R, Ovid Technologies Inc. (2004) Nuclear medicine physics the basics. 6th ed. Philadelphia: Lippincott Williams & Wilkins.
45. Ambrosini V, Nicolini S, Caroli P, Nanni C, Massaro A, et al. (2012) PET/CT imaging in different types of lung cancer: an overview. Eur J Radiol 81: 988-1001.
46. Basu S, Saboury B, Werner T, Alavi A (2011) Clinical utility of FDG-PET and PET/CT in non-malignant thoracic disorders. Mol Imaging Biol 13: 1051-1060.
47. Musch G, Venegas JG (2005) Positron emission tomography imaging of regional pulmonary perfusion and ventilation. Proc Am Thorac Soc 2: 522-527, 508-529.
48. Schroeder T, Vidal Melo MF, Musch G, Harris RS, Winkler T, et al. (2007) PET imaging of regional 18F-FDG uptake and lung function after cigarette smoke inhalation. J Nucl Med 48: 413-419.
49. Vidal Melo MF, Winkler T, Harris RS, Musch G, Greene RE, et al. (2010) Spatial heterogeneity of lung perfusion assessed with (13)N PET as a vascular biomarker in chronic obstructive pulmonary disease. J Nucl Med 51: 57-65.
50. Tgavalekos NT, Musch G, Harris RS, Vidal Melo MF, Winkler T, et al. (2007) Relationship between airway narrowing, patchy ventilation and lung mechanics in asthmatics. Eur Respir J 29: 1174-1181.
51. Beckmann N, Tigani B, Mazzoni L, Fozard JR (2003) Techniques: magnetic resonance imaging of the lung provides potential for non-invasive preclinical evaluation of drugs. Trends Pharmacol Sci 24: 550-554.
52. Washko GR, Parraga G, Coxson HO (2012) Quantitative pulmonary imaging using computed tomography and magnetic resonance imaging. Respirology 17: 432-444.
53. Ley-Zaporozhan J, Ley S, Kauczor HU (2007) Proton MRI in COPD. COPD 4: 55-65.
54. Kirby M, Mathew L, Wheatley A, Santyr GE, McCormack DG, et al. (2010) Chronic obstructive pulmonary disease: longitudinal hyperpolarized (3)He MR imaging. Radiology 256: 280-289.
55. Costella S, Kirby M, Maksym GN, McCormack DG, Paterson NA, et al. (2012) Regional Pulmonary Response to a Methacholine Challenge using Hyperpolarized (3) He Magnetic Resonance Imaging. Respirology.
56. Ambrose J, Hounsfield G (1973) Computerized transverse axial tomography. Br J Radiol 46: 148-149.

57. Buzug TM (2012) Computed Tomography. Springer Handbook of Medical Technology: Springer. pp. 311-342.
58. Hounsfield GN (1973) Computerized transverse axial scanning (tomography). 1. Description of system. Br J Radiol 46: 1016-1022.
59. Bayat S, Porra L, Suhonen H, Janosi T, Strengell S, et al. (2008) Imaging of lung function using synchrotron radiation computed tomography: what's new? Eur J Radiol 68: S78-83.
60. Mos IC, Klok FA, Kroft LJ, de Roos A, Huisman MV (2012) Imaging tests in the diagnosis of pulmonary embolism. Semin Respir Crit Care Med 33: 138-143.
61. Herman GT, Lent A (1976) Iterative reconstruction algorithms. Comput Biol Med 6: 273-294.
62. Dolovich M, Labiris R (2004) Imaging drug delivery and drug responses in the lung. Proc Am Thorac Soc 1: 329-337.
63. Mariani G, Bruselli L, Kuwert T, Kim EE, Flotats A, et al. (2010) A review on the clinical uses of SPECT/CT. Eur J Nucl Med Mol Imaging 37: 1959-1985.
64. Looi K, Sutanto EN, Banerjee B, Garratt L, Ling KM, et al. (2011) Bronchial brushings for investigating airway inflammation and remodelling. Respirology 16: 725-737.
65. Hargreave FE, Leigh R (1999) Induced sputum, eosinophilic bronchitis, and chronic obstructive pulmonary disease. Am J Respir Crit Care Med 160: S53-57.
66. Enright PL (2003) The six-minute walk test. Respir Care 48: 783-785.
67. Bergeron C, Tulic MK, Hamid Q (2007) Tools used to measure airway remodelling in research. Eur Respir J 29: 596-604.
68. Balbi B, Pignatti P, Corradi M, Baiardi P, Bianchi L, et al. (2007) Bronchoalveolar lavage, sputum and exhaled clinically relevant inflammatory markers: values in healthy adults. Eur Respir J 30: 769-781.
69. Weder W, Tutic M, Bloch KE (2009) Lung volume reduction surgery in nonheterogeneous emphysema. Thorac Surg Clin 19: 193-199.
70. Cordova FC (2012) Medical pneumoplasty, surgical resection, or lung transplant. Med Clin North Am 96: 827-847.
71. Hsia CC, Hyde DM, Ochs M, Weibel ER, Structure AEJTFoQAoL (2010) An official research policy statement of the American Thoracic Society/European Respiratory Society: standards for quantitative assessment of lung structure. Am J Respir Crit Care Med 181: 394-418.
72. Liang BM, Lam DC, Feng YL (2012) Clinical applications of lung function tests: a revisit. Respirology 17: 611-619.
73. Jones PW, Agusti AG (2006) Outcomes and markers in the assessment of chronic obstructive pulmonary disease. Eur Respir J 27: 822-832.
74. Parr DG (2011) Patient phenotyping and early disease detection in chronic obstructive pulmonary disease. Proc Am Thorac Soc 8: 338-349.
75. Bousquet J, Khaltaev N (2007) Global surveillance, prevention and control of chronic respiratory diseases: a comprehensive approach.: World Health Organization.
76. Coxson HO, Rogers RM (2005) Quantitative computed tomography of chronic obstructive pulmonary disease. Acad Radiol 12: 1457-1463.

77. Hogg JC, McDonough JE, Sanchez PG, Cooper JD, Coxson HO, et al. (2009) Micro-computed tomography measurements of peripheral lung pathology in chronic obstructive pulmonary disease. Proc Am Thorac Soc 6: 546-549.
78. Wang Z, Gu S, Leader JK, Kundu S, Tedrow JR, et al. (2012) Optimal threshold in CT quantification of emphysema. Eur Radiol.
79. Walker C, Gupta S, Hartley R, Brightling CE (2012) Computed tomography scans in severe asthma: utility and clinical implications. Curr Opin Pulm Med 18: 42-47.
80. Diaz AA, Han MK, Come CE, Estepar RS, Ross JC, et al. (2012) The Effect of Emphysema on Computed Tomographic Measures of Airway Dimensions in Smokers. Chest.
81. Tanabe N, Muro S, Sato S, Tanaka S, Oguma T, et al. (2012) Longitudinal study of spatially heterogeneous emphysema progression in current smokers with chronic obstructive pulmonary disease. PLoS One 7: e44993.
82. Galban CJ, Han MK, Boes JL, Chughtai KA, Meyer CR, et al. (2012) Computed tomography-based biomarker provides unique signature for diagnosis of COPD phenotypes and disease progression. Nat Med.
83. Sylvester JT, Shimoda LA, Aaronson PI, Ward JP (2012) Hypoxic pulmonary vasoconstriction. Physiol Rev 92: 367-520.
84. Sommer N, Dietrich A, Schermuly RT, Ghofrani HA, Gudermann T, et al. (2008) Regulation of hypoxic pulmonary vasoconstriction: basic mechanisms. Eur Respir J 32: 1639-1651.
85. Macintyre N, Crapo RO, Viegi G, Johnson DC, van der Grinten CP, et al. (2005) Standardisation of the single-breath determination of carbon monoxide uptake in the lung. Eur Respir J 26: 720-735.
86. Wagner PD (2008) The multiple inert gas elimination technique (MIGET). Intensive Care Med 34: 994-1001.
87. Hopkins SR, Levin DL, Emami K, Kadlecek S, Yu J, et al. (2007) Advances in magnetic resonance imaging of lung physiology. J Appl Physiol 102: 1244-1254.
88. Kirby M, Mathew L, Heydarian M, Etemad-Rezai R, McCormack DG, et al. (2011) Chronic obstructive pulmonary disease: quantification of bronchodilator effects by using hyperpolarized (3)He MR imaging. Radiology 261: 283-292.
89. Kirby M, Svenningsen S, Owrangi A, Wheatley A, Farag A, et al. (2012) Hyperpolarized 3He and 129Xe MR Imaging in Healthy Volunteers and Patients with Chronic Obstructive Pulmonary Disease. Radiology 265: 600-610.
90. Marshall H, Deppe MH, Parra-Robles J, Hillis S, Billings CG, et al. (2012) Direct visualisation of collateral ventilation in COPD with hyperpolarised gas MRI. Thorax 67: 613-617.
91. Kim WW, Lee CH, Goo JM, Park SJ, Kim JH, et al. (2012) Xenon-Enhanced Dual-Energy CT of Patients With Asthma: Dynamic Ventilation Changes After Methacholine and Salbutamol Inhalation. AJR Am J Roentgenol 199: 975-981.
92. Park EA, Goo JM, Park SJ, Lee HJ, Lee CH, et al. (2010) Chronic obstructive pulmonary disease: quantitative and visual ventilation pattern analysis at xenon ventilation CT performed by using a dual-energy technique. Radiology 256: 985-997.

93. Hachulla AL, Pontana F, Wemeau-Stervinou L, Khung S, Faivre JB, et al. (2012) Krypton ventilation imaging using dual-energy CT in chronic obstructive pulmonary disease patients: initial experience. Radiology 263: 253-259.
94. Musch G, Venegas JG (2006) Positron emission tomography imaging of regional lung function. Minerva Anestesiol 72: 363-367.
95. Harris RS, Winkler T, Tgavalekos N, Musch G, Melo MF, et al. (2006) Regional pulmonary perfusion, inflation, and ventilation defects in bronchoconstricted patients with asthma. Am J Respir Crit Care Med 174: 245-253.
96. King GG, Harris B, Mahadev S (2010) V/Q SPECT: utility for investigation of pulmonary physiology. Semin Nucl Med 40: 467-473.
97. Petersson J, Sanchez-Crespo A, Rohdin M, Montmerle S, Nyren S, et al. (2004) Physiological evaluation of a new quantitative SPECT method measuring regional ventilation and perfusion. J Appl Physiol 96: 1127-1136.
98. Orphanidou D, Hughes JM, Myers MJ, Al-Suhali AR, Henderson B (1986) Tomography of regional ventilation and perfusion using krypton 81m in normal subjects and asthmatic patients. Thorax 41: 542-551.
99. Parameswaran K, Knight AC, Keaney NP, Williams ED, Taylor IK (2007) Ventilation and perfusion lung scintigraphy of allergen-induced airway responses in atopic asthmatic subjects. Can Respir J 14: 285-291.
100. Dai ZK, Chen YW, Hsu JH, Huang MS, Chou SH, et al. (2003) Correlation of pulmonary 99mTc-DTPA ventilation and 99mTc-MAA perfusion scans with pulmonary function tests in asymptomatic asthmatic children. Nucl Med Commun 24: 819-824.
101. Jogi J, Ekberg M, Jonson B, Bozovic G, Bajc M (2011) Ventilation/perfusion SPECT in chronic obstructive pulmonary disease: an evaluation by reference to symptoms, spirometric lung function and emphysema, as assessed with HRCT. Eur J Nucl Med Mol Imaging 38: 1344-1352.
102. Suga K, Kawakami Y, Koike H, Iwanaga H, Tokuda O, et al. (2010) Lung ventilation-perfusion imbalance in pulmonary emphysema: assessment with automated V/Q quotient SPECT. Ann Nucl Med 24: 269-277.
103. Canadian Council on Animal Care: Annual Report 2010-2011.
104. Stevenson CS, Birrell MA (2011) Moving towards a new generation of animal models for asthma and COPD with improved clinical relevance. Pharmacol Ther 130: 93-105.
105. Swirski FK, Gajewska BU, Alvarez D, Ritz SA, Cundall MJ, et al. (2002) Inhalation of a harmless antigen (ovalbumin) elicits immune activation but divergent immunoglobulin and cytokine activities in mice. Clin Exp Allergy 32: 411-421.
106. Cates EC, Gajewska BU, Goncharova S, Alvarez D, Fattouh R, et al. (2003) Effect of GM-CSF on immune, inflammatory, and clinical responses to ragweed in a novel mouse model of mucosal sensitization. J Allergy Clin Immunol 111: 1076-1086.
107. Cates EC, Fattouh R, Wattie J, Inman MD, Goncharova S, et al. (2004) Intranasal exposure of mice to house dust mite elicits allergic airway inflammation via a GM-CSF-mediated mechanism. J Immunol 173: 6384-6392.

108. Johnson JR, Wiley RE, Fattouh R, Swirski FK, Gajewska BU, et al. (2004) Continuous exposure to house dust mite elicits chronic airway inflammation and structural remodeling. Am J Respir Crit Care Med 169: 378-385.
109. Hammad H, Chieppa M, Perros F, Willart MA, Germain RN, et al. (2009) House dust mite allergen induces asthma via Toll-like receptor 4 triggering of airway structural cells. Nat Med 15: 410-416.
110. Hirota JA, Ellis R, Inman MD (2006) Regional differences in the pattern of airway remodeling following chronic allergen exposure in mice. Respir Res 7: 120.
111. Ishii A, Takaoka M, Matsui Y (1977) Production of guinea pig reaginic antibody against the house dust mite extract, Dermatophagoides pteronyssinus, without adjuvant. Jpn J Exp Med 47: 377-383.
112. Singh P, Daniels M, Winsett DW, Richards J, Doerfler D, et al. (2003) Phenotypic comparison of allergic airway responses to house dust mite in three rat strains. Am J Physiol Lung Cell Mol Physiol 284: L588-598.
113. Fournie GJ, Cautain B, Xystrakis E, Damoiseaux J, Mas M, et al. (2001) Cellular and genetic factors involved in the difference between Brown Norway and Lewis rats to develop respectively type-2 and type-1 immune-mediated diseases. Immunol Rev 184: 145-160.
114. Kaplan PD, Kuhn C, Pierce JA (1973) The induction of emphysema with elastase. I. The evolution of the lesion and the influence of serum. J Lab Clin Med 82: 349-356.
115. Stolk J, Rudolphus A, Davies P, Osinga D, Dijkman JH, et al. (1992) Induction of emphysema and bronchial mucus cell hyperplasia by intratracheal instillation of lipopolysaccharide in the hamster. J Pathol 167: 349-356.
116. Bonniaud P, Kolb M, Galt T, Robertson J, Robbins C, et al. (2004) Smad3 null mice develop airspace enlargement and are resistant to TGF-beta-mediated pulmonary fibrosis. J Immunol 173: 2099-2108.
117. Khan MA, Kianpour S, Stampfli MR, Janssen LJ (2007) Kinetics of in vitro bronchoconstriction in an elastolytic mouse model of emphysema. Eur Respir J 30: 691-700.
118. Vernooy JH, Dentener MA, van Suylen RJ, Buurman WA, Wouters EF (2002) Long-term intratracheal lipopolysaccharide exposure in mice results in chronic lung inflammation and persistent pathology. Am J Respir Cell Mol Biol 26: 152-159.
119. Zheng T, Zhu Z, Wang Z, Homer RJ, Ma B, et al. (2000) Inducible targeting of IL-13 to the adult lung causes matrix metalloproteinase- and cathepsin-dependent emphysema. J Clin Invest 106: 1081-1093.
120. Wang Z, Zheng T, Zhu Z, Homer RJ, Riese RJ, et al. (2000) Interferon gamma induction of pulmonary emphysema in the adult murine lung. J Exp Med 192: 1587-1600.
121. Morris DG, Huang X, Kaminski N, Wang Y, Shapiro SD, et al. (2003) Loss of integrin alpha(v)beta6-mediated TGF-beta activation causes Mmp12-dependent emphysema. Nature 422: 169-173.

122. Botelho FM, Gaschler GJ, Kianpour S, Zavitz CC, Trimble NJ, et al. (2010) Innate immune processes are sufficient for driving cigarette smoke-induced inflammation in mice. Am J Respir Cell Mol Biol 42: 394-403.
123. Churg A, Zhou S, Wang X, Wang R, Wright JL (2009) The role of interleukin-1beta in murine cigarette smoke-induced emphysema and small airway remodeling. Am J Respir Cell Mol Biol 40: 482-490.
124. Rinaldi M, Maes K, De Vleeschauwer S, Thomas D, Verbeken EK, et al. (2012) Long-term nose-only cigarette smoke exposure induces emphysema and mild skeletal muscle dysfunction in mice. Dis Model Mech 5: 333-341.
125. Chen K, Pociask DA, McAleer JP, Chan YR, Alcorn JF, et al. (2011) IL-17RA is required for CCL2 expression, macrophage recruitment, and emphysema in response to cigarette smoke. PLoS One 6: e20333.
126. Churg A, Zhou S, Preobrazhenska O, Tai H, Wang R, et al. (2009) Expression of profibrotic mediators in small airways versus parenchyma after cigarette smoke exposure. Am J Respir Cell Mol Biol 40: 268-276.
127. Gaschler GJ, Zavitz CC, Bauer CM, Stampfli MR (2010) Mechanisms of clearance of nontypeable Haemophilus influenzae from cigarette smoke-exposed mouse lungs. Eur Respir J 36: 1131-1142.
128. Balaban RS, Hampshire VA (2001) Challenges in small animal noninvasive imaging. ILAR J 42: 248-262.
129. Lederlin M, Ozier A, Dournes G, Ousova O, Girodet PO, et al. (2012) In Vivo Micro-CT Assessment of Airway Remodeling in a Flexible OVA-Sensitized Murine Model of Asthma. PLoS One 7: e48493.
130. Froese AR, Ask K, Labiris R, Farncombe T, Warburton D, et al. (2007) Three-dimensional computed tomography imaging in an animal model of emphysema. Eur Respir J 30: 1082-1089.
131. Ford NL, Martin EL, Lewis JF, Veldhuizen RA, Holdsworth DW, et al. (2009) Quantifying lung morphology with respiratory-gated micro-CT in a murine model of emphysema. Phys Med Biol 54: 2121-2130.
132. Ask K, Labiris R, Farkas L, Moeller A, Froese A, et al. (2008) Comparison between conventional and "clinical" assessment of experimental lung fibrosis. J Transl Med 6: 16.
133. De Langhe E, Vande Velde G, Hostens J, Himmelreich U, Nemery B, et al. (2012) Quantification of lung fibrosis and emphysema in mice using automated micro-computed tomography. PLoS One 7: e43123.
134. Thomas AC, Potts EN, Chen BT, Slipetz DM, Foster WM, et al. (2009) A robust protocol for regional evaluation of methacholine challenge in mouse models of allergic asthma using hyperpolarized 3He MRI. NMR Biomed 22: 502-515.
135. Mistry NN, Qi Y, Hedlund LW, Johnson GA (2010) Ventilation/perfusion imaging in a rat model of airway obstruction. Magn Reson Med 63: 728-735.
136. Togao O, Ohno Y, Dimitrov I, Hsia CC, Takahashi M (2011) Ventilation/perfusion imaging of the lung using ultra-short echo time (UTE) MRI in an animal model of pulmonary embolism. J Magn Reson Imaging 34: 539-546.

137. Jacob RE, Amidan BG, Soelberg J, Minard KR (2010) In vivo MRI of altered proton signal intensity and T2 relaxation in a bleomycin model of pulmonary inflammation and fibrosis. J Magn Reson Imaging 31: 1091-1099.
138. Ble FX, Cannet C, Zurbruegg S, Karmouty-Quintana H, Bergmann R, et al. (2008) Allergen-induced lung inflammation in actively sensitized mice assessed with MR imaging. Radiology 248: 834-843.
139. Takahashi M, Togao O, Obara M, van Cauteren M, Ohno Y, et al. (2010) Ultra-short echo time (UTE) MR imaging of the lung: comparison between normal and emphysematous lungs in mutant mice. J Magn Reson Imaging 32: 326-333.
140. Locke LW, Williams MB, Fairchild KD, Zhong M, Kundu BK, et al. (2011) FDG-PET Quantification of Lung Inflammation with Image-Derived Blood Input Function in Mice. Int J Mol Imaging 2011: 356730.
141. Gibney BC, Park MA, Chamoto K, Ysasi A, Konerding MA, et al. (2012) Detection of murine post-pneumonectomy lung regeneration by 18FDG PET imaging. EJNMMI Res 2: 48.
142. Hafeli UO, Saatchi K, Elischer P, Misri R, Bokharaei M, et al. (2010) Lung perfusion imaging with monosized biodegradable microspheres. Biomacromolecules 11: 561-567.
143. Pullambhatla M, Tessier J, Beck G, Jedynak B, Wurthner JU, et al. (2012) [(125)I]FIAU imaging in a preclinical model of lung infection: quantification of bacterial load. Am J Nucl Med Mol Imaging 2: 260-270.
144. van Echteld CJ, Beckmann N (2011) A view on imaging in drug research and development for respiratory diseases. J Pharmacol Exp Ther 337: 335-349.
145. Al-Garawi A, Husain M, Ilieva D, Humbles AA, Kolbeck R, et al. (2012) Shifting of immune responsiveness to house dust mite by influenza A infection: genomic insights. J Immunol 188: 832-843.
146. Cardus J, Burgos F, Diaz O, Roca J, Barbera JA, et al. (1997) Increase in pulmonary ventilation-perfusion inequality with age in healthy individuals. Am J Respir Crit Care Med 156: 648-653.
147. Sprung J, Gajic O, Warner DO (2006) Review article: age related alterations in respiratory function - anesthetic considerations. Can J Anaesth 53: 1244-1257.
148. Glenny RW, Lamm WJ, Albert RK, Robertson HT (1991) Gravity is a minor determinant of pulmonary blood flow distribution. J Appl Physiol 71: 620-629.
149. Rodriguez-Roisin R, Drakulovic M, Rodriguez DA, Roca J, Barbera JA, et al. (2009) Ventilation-perfusion imbalance and chronic obstructive pulmonary disease staging severity. J Appl Physiol 106: 1902-1908.
150. Del Guerra A, Belcari N (2007) State-of-the-art of PET, SPECT and CT for small animal imaging. Nuclear Instruments and Methods in Physics Research Section A: Accelerators, Spectrometers, Detectors and Associated Equipment 583: 119-124.
151. Madsen MT (2007) Recent advances in SPECT imaging. J Nucl Med 48: 661-673.
152. Golestani R, Wu C, Tio RA, Zeebregts CJ, Petrov AD, et al. (2010) Small-animal SPECT and SPECT/CT: application in cardiovascular research. Eur J Nucl Med Mol Imaging 37: 1766-1777.

153. Farncombe TH (2008) Software-based respiratory gating for small animal conebeam CT. Med Phys 35: 1785-1792.
154. Bailey EA, Bailey DL, Roach PJ (2010) V/Q imaging in 2010: a quick start guide. Semin Nucl Med 40: 408-414.
155. Jahns J, Anderegg U, Saalbach A, Rosin B, Patties I, et al. (2011) Influence of low dose irradiation on differentiation, maturation and T-cell activation of human dendritic cells. Mutat Res 709-710: 32-39.
156. Schuler E, Parris TZ, Rudqvist N, Helou K, Forssell-Aronsson E (2011) Effects of internal low-dose irradiation from 131I on gene expression in normal tissues in Balb/c mice. EJNMMI Res 1: 29.
157. Travis EL, Peters LJ, McNeill J, Thames HD, Jr., Karolis C (1985) Effect of dose-rate on total body irradiation: lethality and pathologic findings. Radiother Oncol 4: 341-351.
158. Wedzicha JA, Seemungal TA (2007) COPD exacerbations: defining their cause and prevention. Lancet 370: 786-796.
159. Sethi S, Murphy TF (2008) Infection in the pathogenesis and course of chronic obstructive pulmonary disease. N Engl J Med 359: 2355-2365.
160. Suga K, Kawakami Y, Zaki M, Yamashita T, Shimizu K, et al. (2004) Clinical utility of co-registered respiratory-gated( 99m)Tc-Technegas/MAA SPECT-CT images in the assessment of regional lung functional impairment in patients with lung cancer. Eur J Nucl Med Mol Imaging 31: 1280-1290.
161. Taplin GV, MacDonald NS (1971) Radiochemistry of macroaggregated albumin and newer lung scanning agents. Semin Nucl Med 1: 132-152.
162. Coxson HO, Mayo J, Lam S, Santyr G, Parraga G, et al. (2009) New and current clinical imaging techniques to study chronic obstructive pulmonary disease. Am J Respir Crit Care Med 180: 588-597.
163. Amen EM, Becker EM, Truebel H (2011) Analysis of V/Q-matching--a safety "biomarker" in pulmonary drug development? Biomarkers 16 Suppl 1: S5-10.